Reviewed Preprint
v1 • March 12, 2026
Not revised

Reviewed Preprint
v2 • July 6, 2026
Revised by authors

For correspondence:
johnkaranicolas1@gmail.com

† Equal author contributions

Competing interests: No competing interests declared

Funding: See page 54

Reviewing editor: Aaron Frank, Arrakis Therapeutics, United States

Rescuing the Function of Missense-Mutated Tumor Suppressor *VHL* using Stabilizing Small Molecules

Mariam Ahmed Fouad[1,†], Christopher S Parry[1,2,†], Sven A Miller[1], Shipra Malhotra[1], Glenn A Doyle[1], Ezra Shimabenga[1], Mashhura Nurilloeva[1], Elena Bondarenko[1], Grigorii V Andrianov[1], Wayne Childers[3], Benjamin E Blass[3], Petr B Makhov[1], Johnathan R Whetstine[1], Margie L Clapper[1], Erica A Golemis[1,4], John Karanicolas[1,3]

[1]Fox Chase Cancer Center, Philadelphia, United States • [2]MD/PhD Program, Lewis Katz School of Medicine at Temple University, Philadelphia, United States • [3]Moulder Center for Drug Discovery Research, Temple University School of Pharmacy, Philadelphia, United States • [4]Department of Cancer and Cellular Biology, Lewis Katz School of Medicine at Temple University, Philadelphia, United States

eLife Assessment

This study presents **important** findings by identifying small molecules that can stabilize and refold missense-mutated VHL tumor suppressor protein, offering a potential therapeutic approach for clear cell renal cell carcinoma. The computational design approach is well-executed, but the evidence is **incomplete** due to insufficient demonstration that HIF2 downregulation occurs through on-target VHL rescue rather than off-target effects. Additional experiments with appropriate controls are needed to establish the specificity of the mechanism.

https://doi.org/10.7554/eLife.110305.2.sa3

Abstract

Somatic mutations in the *VHL* gene, coupled with *VHL* loss of heterozygosity, drive sporadic clear cell renal cell carcinoma (ccRCC). From structural considerations, we hypothesized that certain mutations in the *VHL* gene thermodynamically destabilize the folded protein product; these mutations would increase the ratio of unfolded:folded pVHL, and thus cause loss of function. To test this, we used computational structure-based screening followed by biophysical characterization and cellular assays to identify small molecules that bind to the folded (native) conformation of pVHL and stabilize it. These studies led to creation of an agent, CP4.29, that stabilizes the native folded structure of mutant pVHL: this in turn restores wild-type pVHL activities to cells that harbor mutant *VHL*. These compounds may serve as starting points for further development into an unprecedented new class of kidney cancer drugs. The approach described herein may also serve as a blueprint for developing agents to correct destabilized mutations underlying other human diseases.

Highlights

- Designed small molecules that re-fold and re-activate destabilized mutant *VHL*
- Lead agent re-folds and re-activates multiple common *VHL* mutants
- This approach may apply to other destabilized proteins that underlie human disease

Introduction

Biallelic loss of tumor suppressor genes (and their associated protein products) represents a key factor in cancer development and progression [1-3]. Germline or somatic mutations in one such tumor suppressor gene, *VHL*, lead to development of von Hippel-Lindau Disease (VHLD) and clear cell renal cell carcinoma (ccRCC), respectively [4-7]. Decades of research have revealed that *VHL*'s protein product, pVHL, serves as an adaptor protein in diverse protein complexes that regulate numerous cellular functions [7-9].

The pVHL / Elongin C / Elongin B ("VCB") complex is the most well studied of these protein complexes. The VCB complex is part of an E3 ubiquitin ligase complex that induces polyubiquitination and proteasomal degradation of substrates bearing a hydroxyproline mark, most notably members of the Hypoxia Inducible Factor Alpha (HIF-α) family [10-13]. Inactivating mutations in *VHL* thus lead to aberrant accumulation of HIF-1α and HIF-2α, which in turn induce transcription of hypoxic response genes including *VEGF-A*, *CCND1* and many more, that collectively drive angiogenesis, cellular metabolism, and cell survival [7,14]. In addition to regulating HIF, pVHL also has many important HIF-independent activities: these include ubiquitinating substrates such as ZHX2 [15], nuclear clusterin [16], IKKβ [17], AURKA [18], RPB1 [19,20], and atypical protein kinase C [21]. pVHL has also been implicated in extracellular matrix assembly, through direct interactions with collagen IV [22,23] and fibronectin-1 [24].

Mechanistic understanding of *VHL* signaling has contributed to targeted therapy for VHLD and ccRCC patients. Dramatic clinical successes came first through inhibition of HIF's downstream effector VEGFR [25-27], and then by inhibiting HIF-2α itself [28-31]. Nonetheless, the fact that *VHL*'s rich tumor suppressive activities clearly extend beyond HIF [15,32-36] suggests that *direct* pharmacological restoration of *VHL* activity may represent a more robust and promising approach than simply targeting individual downstream effectors such as HIF. Attempts to restore the cellular activity of missense *VHL* mutants have been reported [32,37,38], but none of these yielded suitably drug-like hits to serve as a compelling starting point for further translational advancement.

In some kidney cancers *VHL* is inactivated indirectly, through epigenetic silencing or through mutations to accessory proteins such as Elongin C (*TCEB1*) [39]. Among somatic *VHL* missense mutations in kidney cancer, the Catalog of Somatic Mutations in Cancer (COSMIC) database [40] shows that mutation sites are distributed broadly throughout the protein sequence (Figure 1a). Despite the extremely high overall prevalence of *VHL* mutations in in kidney cancer, there are no "hotspot" positions with very high mutation frequency: rather, many different sites are mutated with low frequencies for each. Mapping these positions onto a high resolution crystal structure of the VCB complex (pVHL / Elongin C / Elongin B) bound to a hydroxyprolinated peptide from HIF [41,42] (Figure 1a), about 59% of kidney cancers have *VHL* mutations at sites located in regions that interact with either the Elongins or with the HIF peptide. Importantly though, the other 41% of *VHL* missense mutations in human samples do not localize to surface residues involved in protein interactions, but rather correspond to buried residues comprising the hydrophobic core of the folded protein.

Consistent with the hypothesis that its marginal stability underlies the loss of function associated with single missense mutations in the hydrophobic core, prior studies also found that isolated (WT) pVHL is not fully folded but rather occupies a molten globule state that is particularly susceptible to aggregation [43]. Stability of pVHL in cells is dependent on the presence of Elongins B and C [44], and indeed crystallographic studies of pVHL inevitably also use the VCB complex [41,42]. Recognizing that certain disease-associated *VHL* mutations affect protein stability [45-47], a recent machine learning model employed protein stability predictions to assess the risk of ccRCC associated with a given *VHL* mutation [48]. Collectively, these observations suggest that small molecules binding to the wild-type conformation of mutant pVHL in cells ought to enhance the protein's thermodynamic stability, thus reversing the destabilizing effect of the mutation (Figure 1b).

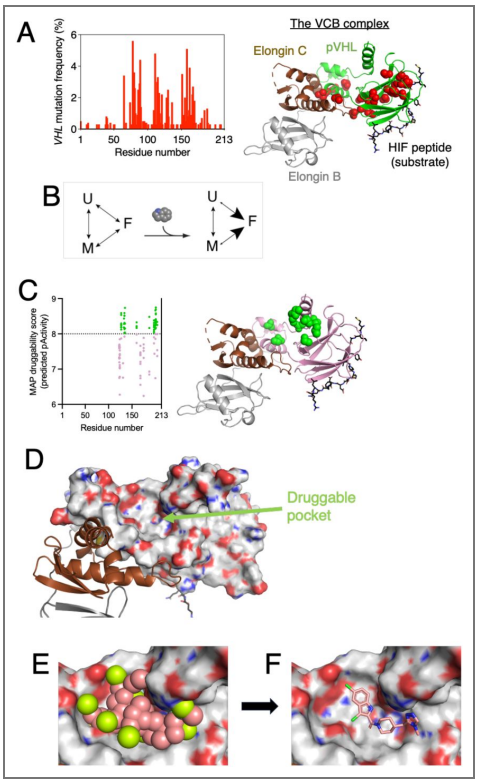

Figure 1. Designing pharmacological pVHL refolders by targeting a distinct surface pocket.

(A) Missense mutations observed in kidney cancer are broadly distributed across the VHL sequence, and mapping them to the protein structure (PDB 1LM8) shows that many of the 20 most frequently occurring mutations (*red*) are located in the hydrophobic core of the folded protein structure. **(B)** Overarching design strategy for re-folders / re-activators. In principle, ligands that preferentially bind to the folded/active conformation of a protein (F) will shift the conformation equilibrium towards this state, at the expense of unfolded (U) or misfolded (M) states. **(C)** The MAP druggability score is intended to provide a measure of how potently some (yet unknown) ligand might engage a given protein surface. With respect to pVHL, multiple simulations implicated the same surface pockets as having the highest MAP score. Spheres in this figure (*green*) indicate locations of residues with the highest MAP score. **(D)** The location of this druggable pocket is distinct from the binding surfaces of the Elongins, and of the HIF recognition site. **(E)** Building an exemplar indicates how an ideal ligand would engage this surface pocket. Spheres indicate volume that would be filled by an ideal ligand, marked by lipophilic (*pink*) or polar atoms (*yellow*). **(F)** Using this exemplar as a template, virtual screening provides models of specific ligands that complement this surface pocket.

Here, we report a computational structure-based screening approach and initial optimization leading to a chemical probe (CP4.29) that directly engages the VCB complex and functionally restores *VHL* activity to different mutants in assorted ccRCC cell lines. This represents the first drug-like agent that directly restores stability and activity to mutant pVHL. We expect that this compound will serve as an entry point for developing pVHL refolders as an entirely new class of therapeutics for ccRCC and VHLD.

Results

Computational design of pVHL binders

In principle, binding of a small molecule to the transiently folded conformation (F) of mutant pVHL would stabilize this conformation, thus shifting the conformational equilibrium away from misfolded (M) or unfolded (U) states (Figure 1b). The potential binding site for such a ligand is not known *a priori*; however, targeting some non-functional region of the protein surface would be preferred, to avoid competitive inhibition with pVHL's endogenous interaction partners. Rather than simply search for druggable pockets on the surface of the pVHL crystal structure, we expanded the potential binding sites we considered by additionally evaluating cryptic pockets transiently sampled on the protein surface [49,50]. To this end, we used a biased conformational sampling strategy [50,51] implemented in the Rosetta software suite [52] to generate low-energy pocket-containing conformations of pVHL. To ensure that formation of a cryptic pocket would not allosterically inhibit pVHL's interaction with either the Elongins or its substrate(s), we carried out these simulations in the context of the (wild-type) pVHL / Elongin C / Elongin B / HIF-1α complex.

We carried out a focused set of individual simulations on each of pVHL's surface-exposed residues (see Supplemental Methods). For each pocket observed in these simulations, we applied a gradient boosting machine learning model (GBM) to predict the "Maximum Achievable Potency" (MAP) value for each surface pocket [53-55]. Briefly, this model was developed by extracting pockets from a diverse collection of experimentally characterized protein-ligand complexes, then discarding the ligand and training the model to predict the ligand's potency using only features from the protein pocket (primarily hydrophobicity and concavity). By applying this analysis to pockets from simulations of the pVHL surface, we identified a collection of pockets predicted to enable development of a ligand with potency in the 1-10 nM range (MAP values between 8 and 9) (Figure 1c). Mapping the location of these pockets to the protein structure revealed that each of these simulations had identified small structural variations of a large pocket already evident from the crystal structure of the VCB complex (Figure 1d). In principle, conformational variations of this pocket could allow for discovery of different and complementary collections of ligands. Accordingly, we advanced each low-energy conformation with a highly druggable pocket (MAP>8) for virtual screening.

For each protein conformation, we built an "exemplar" [56]: essentially a receptor-based pharmacophore that defines the shape and relative positioning of hydrogen bond donors/acceptors for a ligand that would optimally complement the protein surface (Figure 1e). We then used these exemplars to carry out a two-step virtual screen of chemical vendor Enamine's collection of make-on-demand compounds. In the first phase, we screened a set of 12.5 million diverse compounds to identify 100 chemical scaffolds complementary to this region of the protein surface. In the second phase, we identified 100 analogs of each initial scaffold and combined these into a target-focused library of 10,000 compounds. We aligned each of these onto the parent scaffold, used Rosetta to refine the protein/ligand structure, and then used the vScreenML machine learning classifier [57] to distinguish likely binders from likely computational artifacts. The *Supporting Information* contains complete details of this computational protocol, including a summary of the workflow (Figure S1).

The resulting models, as exemplified by the compound designated "CP4", show clear complementarity to this surface of pVHL, both in terms of shape and hydrogen bonding groups (Figure 1f). The top 18 compounds based on vScreenML score were selected (Table S1), and these were requisitioned via Enamine's on-demand synthesis.

CP4 directly engages the VCB complex consistent with the intended binding mode

Having acquired 18 initial compounds from this virtual screen, we first sought to assess each for binding to purified (WT) pVHL. As noted earlier, pVHL is not stable in the absence of Elongins B and C [44], and accordingly studies of purified pVHL use the VCB complex [41,42]. For these reasons, we elected to test our initial designed hits using label-free binding assays that could be applied in the context of the VCB complex, rather than pVHL alone. Further, since our compounds are intended to bind to the folded conformation of pVHL, we elected to use WT pVHL for primary testing rather than a destabilized mutant.

We therefore purified the recombinant (WT) pVHL / Elongin C / Elongin B ("VCB") protein complex, and we evaluated the 18 hit compounds via Saturation Transfer Difference (STD) NMR. Among the compounds showing evidence of binding was CP4 (Figure 2a). To fully confirm direct binding of CP4 to the VCB complex, we evaluated binding using three separate and orthogonal ligand-observed NMR assays: STD-NMR, WaterLOGSY, and CPMG [58,59]. Parenthetically, all three NMR techniques have already been used in the context of fragment screening against the VCB complex [60,61], albeit with the intention of designing new warheads for targeted protein degradation (e.g. PROTACs) to replace the widely used HIF-α peptidomimetic VH298 [62,63].

An advantage of ligand-observed NMR assays is that multiple compounds can be tested in a single tube, provided that their ^{1}H spectra are non-overlapping. As a positive control in these assays, we therefore included the above-referenced HIF-α peptidomimetic VH298 (Figure 2a). As a negative control, we sought to include a readily available compound with physicochemical properties matched to those of CP4: this led us to select the anti-diabetes drug sitagliptin (Figure 2a). By comparing with individual spectra for each compound, the peaks in this mixture could be unambiguously assigned as belonging either to CP4, to sitagliptin, or to VH298 (Figure S2-S4).

In the STD-NMR experiment, addition of VCB complex to the mixture yielded clear saturation transfer differences for peaks in the aromatic region corresponding to CP4 and VH298 (indicating binding), but not for sitagliptin (Figure 2b, *top*). Importantly, none of the aromatic protons show appreciable STD signal in the absence of protein: this rules out direct irradiation of these protons as an artifactual source of the STD signal [64]. Additionally, the observation of STD signal for protons from positive control compound VH298 also confirm that (WT) VHL is correctly folded in the sample, making it unlikely that CP4 is interacting non-specifically with some unfolded/misfolded form of the protein.

In the WaterLOGSY experiment, all non-exchangeable protons on the small molecules phase down in the absence of protein, as expected; the only peaks phased upward correspond to a doublet at 7.24 ppm from an exchangeable proton on VH298. Upon addition of the VCB complex, CP4 peaks flip from phased down to phased up, consistent with an interaction between the two (Figure 2b, *middle*). While peaks from VH298 do not change phase, the magnitude of their downward phase is diminished by the interaction with VCB; by contrast, peaks from negative control sitagliptin are unaffected.

In contrast to the first two experiments, which probe effects of magnetization transfer (either from the protein itself or bulk water), the CPMG experiment probes differences in T2 relaxation time associated with binding to a macromolecule [65,66]. Here too, peaks corresponding to CP4 exhibit dramatic loss of intensity upon addition of the VCB complex, consistent with binding (Figure 2b, *bottom*). The peaks from positive control VH298 also lose intensity, whereas peaks from negative control sitagliptin do not. Collectively then, all three ligand-observed NMR experiments are consistent in their demonstration of a direct interaction between CP4 and the VCB complex.

To determine whether CP4 indeed engages the intended pocket on the surface of VHL, we designed a mutation at the base of the binding site, D197K (Figure 2c). As noted earlier, HIF-α and its peptidomimetic VH298 both bind at a site that is distant from our intended binding surface target

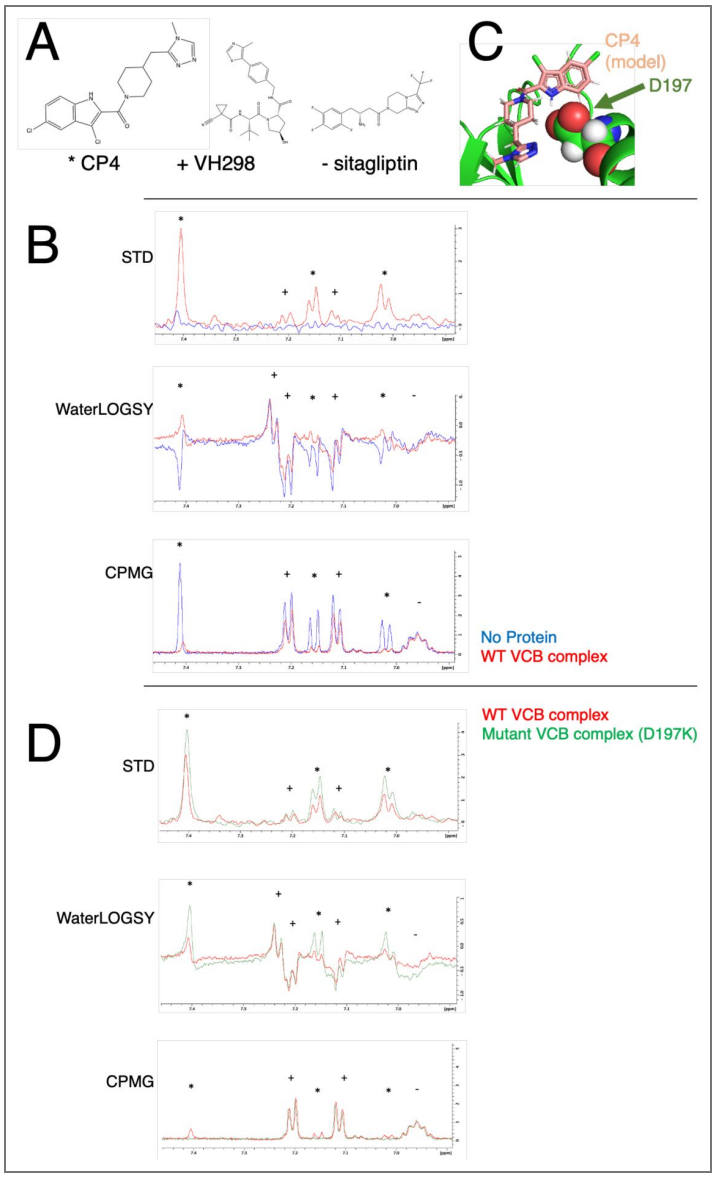

Figure 2. Direct evidence of CP4 binding to the VCB complex.

(A) Chemical structure of CP4, as well as those of VH298 (positive control) and sitagliptin (negative control). **(B)** Orthogonal ligand-observed NMR spectra for three separate experiments: STD-NMR, WaterLOGSY, and CPMG. Each sample contains a mixture of CP4, sitagliptin, and VH298 in the presence (*red*) or absence (*blue*) of the VCB complex. Peaks are labeled based on whether they belong to CP4 (*), VH298 (+), or sitagliptin (-). **(C)** Based on our model of CP4 engaging the VCB complex, we elected to mutate *VHL* Asp197, a residue in the intended binding pocket. **(D)** The same three ligand-observed NMR assays were carried out using VCB complex harboring designed *VHL* mutant D197K. This mutant complex does not show any change in binding for VH298 or sitagliptin (relative to the WT VCB complex), but it *does* show a difference in binding for CP4. Due to the kinetic nature of these experiments, they cannot be used to differentiate between enhanced versus diminished CP4 binding. Full spectra from these experiments are included as Figures S5-S10.

pocket, leading us to expect that this mutation would not affect binding of VH298 to the protein complex. Upon expressing and purifying the $V_{D197K}CB$ protein complex, we applied the same suite of NMR experiments described above.

In all three experiments, VH298 binding was indeed unaffected by the mutation: this observation also confirms that the D197K mutation did not affect foldedness of the protein complex. Conversely, all three experiments show differences in CP4 binding (Figure 2d), consistent with CP4 binding at the intended site from our computational designs.

We note that the magnitude of each probed effect is greater for the mutant complex $V_{D197K}CB$ than for WT VCB. A key limitation of ligand-observed NMR methods is that evidence of binding diminishes when the binding affinity is *either* too weak or strong to be observed via this class of methods [67,68]. The observed signal these techniques scales with the number of binding/unbinding events, because these events are responsible for observed signal that underlies all three methods. For this reason, changes to the protein structure that lead to faster off-rate (i.e. weaker affinity) would result in more binding/unbinding events, and thus greater signal as detected by these methods. These methods are best suited for determination of binding affinities in the 10 μM to 1 mM range, with observed signal diminishing as binding affinity is outside this range in either direction.

Ultimately, we hypothesize that the D197K mutation indeed weakens the VHL's interaction with CP4, leading to faster off-rate (and thus more binding/unbinding events in the NMR timescale). We can rule out the fact that the mutation affects the amount of folded VHL, because the mutation does not affect the signal from VH298. Regardless of the specific effect on binding affinity, however, these data strongly corroborate the hypothesis that CP4 binds to the VCB complex near pVHL's Asp197, as designed in the computational model. Alternative biophysical methods to directly probe binding / protein stability are confounded by the fact that pVHL is not readily purified without the Elongins present, and such characterization will therefore be deferred for a future study.

CP4 stabilizes mutant pVHL in ccRCC cell lines

Having observed CP4's direct engagement of purified WT pVHL, we next sought to evaluate the effect of CP4 on mutant pVHL in a more relevant cellular context. Accordingly, we obtained three different cell lines from human ccRCC that each harbor a different *VHL* missense mutation: RCC-MF (*VHL* P86S), RCC4 (*VHL* S65W), and 769-P (*VHL* I180N). Each mutation is at a buried/interfacial position in the VCB complex, but they map to different parts of the pVHL structure: P86S is in the central core, S65W is near the HIF-α binding site, and I180N is near the Elongin C binding surface (Figure 3a). The latter mutation is of particular interest, because mutations in the interfacial region between pVHL and the Elongins have been shown to disrupt both pVHL and Elongin stability, suggesting that each component of the VCB complex is dependent on the others for cellular stability [44]. In fact, the 769-P cell line is sometimes (misleadingly) described as "VHL null" because of the extremely low abundance of mutant pVHL [69,70]. Importantly though, none of these mutation sites are close to the CP4 binding site, allowing us to test the hypothesis that ligand binding can rescue the effect of a mutation at a distant site.

Many *VHL* mutants have been found at lower cellular abundance than the WT protein, due to shortened cellular half-life [38]. Accordingly, we hypothesized that treatment with CP4 would increase cellular abundance of mutant pVHL by extending its half-life. To test this, we treated each cell line with an increasing concentration of CP4 for 1 hour, and we probed for pVHL abundance via Western blot. Cells produce pVHL in two isoforms, pVHL19 and pVHL30. pVHL19 arises due to an alternative initiation site at Met54, thus resulting in a protein product that lacks 53 residues in the disordered N-terminus of pVHL30. Despite slightly different subcellular localization, the shared folded structure of these isoforms allow both to bind Elongins and recognize substrates including HIF-α [71]. We find that treatment with CP4 leads to accumulation of both pVHL isoforms, in all three cell lines (Figure 3b).

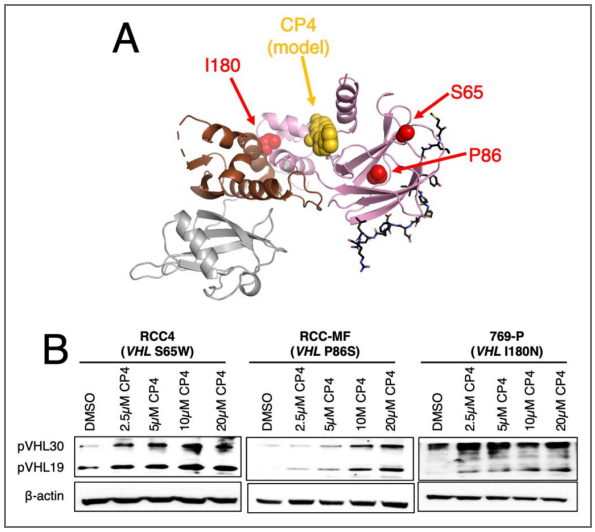

Figure 3. **CP4 stabilizes pVHL in ccRCC cell lines harboring *VHL* missense mutations.**

(A) Our cellular studies use three cell lines that each harbor a different *VHL* missense mutations. The sites of these three mutations are structurally remote: P86 is in the central core, S65 is near the HIF-α binding site, and I180 is near the Elongin C binding surface. None of these positions are in direct contact with the CP4 designed binding site. **(B)** CP4 treatment for 1 hour leads to accumulation of both isoforms of mutant pVHL.

CP4.29 induces VHL-dependent depletion of HIF-2α

The most relevant HIF isoform in the context of ccRCC is HIF-2α [72,73]. Given that CP4 induces refolding of mutant pVHL in cells, we expected that CP4 treatment would also restore pVHL activity in cells – most notably including the ubiquitin-mediated destruction of HIF-2α. Initial experiments evaluating CP4 in this context showed little to no reduction in HIF-2α, however, despite CP4 stabilizing mutant pVHL isoforms in the same cell lines.

In past studies using an artificial system, we screened small molecules to evaluate their complementation of a designed cavity introduced by mutation into an enzyme [74]. We found that certain ligands bound to this cavity but led to slight distortions in the protein structure, such that enzyme activity was not rescued. In fact, restoring enzyme activity required that the ligand bind to the designed cavity in a manner that precisely recovered the original enzyme conformation [75]. Thus, close analogs could have dramatic differences in their rescue of enzyme activity, that were not simply attributable to differences in binding affinity [74].

We therefore surmised that CP4 may bind to mutant pVHL such that the resulting conformation is very close to that of the WT protein, but not precisely so. While CP4 itself did not recover HIF-2α degradation by mutant pVHL, we hypothesized that a close chemical analog of CP4 might do so. Accordingly, we relied on the straightforward synthetic accessibility of CP4 (Figure 4a) to prepare a library of close analogs, and then supplemented this collection using additional analogs available from Enamine for a total of 46 compounds (Table S2).

We evaluated this panel in RCC-MF cells (*VHL* P86S), by applying a 2 hour treatment of each compound at 20 μM, then probing for HIF-2α by ELISA. Whereas most CP4 derivatives (and CP4 itself) did not lead to any appreciable difference in HIF-2α, related compounds CP4.29 and CP4.30 induced a dramatic reduction of HIF-2α (Figure 4b). To test whether a single compound could recover activity of multiple *VHL* mutants, we applied CP4.29 to all three cell lines, and we observed depletion of both HIF-2α (Figure 4c) and HIF-1α (Figure S11) in all three cell lines.

The distinction between CP4 and CP4.29 is remarkably modest. Relative to CP4, derivative CP4.29 replaces a 4-methyltriazole with a 3-isopropylozadiazole. While we cannot rule out subtle differences in the compounds' physical properties that may have led to enhanced cell permeability, the fact that other substitutions did not confer this activity implies that this is not the case (Table S2). In our model of CP4 bound to the VCB complex, this substituent that differentiates CP4.29 and CP4.30 from CP4 is in direct contact with a long loop that connects the two halves of pVHL's β-sandwich, about 20 Å from the bound HIF-α peptide (Figure 4d). The surprising impact of these specific substitutions suggests an unexpected allosteric coupling between the two sides of the β-sandwich, such that subtle structural differences on one side can impact binding at the other side. Through evaluation of further CP4.29 analogs (Table S3), we identified alternate substituents with similar activity to CP4.29. Changes to the dichloroindole group inevitably led to loss of activity, suggesting that this side of the ligand is already well-optimized for binding to pVHL.

A key consequence of HIF-α destruction is the expected downregulation of HIF target genes. Due to the role of HIF-α in transcriptional activation, the principal activity of HIF-2α antagonists (including approved drug belzutifan) is to inhibit expression of HIF-2α dependent genes such as *CCND1* (cyclin D) and *VEGF-A* (VEGF-A) [76]. Using the 769-P cell line that contained very little pVHL in the absence of our stabilizers, we applied RT-PCR to probe the activity of CP4.29 on mRNA levels of both genes, using belzutifan as a positive control. Remarkably, CP4.29 showed similar activity and kinetics as belzutifan (Figure 4e), despite their very different mechanisms of action.

Having established CP4.29 as our most promising degrader of HIF-2α, we next sought to evaluate its mechanism of action. As noted earlier, pVHL recognition of HIF-2α depends on the latter bearing a hydroxyproline post-translational modification in response to a normoxic environment (high O_2). Under hypoxic conditions (low O_2), HIF-2α does not receive this modification and is not targeted by pVHL for destruction [7,10,11,14]. To test whether CP4.29 induces HIF-2α degradation in an oxygen-dependent manner, we applied 5 μM CP4.29 to RCC-MF cells that had been

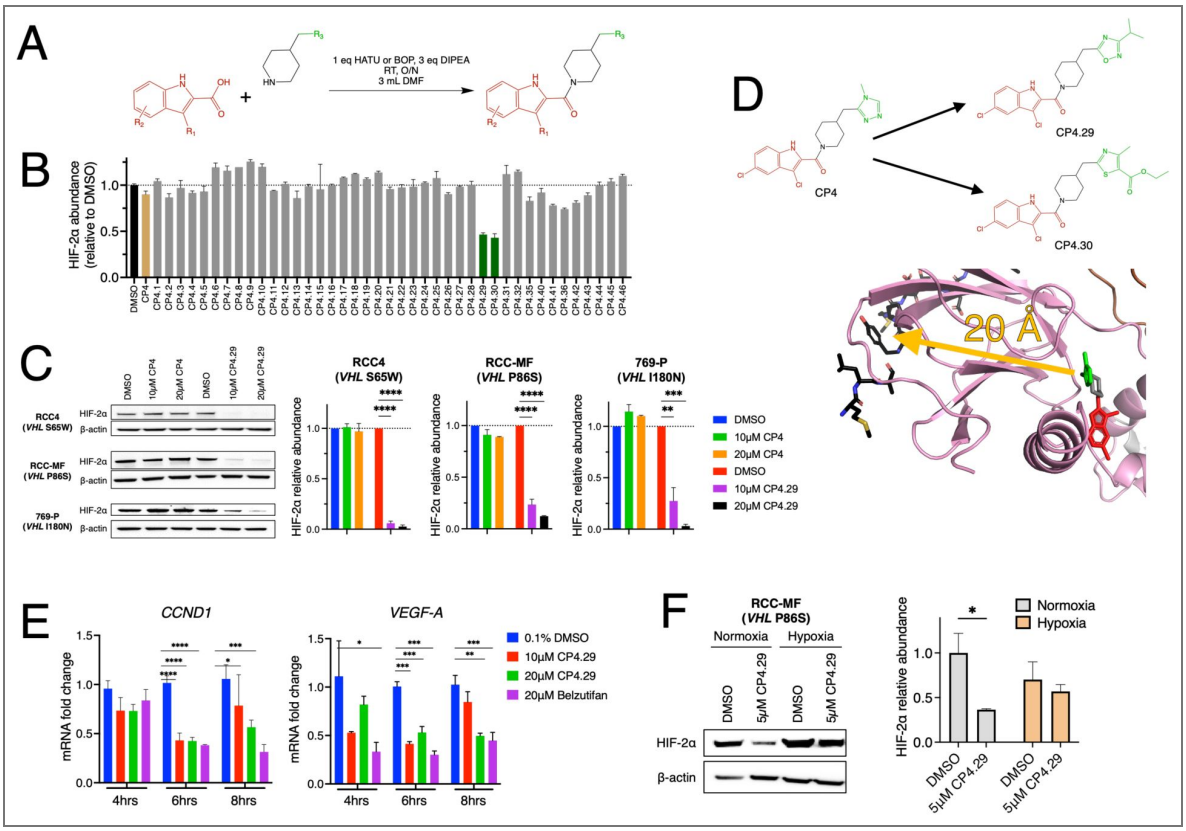

Figure 4. CP4.29 degrades HIF-2α by re-activating mutant pVHL in ccRCC cell lines.

(A) Reaction scheme for preparing CP4 derivatives. **(B)** CP4 derivatives were screened at 20 μM in RCC-MF cells, by using ELISA to probe HIF-2α abundance after 2 hour treatment with each compound. **(C)** Treatment with CP4.29 for 2 hours led to depletion of HIF-2α in RCC4, RCC-MF, and 769-P cell lines. **(D)** CP4 and CP4.29 differ only slightly in chemical structure, at a site approximately 20 Å from substrate HIF-α in our model of target engagement. **(E)** Application of CP4.29 to 769-P cells reduced mRNA levels of HIF-2α target genes *CCND1* and *VEGF-A*. **(F)** CP4.29 treatment for 4 hours induces HIF-2α degradation in RCC-MF cells under normoxic conditions (20% O_2) but not hypoxic conditions (2% O_2), consistent with pVHL-mediated recognition of HIF-2α.

acclimated for 24 hours at either a normoxic environment (20% O_2) or a hypoxic environment (2% O_2). Consistent with a pVHL-dependent mechanism of CP4.29, we observe HIF-2α degradation only under normoxic conditions (Figure 4f).

CP4.29 restores pVHL's ubiquitin ligase activity against multiple substrates

VHL tumor suppressive activity derives not just from degrading HIF-α: it also induces degradation of other oncogenic substrates including Aurora kinase A (AURKA) [18] and ZHX2 [15]. Using the same 769-P cell line (*VHL* I180N), we therefore probed for depletion of these substrates and found that CP4.29 rescues these activities of mutant pVHL as well (Figure 5a). This observation is important because CP4.29 was selected based on its activity in rescuing HIF-2α depletion: the fact that CP4.29 also depletes other pVHL targets provides more stringent evidence that CP4.29 may be fully recapitulating the WT pVHL structure, rather than simply re-constructing a few key interactions sufficient for recruiting HIF-α.

To establish that the observed depletion of these pVHL substrates is indeed dependent on the ubiquitin ligase pathway, we applied several complementary pharmacological controls. First, we co-treated cells with CP4.29 and MLN4924, an inhibitor of NEDD8-activating enzyme (NAE) [77]. Cullin-RING E3 ligases (CRLs) require NEDD8ylation of the cullin to assemble into active complexes; thus, inhibiting the NEDD8ylation cascade using MLN4924 disrupts ubiquitination by CRLs (including pVHL). We found that treatment with MLN4924 abrogated the effect of CP4.29 (Figure 5b), confirming that our observed depletion of HIF-2α, AURKA, and ZHX2 is dependent on a CRL.

Second, we co-treated cells with CP4.29 and JNJ42041935, an inhibitor of prolyl hydroxylase (PHD) enzymes [78]. Hypoxia-dependent recognition of HIF-α and ZHX2 by pVHL depend on their bearing a hydroxyproline post-translational modification; this mark is added by the PHD family of enzymes. By contrast, AURKA is degraded by pVHL in a hypoxia-independent manner [18]. We found that treatment with JNJ42041935 protected hypoxia-dependent substrates HIF-2α and ZHX2 from depletion by CP4.29, but not AURKA (Figure 5c). Thus, this observation implies that CP4.29-mediated depletion of these three targets is consistent with the same modes of recognition used by WT pVHL.

Next, we co-treated cells with CP4.29 and MG132, a direct inhibitor of the 26S proteasome [79,80]. If depletion of these three targets is indeed due to ubiquitination by re-activated mutant pVHL, their ultimate destruction would occur at the proteasome. In the presence of MG132 to block the proteasome's ability to degrade ubiquitinated proteins, we observe markedly less depletion of HIF-2α, AURKA, and ZHX2 (Figure 5d), confirming that their destruction by CP4.29 is indeed primarily through the proteasome.

To confirm that the observations from this mechanistic analysis was robust towards the *VHL* mutation / cell line selected, we applied similar pharmacological controls using the RCC4 cell line (*VHL* S65W) and obtained analogous findings (Figures S12 and S13). Finally, we sought to directly confirm that CP4.29-induced re-activation of mutant pVHL leads to enhanced (poly-)ubiquitination of these three targets. We used the cell lysates from the 769-P cells co-treated with MG132 (Figure 5d), to trap ubiquitinated proteins without allowing their degradation. We then used immunoprecipitation against each of the three pVHL substrates, followed by Western blotting against ubiquitin. We observed high molecular weight species for all three substrates upon treatment with CP4.29, but only in parental 769-P cells and not in an isogenic *VHL*$^{-/-}$ knockout line (Figure S14 and S15).

Taken together, these results demonstrate that CP4.29 re-activates ubiquitination patterns associated with WT *VHL*, in cells harboring mutant *VHL*. Ahead of characterizing CP4.29 through *in vivo* studies, further development of this agent will be needed. Whereas our initial optimization focused solely on achieving on-target cellular activity, the ADME properties of CP4.29 must next be improved. Specifically, this agent is too lipophilic for immediate advancement, as evidenced by its poor solubility in the absence of DMSO and its high plasma protein binding (Figure S16), and

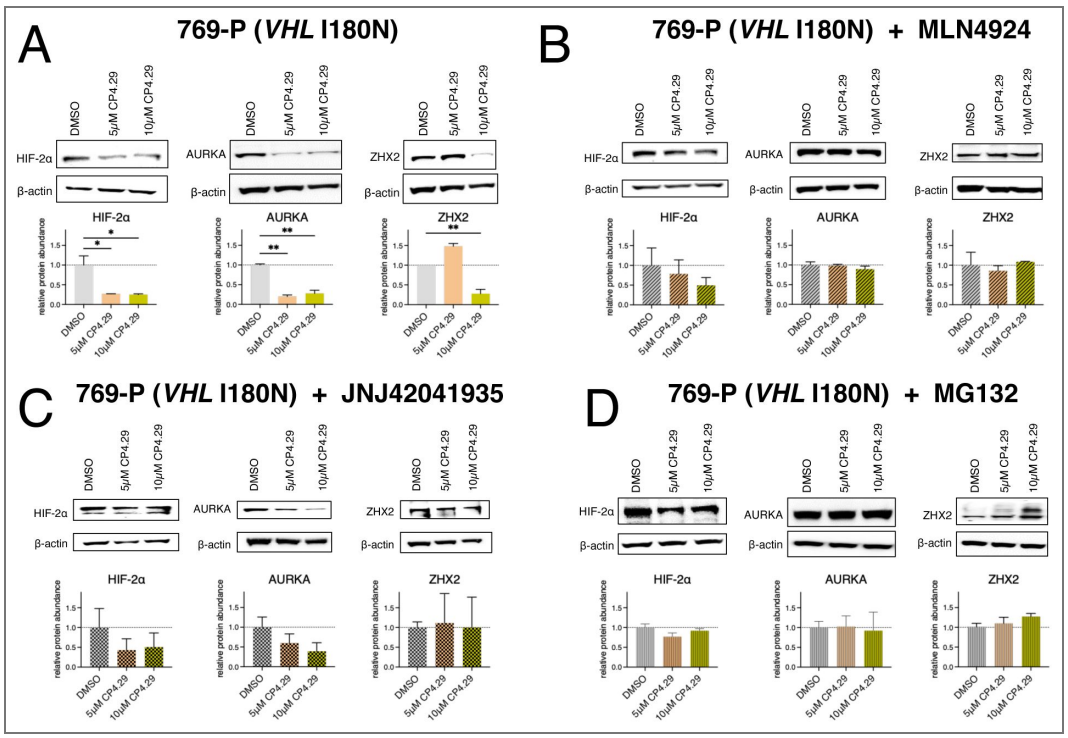

Figure 5. Activity of CP4.29 using mutant pVHL recapitulates the expected dependencies of recognition by WT pVHL.

(A) In 769-P cells (*VHL* I180N) treatment with CP4.29 induces depletion of HIF-2α, and also depletion of additional pVHL substrates AURKA and ZHX2. Analysis of HIF-2α was obtained after 2 hr treatment, whereas analysis of AURKA and ZHX2 were obtained after 24 hr treatment. **(B)** CP4.29's depletion of all three substrates is mitigated by co-treatment with 1 μM neddylation inhibitor MLN4924, demonstrating that CP4.29 activity is dependent on a cullin-RING E3 ligase. **(C)** CP4.29's depletion of HIF-2α and ZHX2 (but not AURKA) is mitigated by co-treatment with 50 μM PHD inhibitor JNJ42041935, demonstrating that CP4.29 activity in this mutant *VHL* cell line recapitulates the molecular recognition patterns of WT pVHL. **(D)** CP4.29's depletion of all three substrates is mitigated by co-treatment with 20 μM proteasome inhibitor MG132, consistent with a ubiquitin-mediated (proteasomal) path to their destruction.

affirmed by its high calculated logP value (cLogP=4.95 per ALOGPS 2.1 [81]). In addition to improving potency of pVHL re-activation into the nanomolar range, careful experimentation will also focus on probing for potential off-target activities at the physiologically relevant concentrations of next-generation pVHL re-folders.

Discussion

Clear cell renal cell carcinoma (ccRCC) and von Hippel-Lindau disease (VHLD) represent two distinct cancer phenotypes linked by their shared molecular underpinnings: loss of *VHL* activity [4,7]. Treatment paradigms for both ccRCC and VHLD initially focused on inhibiting angiogenesis using VEGFR inhibitors, thus disabling a key downstream effector of HIF-2α [25-27]. More recently, the breakthrough drug belzutifan showed impressive clinical responses by inhibiting HIF-2α directly [28-31], thus blunting all of HIF-2α's downstream effectors rather than a subset of them. Nonetheless, the basis for *VHL* tumor suppression extends beyond its ability to degrade HIF-2α [15,32-36]. Because of this, there remains an unmet opportunity for improved therapeutic intervention in *VHL*-mutated cancers, and perhaps even for cancer prevention in VHLD individuals who harbor germline mutations in *VHL*.

Despite pVHL having been identified as the unambiguous driver of these diseases for many years, campaigns to pharmacologically restore pVHL activity have met with limited success [32,37,38]. Challenges developing suitable assays have certainly hampered these efforts. The fact that mutant pVHL is not amenable to purification – as even the WT protein requires partners Elongin B and C for stability – diminishes opportunities to use biochemical or biophysical screening techniques. Separately, phenotypic screens can be difficult to implement due to pVHL's many activities; further, they tend to uncover compounds that act on the *VHL* axis indirectly, such as inhibitors of histone deacetylases that modulate cellular chaperones including Hsp90 [38,82]. While manipulating cellular proteostasis may yet provide favorable clinical outcomes [83], these agents' broad pharmacology and indirect mechanism of action leaves open concerns surrounding what other cellular changes may arise from their use.

For identifying refolder agents, then, structure-based computational design presents a natural alternative to traditional screening methods. As demonstrated in this study, computational methods can be applied to identify a suitably druggable region on the folded protein (Figure 1), and then to select compounds that engage this surface in a targeted manner (Figure 2). Many approved drugs act via allosteric mechanisms, including GPCR agonists that bind to the active receptor conformation at the (extracellular) orthosteric site and thus activate (intracellular) signaling. The refolding strategy we describe here is a select example of this general mechanism, differentiated by the fact that the unliganded (inactive) protein target resides in an unfolded conformation.

Importantly, however, an agent that binds to the target protein and induces refolding does *not* necessarily re-activate the protein's activity. Whereas computational design provided an initial ligand CP4 to bind the intended pocket on pVHL and confer cellular stability (Figure 3), further development into derivative CP4.29 was necessary before pVHL activities were restored. This finding points to the inadequacy of our initial model for pVHL re-activation (Figure 1b): re-folding the protein target is necessary but not sufficient for re-activating it. In retrospect, this insight speaks in direct analogy to biased agonism of GPCR ligands [84,85]. In such examples, synthetic ligands can engage a receptor and impact its structure or dynamics in a manner that nearly – but not quite – recapitulates that of the natural ligand. Due to the resulting differences in the bound receptor, downstream signaling can be affected in subtle and complex ways.

In this context, a further challenge identifying re-activators of destabilized pVHL comes into focus: the "steepness" of the structure-activity relationships (SAR) surrounding CP4.29. In the case of a phenotypic screen searching for agents that induce depletion of pVHL targets, compounds such as CP4 or many of its analogs would not be recognized (Figure 4b). Searching at the outset for pVHL re-activators would therefore have necessitated extremely dense coverage of chemical space in an initial hit-finding campaign, due to the apparent sensitivity of re-activation to relatively

subtle chemical substitutions (Figure 4d). Despite this apparent sensitivity, however, CP4.29 re-activates pVHL variants in which the mutation occurs at diverse locations in the protein structure (Figure 3a).

Analysis of sequencing data from human tumors implicated a set of 125 genes as harboring cancer driving mutations: 71 of these genes are tumor suppressors, and 54 are oncogenes [86]. Despite the abundance of well-validated tumor suppressor targets, however, nearly all targeted therapies in oncology address oncogenes rather than tumor suppressors [87]. This is a consequence of the fact that it is inherently easier to develop molecular agents that inhibit the activity of a molecular target, rather than to develop agents that re-awaken the lost activity of a mutated target; and accordingly, it remains standard practice to address tumor suppressors by targeting their downstream effectors.

As demonstrated above, both CP4.29 (pVHL re-folder) and belzutifan (HIF-2α antagonist) inhibit HIF-2α dependent gene expression (Figure 4e). Because of their fundamentally different mechanisms of action, however, CP4.29 also rescues pVHL's activity on additional substrates (Figure 5), and thus may restore additional (HIF-2α independent) tumor suppressive activities that belzutifan does not. As with many other multi-functional tumor suppressors that can become inactivated by destabilizing mutations [88,89], this example demonstrates that direct pharmacological re-activation of a mutant tumor suppressor holds the potential for restoring *all* dysregulated activities, rather than just the subset associated with a single downstream effector.

Availability of cancer genomic data makes it tempting to speculate what fraction of ccRCC and VHLD cases harbor mutations that could be addressed by compounds such as CP4.29. Such an analysis is premature at this stage, however, because cellular rescue is confounded by a variety of factors including the extent of destabilization conferred by the mutation, the concentration of Elongin proteins (which indirectly impact pVHL stability), and more. For these reasons, future studies must also include direct evaluation of the impact of CP4.29 on a broader collection of cancer cell lines. This will allow the domain of applicability for CP4.29 to be unambiguously determined, and such studies may also guide development of analogs that expand the set of mutants which can be addressed. Ultimately, the *in vivo* applicability of future CP4.29 analogs will be critical to determine across multiple heterogeneous patient-derived samples, and ongoing developments in new preclinical models will certainly enable such efforts [90].

Conclusions

Given the broad assortment of human diseases causally linked to protein folding defects, there has long been enthusiasm for developing "pharmacological chaperones" to reverse the effect of destabilizing pathogenic mutations [91]. Despite the simple conceptual framework by which such agents might act (Figure 1b), there are only four examples that have reached FDA/EMA approval; moreover, the mechanisms of action underlying these four examples are somewhat complicated by the nature of their respective targets [92,93]. Here, we describe CP4.29 as a new pharmacological agent that re-folds and re-activates mutant pVHL, which may serve as a starting point for focused drug discovery efforts. Equally important, however, these studies define the challenges associated with identifying pharmacological re-activators for other tumor suppressors, and they demonstrate how structure-based computational design is well-positioned to address such targets.

Methods

Detailed descriptions of computational and experimental methods are provided in the *Supporting Methods* section.

Data availability

No relevant datasets.

Supporting Information

Supporting Methods

Details of Computational Methods

Computationally generating pocket-containing conformations of pVHL

The presence of a surface pocket is necessary, but not sufficient, for the druggability of a protein. Druggable low-energy pockets may or may not be evident from a crystal structure of the unbound protein [S1,2]: accordingly, it can be beneficial to explore alternate low-energy protein conformations [S3,4].

Simulations were started from the crystal structure of the VCB complex bound to a hydroxyproline containing HIF-1α peptide (the "VCBH" complex), PDB ID: 1LM8 [S5]. All usage of the Rosetta3 software suite used developer version: 7dc49c1abe6a9b8aa9c0c5dc3cc2e81968ad1198.

Prior to (biased) pocket opening simulations [S3], a set of 100 unbiased trajectories were first generated using Rosetta's "relax" application then the "minimize" application [S6,7] as follows:

```
relax.default.linuxgccrelease -s 1lm8.pdb -relax:fast -nstruct 100 -ex1 -ex2 -ex1aro
      -ignore_unrecognized_res -database <path_to_Rosetta>/database
minimize.default.linuxgccrelease -s 1lm8_00##.pdb -out:file:scorefile miniscore.sc
      -database <path_to_Rosetta>/database
```

Individual pocket opening simulations seek to find cryptic pockets in direct contact with some pre-specified "target" residue [S3]. To select all reasonable target residues for pVHL, we calculated the solvent accessible surface area (SASA) for each pVHL residue in the context of the VCBH complex as follows:

```
sasa_list_v2.default.linuxgccrelease -s 1lm8.pdb
```

A target residue was defined as any pVHL residue that 1) had no difference in SASA between the VCBH complex and pVHL alone, and 2) had SASA value > 10 $Å^2$. The first criterion in this definition rules out any residues at the interface between two protein partners (thus preventing the inadvertent design of direct inhibitors of VHL activity). The second criterion avoids any target residues that would dramatically change the protein conformation, since the residue would otherwise be completely buried.

Using the lowest-energy conformation from the unbiased simulation, a set of 100 biased simulations [S3] were initiated for each target residue as follows:

```
relax.default.linuxgccrelease -s 1lm8.pdb -relax:fast
            -nstruct 10 -ex1 -ex2 -ex1aro -ignore_unrecognized_res
            -pocket_zero_derivatives -pocket_max_spacing 12
            -pocket_psp false -pocket_sps -pocket_num_angles 2
            -score:patch pocket.wts.patch -constraints:cst_file constraint
            -pocket_grid_size 10 -database <path_to_Rosetta>/database
```

Here, "pocket.wts.patch" is a text file containing a single line reading "pocket_constraint = 1.0" and "constraint" is a text file containing a single line consisting of the strength of the biasing term (we used -0.25) followed by a space and then the target residue).

Following generation of these "pocket opened" structures, each was subjected to (unbiased) minimization as shown earlier, to enabling fair energetic comparison between unbiased and biased structures. As in earlier studies [S3], output structures from the biased simulations were discarded if they were more than 2.5 REU worse than the maximum energy from the unbiased collection.

For the remaining output structures from the biased simulations, the pocket volume at the target residue was determined as follows (where ## refers to the relaxed/minimized index number in the file name, and "#:V" target residue number ("#") on chain V (":V") in the PDB file):

```
pocket_measure.default.linuxgccrelease -s 1lm8_00##_0001.pdb
       -num_angles 100 -pocket_max_spacing 12 -pocket_psp false -pocket_sps
       -central_relax_pdb_num #:V -database <path_to_Rosetta>/database
```

Any pockets that had volume of less than 150 $Å^3$ were excluded from further analysis.

Computationally generating exemplars from pocket-containing conformations of pVHL

For each of the pocket-containing conformations generated above, exemplars were built at the target residue pocket as described previously [S4,8], using the following command:

```
make_exemplar.default.linuxgccrelease -s 1lm8_00#_0001.pdb
       -pocket_num_angles 100 -pocket_psp -pocket_grid_size 10 -pocket_max_spacing 12
       -central_relax_pdb_num ##:V -pocket_filter_by_exemplar -pocket_static_grid
       -pocket_limit_exemplar_color -pocket_dump_exemplars -min_atoms 1 -max_atoms 65
       -database <path_to_Rosetta>/database
```

Concatenating the PDB files for the protein and an exemplar together produced a VCBH:exemplar complex, as shown in Figure 1d.

Computational predictions of pocket druggability

The "Maximum Achievable Potency" (MAP) that a ligand might obtain for a given surface pocket was predicted using a recently-developed machine learning model [S9-11]. The PDB file containing the VCBH:exemplar complex was first used to define all protein atoms within 4.0 Å of any exemplar atom, using a script provided in GitHub [S10]. Input features for the ML model were calculated using these atoms, and these served as the basis for predicting the MAP value (in units of -log(potency)).

Individual exemplars were carried forward for virtual screening only if the yielded a MAP value greater than 8 (implying that thorough optimization could yield a small molecule with Kd better than 10 nM).

Virtual screening to identify pVHL binders

Virtual screening was carried out in two phases: an initial screen to select chemical scaffolds complementary to the pVHL surface, and then a second screen to explore more deeply available compounds based on these scaffolds.

To prepare a suitable database for the first phase of screening, we began with Enamine's REAL Space Diverse Set, corresponding to ~15M distinct small molecules at the time. Compounds with molecular weight below 300 Da or above 550 Da were removed using OpenEye's "filter" application in Omega2 [S12-14]. Removing these compounds left a set of ~12.5M compounds available for screening.

The initial library (as SMILES strings) was split into smaller files each containing ~50,000 SMILES strings. Omega2 was then used to build conformers for the compounds in each file, as follows:

```
omega2 -in <input_file>.smi -out <output_file>.oeb.gz
       -prefix <insert_prefix_name> -warts -strictstereo false
```

Each pVHL exemplar was then used as the basis for screening this library, as described earlier [S8]. Briefly, OpenEye's ROCS software [S15,16] was used to align each conformer from the database onto the exemplar and provide a quantitative measurement of similarity for both geometric and chemical features. As in our previous studies [S8], an initial overlay was generated using FastROCS [S17] and then refined using the standard ROCS application. Prior to the second ROCS step, compounds' protonation states were adjusted using OpenEye's "fixpka" application in QUACPAC [S18] with default parameters. To allow for fair comparison between hits coming from different exemplars, aligned scores were expressed as a Z-score relative to all compounds screened against that exemplar. In contrast to previous work [S8], the TanimotoCombo score was used rather than the TverskyCombo score.

The top-scoring 20,000 matches were converted from ".oeb.gz" files to ".sdf" file format using the convert.py script in the OpenEye OEChem toolkit [S17]. From the ".sdf" file format, each was parameterized for use in Rosetta using the following command:

```
Rosetta/main/source/scripts/python/public/molfile_to_params.py
       <ligand_conformer>.sdf -p <ligand_conformer>
```

The resulting .pdb files for each of the top 20,000 hits were concatenated into the corresponding pocket-opened structure, to yield an initial docked complex. Full-atom Rosetta minimization was carried out on each protein:ligand complexes as follows:

```
minimize_ppi.default.linuxgccrelease -extra_res_fa <conformer_params_file>.params
      -s <cat_protein_ligand_structure>.pdb -database Path_to_Rosetta/main/database
```

Minimized complexes were then used as input into the vScreenML machine learning classifier [S19]. Based on vScreenML scores, the top 100 compounds were selected for further exploration of these scaffolds.

Using the Enamine REAL Space Navigator application [S20], 100 analogs for each of these initial scaffolds were identified from amongst a total of ~21 billion compounds: collectively then, these served as a new focused library of 10,000 compounds. Conformers for each of these 10,000 compounds were generated using Omega2 as described above. Following conformer generation, each conformer for a given compound was aligned onto the parent scaffold in the minimized model, using the following command in ROCS:

```
rocs -query <parent_compound_conformer_post_minimization>.pdb
      -dbase <analog_id>.oeb.gz -prefix <analog_id> -status none
      -rankby TanimotoCombo -besthits 1
```

Following the identification of the best overlapping analog conformer, the resulting conformer was converted from ".oeb.gz file" format to .sdf file format using the following OEChem [S17] command:

```
python openeye/examples/oechem/convert.py
       <top_analog_conformer>.oeb.gz <top_analog_conformer>.sdf
```

Since standard output files from ROCS contain both the initial conformer used as query (in this case the parent scaffold) and the top scoring database conformer (the top conformer of the aligned analog), the resulting .sdf file was split into two pieces using OpenEye's "chunker" application [S15,16] as follows:

```
chunker -in <analog_ID>.sdf -base <analog_ID__chunk_> -chunksize 1
```

The standard output from ROCS lists the query molecule first, and so only the second chunk file (containing the top conformer of the analog) was selected. To ensure the top conformer was properly protonated, the resulting .sdf file was run through the "fixpka" application in OpenEye's QUACPAC [S18] with the following command:

```
fixpka -in <analog_ID__chunk_0000002.sdf> -out <analog_ID__chunk_0000002_FIXPKA>.sdf
```

Finally, the analog's top scoring conformer following this step was parameterized for Rosetta compatibility and minimized as described above. The resulting minimized models were again ranked using vScreenML.

The top-scoring 18 compounds from vScreenML were visually inspected, then purchased directly from Enamine (Table S1).

Identification of additional Enamine analogs for CP4.29

Once our wetlab studies led us to prioritize CP4.29, we searched for additional analogs that could enrich our understanding of structure-activity relationships (SAR). By this time the REAL Space Navigator application had been discontinued, and so we used the newer infiniSee application [S21] to search the Enamine REAL Space database for additional analogs (version 2021-10, 21 billion compounds). Compounds that afforded the opportunity to evaluate the effect of individual substitutions (relative to CP4 or CP4.29) were selected for purchase.

Plasmids, Cloning, and Site Directed Mutagenesis

A polycistronic expression vector containing coding regions for an N-terminal 6xHis-Trx tagged pVHL19 protein construct, full length Elongin B, and Elongin C (residues 17-112) was generously provided by Dr. Song Tan [S22]. The plasmid was transformed into BL21(DE3) competent *E. Coli* according to manufacturer's protocols (New England Biolabs, catalog number C2527H), plated onto pre-warmed 100 µg/mL ampicillin containing LBBA agar plates, and grown overnight at 37°C. A single colony was selected and transferred to LB media with 100 µg/mL ampicillin sulfate. The starter culture was subsequently placed in a 37°C shaker at 250 rpm overnight. The resulting plasmid DNA was extracted from the starter culture using a QIAprep Spin Miniprep Kit (Qiagen USA, catalog number 27140 or 27106) according to manufacturer's protocols. Final aliquots of the plasmid at a concentration of 50 ng/µL were frozen at -80°C.

To incorporate the D197K mutation into VHL, two primers were purchased as HPLC purified oligomers with the following sequences: 5'-CAC CCA AAT GTG CAG AAA AAG CTG GAG CGG CTG ACA CAG-3' (forward) and 5'-CTG TGT CAG CCG CTC CAG CTT TTT CTG CAC ATT TGG GTG -3' (reverse). These were diluted to 100 µM in low EDTA, TE buffer. Using the QuikChange II Site-Directed Mutagenesis Kit (Agilent Technologies, catalog number 200523), the wild-type plasmid and primers were used to generate the $V_{D197K}CB$ plasmid in accordance with manufacturer's protocols. The resulting $V_{D197K}CB$ plasmid was transformed into Stellar chemically competent *E.*

Coli (Takara Bio USA, catalog number 636763). Starter cultures were prepared, and plasmid DNA was isolated using the same method as described above. The sequence of the wild type and $V_{D197K}CB$ constructs were validated using Sanger sequencing.

Expression and Purification of the VCB and $V_{D197K}CB$ Complexes

To begin expression/purification of either WT VCB or mutant ($V_{D197K}CB$) complex, 2 µL of 50 ng/µL of the corresponding plasmid was transformed into BL21(DE3) *E. coli* according to manufacturer's protocols (New England Biolabs, Ipswich, MA; C2527H). After overnight growth of colonies at 37°C on 100 µg/mL ampicillin containing LBBA agar plates, single colonies of each respective construct containing bacteria were transferred to one of two 300 mL Erlenmeyer flasks containing 100 mL of LB media with 100 µg/mL ampicillin sulfate and left to shake at 37°C for 6 hours at 250 rpm. Starter cultures were subsequently diluted 1:100 into 2L of LB media containing the same concentration of ampicillin in appropriately labelled (i.e. "wild type" or "D197K") 4L Erlenmeyer flasks and left to shake at 190 rpm and 37°C until the OD_{600} = 0.6. Flasks were then placed at 4°C for approximately one hour at which time IPTG was added to a final concentration of 200 µM to induce expression. After addition of IPTG, the flasks were placed back into a 16°C shaker and left to shake overnight at 190 rpm. The following morning, bacteria expressing either construct were pelleted by centrifugation at 3,057xg at 4°C for 20 minutes. Pellets from 4L worth of bacteria expressing wildtype VCB or pellets from 4L of bacteria expressing $V_{D197K}CB$ were combined appropriately and frozen at -20°C.

Both VCB and $V_{D197K}CB$ were purified from their respective pellets using the same method described below. Pellets were first resuspended in 100-150 mL of 20 mM Tris, 500 mM NaCl, pH=7.5 buffer. After the addition of benzamidine HCl, lysozyme, and DNAse I from bovine pancreas, the suspension was left to stir vigorously at room temperature for at least 30 minutes. Bacteria were lysed by 3 rounds of French press (pressure between 500 – 1000 psi) at 4°C. The lysates were cleared by centrifugation at 17,418xg for 20 min at 4°C and supernatants were filtered through a syringe driven 0.2 µm PES filter. All remaining steps were conducted at 4°C unless otherwise noted.

A HisTrap HP 5 mL affinity chromatography column (Cytiva Life Sciences; Marlborough, MA) was equilibrated with 10 CVs of 20 mM Tris, 500 mM NaCl, pH=7.5 buffer attached to an AKTA Pure protein purification system. Following equilibration, the column was detached and hooked up to a peristaltic pump (pre-equilibrated in the same buffer). The filtered supernatant was subsequently loaded onto the column using the peristaltic pump at a speed of approximately 3 mL/min. After loading, the column was re-attached to the AKTA system and washed at a flow rate of 3 mL/min for a total of 70 mL with 20 mM Tris, 500 mM NaCl, 20 mM imidazole, pH=7.5 buffer while collecting 2 mL fractions. Protein was eluted from the column over a 40 mL stretch using a linear gradient of the same buffer in which the imidazole concentration increased from 20 to 500 mM while taking 2 mL fractions. Fractions were analyzed for the target protein using SDS-PAGE and those confirmed to contain tagged VCB (or tagged $V_{D197K}CB$) were pooled.

The 6xHis-Trx tag was removed by placing the pooled fractions into a pre-soaked 15 mL dialysis cassette (10K MWCO) along with 3 mL of A280=4.0 TEV protease (stored at -20°C in 20% glycerol containing buffer). The entire cassette was placed into 1 L of 20 mM Tris, 500 mM NaCl, pH=7.5 buffer overnight at 4°C with slow stirring to ensure efficient dialysis of the imidazole. The following morning, the protein was removed from dialysis and manually loaded via syringe onto a HisTrap HP 5 mL column (pre-equilibrated with 10 CVs of 20 mM Tris, 500 mM NaCl, pH=7.5 buffer) at 4°C and a rate of approximately 3 mL/min. The column was loaded back onto the AKTA and subjected to the same wash/elution steps already described. Consistent with efficient tag cleavage, the untagged VCB (or $V_{D197K}CB$) was identified in the wash fractions. The three most concentrated fractions were subsequently pooled and stored at 4°C.

The pooled fractions were further purified using size exclusion chromatography with either a HiLoad 16/600 Superdex 200 pg or HiLoad 16/60 Superdex 75 pg column (Cytiva Life Sciences; Marlborough, MA) equilibrated in 20 mM Tris, 150 mM NaCl, 2 mM DTT, pH=7.0 buffer. Samples of 2 mL of either respective protein construct were injected onto the column at a rate of 1 mL/min.

The protein was eluted using an isocratic elution in the same buffer at a rate of 1 mL/min and collected in 2 mL fractions. Fractions eluting at a rate consistent with the proper molecular weight were pooled and final protein purity was assessed by SDS-PAGE.

Ligand Observed NMR Experiments

Three separate ligand-observed NMR approaches were utilized to assess CP4 binding to the VCB complex: Saturation Transfer Difference (STD-NMR), WaterLOGSY, and Relaxation Filtered (or "CPMG") experiments. Each of these experiments is independently capable of detecting binding and can be considered orthogonal (with the caveat that STD and WaterLOGSY do leverage a similar underlying principle of magnetization transfer) [S23].

As a starting point, aliquots of 80 mM CP4, 49.6 mM sitagliptin phosphate, and 40 mM VH298 in DMSO-d6 were thawed from -80°C to room temperature. CP4 was diluted to a working concentration of 40 mM with additional DMSO-d6. 1 µL of 40 mM CP4, 1 µL of 49.6 mM sitagliptin phosphate, 1 µL of 40 mM VH298, and 1 µL of DMSO-d6 were added to 3x1.5 mL microcentrifuge tubes and mixed gently by pipette. Tubes were capped and frozen at -80°C until ready for use. Meanwhile, 2x15 mL Amicon 10K MWCO concentrators were used to concentrate the pooled fractions of VCB or $V_{D197K}CB$ (following size exclusion chromatography) to a final volume of approximately 1 mL by centrifugation at 3000xg and 4°C. Protein was subsequently placed on ice.

Meanwhile, two Nap-10 Sephadex G-25 DNA grade columns were drained of storage solution and washed with at least 15 mL of MilliQ water. Columns were equilibrated in 3x5 mL washes with ice cold 50 mM sodium phosphate buffer containing 10% D_2O/90% MilliQ water (v/v), pH=6.92 (here after referred to as "NMR buffer"). VCB or $V_{D197K}CB$ samples (approximately 1 mL) were removed from ice and loaded onto Nap columns and allowed to drip through. Protein was eluted using 1.5 mL of NMR buffer, diluted to a final volume of 2 mL in 2 mL tubes, and placed on ice. Concentration of each protein was determined by absorbance at 280 nm (ε = 25900 M^{-1} cm^{-1}, MW = 42497 g/mole for VCB and MW=42510 g/mole for $V_{D197K}CB$) using a ThermoFisher NanoDrop 1000 spectrophotometer [S24]. Each solution of protein was measured five times to ensure robust determination of protein concentration. Since the $V_{D197K}CB$ protein was the more dilute of the two (measured at 7.7 µM), an aliquot of the more concentrated wild type VCB was diluted in NMR buffer to the same concentration and a final volume of 2 mL. To ensure this dilution was done correctly, the concentration of this diluted wild type VCB was measured five times and found to also equal 7.7 µM. Final solutions of wild type VCB and $V_{D197K}CB$ were immediately placed on ice.

Samples for NMR analysis were prepared by taking one of the tubes containing 4 µL of combined CP4/sitagliptin phosphate/VH298/DMSO-d6 and adding 396 µL of either 1) NMR buffer (kept on ice), 7.7 µM VCB (in NMR buffer), or 3) 7.7 µM $V_{D197K}CB$ (in NMR buffer) and mixing gently by pipette. The inclusion of a control sample containing no VCB (sample 1) for each experiment greatly diminishes the chances of a false positive result, while the matched concentrations of VCB and $V_{D197K}CB$ rule out different protein concentrations as a potentially confounding variable.

For each sample, final compound concentrations were 100 µM for each of CP4, sitagliptin (after accounting for the phosphate), and VH298. DMSO-d6 was kept at 1%. Samples were transferred to NMR tubes and immediately placed into a 600 MHz Bruker NMR with TCI CryoProbe and Bruker Avance Neo console (running TopSpin 4.2.0) equilibrated at 278K. Four experiments consisting of a ^1H NMR with excitation sculpting water suppression, STD NMR, WaterLOGSY, and CPMG NMR were carried out in sequential order prior to preparing the next sample and repeating the process using protocols adapted from others' work [S25-27]. A detailed description of the protocol is provided below.

The sequence of experiments run on a given sample is as follows: 1) ^1H NMR with excitation sculpting water suppression (ZGESGP), 2) Saturation Transfer Difference NMR (SCREEN_STD), WaterLOGSY (SCREEN_WLOGSY), and 4) CPMG (CPMGPR1D). To start, an existing experiment saved on the instrument was opened and the command "new" was typed into the command line. In the resulting dialogue box, a new folder name was entered and the EXPNO was changed to 1. Additionally, the "read parameterset" bubble was selected and the option for "ZGESGP" was selected. The checkbox for "Set solvent" was also checked and the "H2O+D2O" solvent option was

chosen from the list. Under the "Additional action" section, the bubble for "Execute getprosol" was selected. In the title box, the experiment description was written and then the "OK" button was clicked. This resulted in a new experiment being opened in TopSpin. To lock onto the solvent, the command "lock" was typed into the command line and the option for "H2O+D2O" was selected. Once locked, the instrument was tuned by typing "atma" into the command line. Upon completion of tuning, the instrument was shimmed by first typing "topshim gui" into the command line. In the resulting dialog box, the "Dimension" option was set to "1D," the "Optimisation" option was set to "solvent suppression," the "Optimise for" option was set to "1H," and the "Use Z6" option was left unchecked. Under the "Tune" section of the dialog box, the "Before" and "After" were both set to "Z-X-Y-XZ-YZ-Z" and "Start" was clicked. Once shimming was complete, the sample icon was double clicked and the "Shim" tab was selected followed by the "Power" option. The power was adjusted until the lock signal was approximately 75% of the way to the top of the screen and "STDBY" was clicked. To determine the pulse length, the command "pulsecal -auto" was used and the number under "5.702W" was recorded. The pulse length was subsequently set for the experiment by typing "getprosol 1H #.## 5.7021W" where "#.##" was the pulse length recorded in the previous step. The receiver gain was set automatically using the command "rga" and the number of scans was set to 64 through the "ns" command. Finally, expected time for the experiment was determined via the "expt" command and the experiment was started via the "zg" command.

To begin the Saturation Transfer Difference (STD) experiment, the flask icon on the left side of the screen was clicked, followed by double clicking the "SCREEN_STD" option in the "Drug_discovery" library. In the resulting dialog box, the same options as described above for the "new" command were selected (with the EXPNO being updated to "2"). The newly created experiment (EXPNO 2) was double clicked in the "Data" list and the pulse length set with the following command "getprosol 1H #.## 5.7021W" as before using the same value for "#.##". The number of scans was set to 128 using the "ns" command and the expected time of experiment was determined by the "expt" command. Finally, the experiment was started using the "zg" commad.

While the STD experiment was running, the WaterLOGSY experiment was queued up using the following protocol. To find the proper experiment, the flask icon was clicked and the "SCREEN_WLOGSY" option under the "Drug_discovery" library was selected. The same options as described above were selected in the dialog box (except for the appropriate change in the "EXPNO" value). The newly created experiment was selected in the "Data" list and the pulse length was set using same command ("getprosol 1H #.## 5.7021W"). The number of scans was set to 512 using the "ns" command. The number of dummy scans was adjusted to 4 by first clicking the "ACQUPARS" tab and changing the value in the "DS" box. The "SPECTRUM" button was clicked to close the "ACQUPARS" tab. Time of experiment was determined by the "expt" command. In order to queue up the next job in the scheduler, the Spooler icon was clicked and the "Job" button in the toolbar was clicked, followed by the "new" button. In the resulting box, the command "rga" was typed and OK was clicked. This same process was repeated with the "zg" command instead of the "rga" command to queue up the experiment.

Finally, a CPMG experiment was queued up on the sample using a similar protocol. First, the 1H excitation sculpting experiment (EXPNO 1) was opened and the "new" command was entered. The dialog box was filled in according to the same method described earlier for the first experiment with the EXPNO set to 4 (ZGESGP was still set as the "Read parameterset" option). After the new experiment was created, it was selected from the "Data" list. Under ACQUPARS, the pulse program was changed from "zgesgp" to "cpmgpr1d" by clicking the "…" icon across from the "PULPROG" option and selecting "cpmgpr1d" and clicking "Set PULPROG to Dataset." The pulse length was set to the same value as all other experiments for the sample using the same "getprosol 1H #.## 5.7021W" command. The loop counter was set to a value of 400 (corresponding to a KD value in the uM range)[S25] by typing the "L4" command and entering "400" into the box. The relaxation delay was set to 15 seconds using the "D1" command and entering "15" in the dialog box. The mixing time was set to 0.001 seconds by typing "D20" and setting the value to 0.001 seconds. The

number of scans was set to 64 using the “ns” command. The length of the experiment was predicted using the “expt” command and the job was queued up using the same Spooler protocol described above for WaterLOGSY.

Upon completion of the experiments for a given sample, initial data processing was done for each experiment using TopSpin 4.2.0. For the 1H excitation sculpting water suppression experiment (zgesgp), the raw data was opened by double clicking the experiment from the “Data” list. The spectrum was viewed using the “efp” command and phased using the “apk” command. The WaterLOGSY experiments were processed simply by clicking the experiment and typing the “efp” command. The CPMG experiments were analyzed by opening the experiment, typing the “efp” command, and phasing the spectrum using the “apk” command.

Analysis of the STD experiment was carried out by adapting others’ protocol [S26]. The initial 2D experiment was opened by double clicking the experiment from the “Data” list. The line broadening was set to a value of 3.0 Hz using the “lb 3” command. The “off resonance” spectrum was extracted using the “efp 1 2” command. The spectrum was phased using the “apk” command. To ensure the phasing was saved properly, the “.ph” command was entered followed by the “.s2d” and “.sret” commands. The original 2D experiment was reopened by typing the “rep 1” command. The “on” resonance spectrum was extracted using the “efp 2 3” command. The original 2D experiment was reopened using the same command as above and the “off” resonance spectrum was opened using the “rep 2” command. Multiple Display mode was opened and the “on” resonance spectrum was pulled up by typing the “rep 2; .md” and “rep 3” commands, respectively. To calculate the difference between the “off” and “on” resonance spectra (i.e. the saturation transfer difference), the delta icon followed by the floppy disk icon was clicked. In the resulting dialog box, the number “5” was entered.

Cell Culture and Reagents

Human renal cell carcinoma (ccRCC) cell lines, including Caki-1 (CVCL_0234), 769-P (CVCL_1050), and RCC4 (CVCL_0498) were obtained from Fox Chase Cancer Center’s Cell Culture Facility (Philadelphia, PA). The RCC-MF (KTCTL-1M) cell line was generously provided by Dr. Philip Abbosh (Fox Chase Cancer Center, Philadelphia, PA).

Initial stocks were cryopreserved in FBS with 10% DMSO, and at every 6-month interval, a fresh aliquot of frozen cells was thawed and passaged for subsequent experiments. Cells were grown as monolayer in T75 flasks using RPMI- 1640 media supplemented with 10% fetal bovine serum, sodium pyruvate (1 mM), and non-essential amino acids (0.1 mM) and 1% penicillin/streptomycin at 37°C in 5% CO_2 atmosphere.

To compare the effect of CP4.29 under normoxic versus hypoxic conditions, a hypoxic culture glove box and incubator (Terra Universal) was used for continuous (uninterrupted) treatment and incubation of cells with 5μM CP4.29 at low oxygen conditions. Cells were first cultured on two 6-well plates at normoxic conditions (about 20% O_2) in the 5% CO_2 incubator until attachment. One plate was then transferred into hypoxic conditions (2% O_2 / 5% CO_2) in the glove box. Cells were left for 24 hours at each condition, then were treated with 5uM CP4.29 for 2 hours, then were lysed for Western blotting.

VHL knockout cells were generated by using Fugene lipofectamine from Promega (# E5911) to transfect cells with pLenti-Cas9-GFP (Addgene, # 83165) and sgRNA for *VHL* (Sg.VHL_1: 5'-CGCGGA GGGAATGCCCCGGA-3', Sg.VHL_2: 5'-CCTCGGCGCCCAGTTCCTCC-3', Sg.VHL_3: 5'-CCTCCCCGCCGTCTT CTTCA-3'). Knocked out clones were segregated into individual cells via FACS cell sorting guided by the green florescence signal from the GFP-tag fused to Cas9. Effectiveness of the knockouts was verified in the expanded clones via Western blotting (Figure S13).

All reagents were of high purity grade and for use in cell culture experiments. MG132 and JNJ42041935 were obtained from EMD Millipore Corp. (# 474791 and # 400093, respectively). VH298 and MLN4924 were from Sigma Aldrich (# 1896, and # 951950, respectively). Belzutifan was from MedChemExpress (# HY-125840). Each was prepared in a stock of 40 mM and diluted to the desired culture treatment concentration.

Western Blotting and Immunoprecipitation

Adherent cells were rinsed once with ice-cold phosphate-buffered saline (PBS) (pH 7.4) and scraped in 100 µL of 2% SDS lysis buffer supplemented with complete protease inhibitors. Protein concentration of the resulting whole-cell lysates was determined by Pierce BCA Protein assay Kit (Thermo Scientific # 23228). For Western blotting, 20 µg of total protein for each sample was diluted in Laemmli sample buffer, heated at 95 °C for 5 min, loaded into 4- 20% Sure PAGE^{TM}, Bis-Tris gels (Gene Script # M00657), separated by sodium dodecyl sulfate polyacrylamide gel electrophoresis, and transferred to iBlot2 PVDF Regular Stacks System (Invitrogen # IB24001) according to the manufacturer's specifications. The membrane was then incubated for 40 min. at room temperature in 5% nonfat milk in TBS-T to block nonspecific antibody binding with constant agitation. Milk was washed off the membrane by two 5-min washes in TBS-T. The membrane was incubated overnight with constant agitation at 4 °C with primary antibodies (listed below) diluted in TBS-T supplemented with 1% protease-free bovine serum albumin and 0.05% sodium azide. The following day, the primary antibody solution was removed, and the membrane was washed three times with TBS-T for 5 min. Washed membranes were incubated with horseradish peroxidase (HRP)–conjugated secondary antibodies (goat anti-mouse immunoglobulin G [IgG] (Invitrogen # G21040) or goat anti-rabbit IgG (Invitrogen # G21234) diluted 1:5,000 in TBT-T containing 1% nonfat milk for 1 h at room temperature with constant agitation. The secondary-antibody solution was removed, and the membrane was washed three times with TBS-T for 5 min. Bound antibodies were detected with enhanced chemiluminescent HRP substrates SuperSignal West Pico PLUS Chemiluminescent Substrate (Thermo Scientific # 34578), or West Femto Maximum Sensitivity Substrate (Thermo Scientific # 34095), or West Atto Ultimate Sensitivity Substrate (Thermo Fisher # A38555), each used based on the intracellular protein level. Chemiluminescent signal was detected with (Fluorchem # E3031).

For immunoprecipitation (IP), cells were grown for treatment with either 0.1% DMSO or 5µM CP4.29 for 4 hours till harvesting with cold non-denaturing cell lysis buffer containing 1X complete protease inhibitor. The lysates were immunoprecipitated overnight using an anti-HIF2a or anti-AURKA or anti-ZHX2 primary antibodies. The immune complexes were incubated with pre-washed Protein A/G Sepharose Beads (Abcam, ab206996) for 4 hours, and washed three times with 1X cell lysis buffer before resuspending the pellet in loading dye and boiling for 5 min at 95 °C. Eluted proteins were immunoblotted with anti-ubiquitin.

Primary antibodies were used at the following dilutions:

- Rabbit anti-HIF2α, Cell Signaling Technologies (# 7096S), used at 1:1,000
- Mouse HIF1α, BD Biosciences (# 610958), used at 1:1,000
- Rabbit anti-VHL, Cell Signaling Technologies (# 68547S), used at 1:1,000
- Rabbit anti-AURKA, Cell Signaling Technologies (# 3092S), used at 1:1,000
- Rabbit anti-Fibronectin-1, Cell Signaling Technologies (# 26836S), used at 1:1,000
- Rabbit anti-ZHX2, Cell Signaling Technologies (# 20937S), used at 1:1,000
- Mouse anti-ubiquitin, Invitrogen (# 13-1600), used at 1:10,000

Screening small molecules with Enzyme Linked Immunosorbent Assay (ELISA)

Capture assay "sandwich" ELISAs were used to determine the levels of HIF2a (DuoSet IC ELISA, R&D Systems # DYC2997-2) after treatment with small molecules. RCC-MF cells were grown in 6-well plates overnight, treated with 20µM of small molecules for 2 hours, then lysed with a cocktail of 1mM EDTA, 0.5% TritonX-100, 5mM NaF, 6M urea, 1mM activated sodium orthovanadate, 2.5mM sodium pyrophosphate, 10 µg/ml leupeptin, 10 µg/ml pepstatin, 100 µM PMSF, 3 µg/ml aprotinin in PBS- pH 7.2-7.4. The protein concentration of each treatment was determined by BCA (ThermoFisher # 23228). Cell lysates were added to the pre-coated 96-well plates with HIF2a and the biotinylated detection antibody specific for HIF2a/ EPAS1 is used to detect the protein utilizing a standard Streptavidin-HRP format, with Spectromax Plate Reader.

Reverse Transcription and qPCR

769-P cells were treated with DMSO (vehicle control), 10 and 20 μM concentrations of CP4.29 along 20 μM belzutifan (positive control) for 4, 6, and 8 hours. RNA was extracted using phenol-chloroform based method with Trizol (Life Technologies # 15596018). RNA concentration was measured using NanoDrop Lite (ThermoFisher Scientific). First strand cDNA synthesis was performed with High-Capacity cDNA Reverse Transcription kit (Applied Biosystems # 4368814) according to manufacturer's instructions. The generated cDNA was diluted tenfold and used as a template for qPCR, which was performed with Applied Biosystems QuantStudio 5 system using PowerTrack™ SYBR Green Master Mix (Applied Biosystems # 4309155). Relative quantification of genes expression was performed using $2^{-\Delta\Delta Ct}$ method, and the primer sequences were:

CCND1 forward: CCGTCCATGCGGAAGATC
CCND1 reverse: ATGGCCAGCGGGAAGAC
VEGF forward: CGAAACCATGAACTTTCTGC
VEGF reverse: CATCCATGAACTTCACCACTTC
Actin forward: ACCAACTGGGACGACATGGAGAAA
Actin reverse: TAGCACAGCCTGGATAGCAACGTA.

Cell proliferation assay

Cells were plated in 8 replicates in 96-well plates (2000 cells/well) in 200 μL growth medium. Cells were treated with increasing concentrations of CP4.29 (0.05, 0.5, 5, and 10 μM) for 24, 48 and 72 hours. At the indicated time points, cells were changed with 190 μL fresh growth medium supplemented with 10 μL 12mM MTT reagent (Invitrogen # M6494) at 37 °C for 1-4 hours. The optical density value was detected at 540 nm using a 96-well plate reader.

Colony formation assay

A colony formation assay was used to analyze the effect of CP4.29 on cell growth. 769-P cells were used along their CRISPR knocked out generated clones of cells. Cells were seeded into six-well plates (20,000 cells/well). After four days, the colonies were stained with 0.5% crystal violet (Thermo Scientific # 40583-0250). The density of colonies formed in each well was measured using imageJ and then normalized to control wells (0.1% DMSO treated). Experiments were performed in triplicate, and pairwise test of comparison in the one-way ANOVA was used to analyze the difference between control and treatment groups.

Wound healing assay

Parental 769-P cells and *VHL* CRISPR-KO cells were seeded into six-well plates with a density of approximately 95% confluence after 24 h. The monolayer was lightly scratched with a 10-μl pipette tip across the well. After scratching, the well was washed with PBS and then replenished with serum-free medium supplemented with either 0.1% DMSO or 5 μM CP4.29 or 10 μM CP4.29 for 24 h. Wells were stained with 0.5% crystal violet (Thermo Scientific # 40583-0250) and the scratch area was measured with imageJ. Experiments were performed in triplicate, and pairwise test of comparison in the one-way ANOVA was used to analyze the difference between control and treatment groups.

Statistical Analysis

GraphPad Prism was used to analyze the statistical significances of data. All graphs depict mean ± SEM. *, ** and *** represent P value of < 0.05, 0.01, and 0.001, respectively. GraphPad Prism was used to generate all the graphs.

Compound storage / preparation of purchased compounds

Compounds purchased from Enamine arrived as dried powders/oils in amber vials. The initial 18 CP series compounds were dissolved in DMSO to a final concentration of 40 mM and several initial 40 μL aliquots were prepared in small amber vials. Aliquots (along with remaining volume in original vials) were frozen at -20°C. Prior to initial screening experiment using STD-NMR, aliquots of each compound were pooled into a pre-weighed vial and lyophilized overnight to dryness.

Compounds were subsequently re-dissolved in DMSO-d6 to a final concentration of 160 mM (CP1, CP3, CP4, CP9, CP10, CP11, CP12, CP14, CP17, CP18), 80 mM (CP2, CP5), or 40 mM (CP6, CP7, CP8, CP13, CP15) depending on solubility and frozen at -20°C. The compound designated CP16 was not included in the initial screen.

Subsequent batches of CP4 were later delivered from Enamine and diluted to 80 mM in DMSO-d6. 10 µL aliquots were prepared in amber 1.5 mL microcentrifuge tubes and frozen at -80°C.

Compounds synthesized in-house (including CP4.29, CP4.35, CP4.36, CP4.40, CP4.41, CP4.42, CP4.43, CP4.44, CP4.45, and CP4.46) were dissolved into DMSO-d6 at a concentration of 160 mM and aliquoted. A single aliquot of each compound was further diluted to 40 mM, aliquoted, and frozen at -20°C in anticipation of cellular testing. Remaining aliquots of the 160 mM stocks were frozen at -80°C.

Additional analogs of CP4.29, termed CP4.1-CP4.34, were delivered from Enamine as either dry powders or oils in amber vials. The compounds designated CP4.33 and CP4.34 were not included in experimental characterization. Compounds were dissolved to a final concentration of either 80 mM or 160 mM in DMSO-d6 (depending on solubility) and frozen at -20°C.

Additional batches of CP4.29 used for experiments other than the initial screen were purchased directly from Enamine (catalog number Z5717230270), dissolved to 160 mM in DMSO-d6, and frozen at -80°C. The equivalence of our synthesized CP4.29 and the batches purchased from Enamine was confirmed by comparing each purchased batch to our reference ^{1}H and ^{13}C NMR spectra (Figures S17-S18).

Synthesized derivatives of CP4.29 were dissolved in DMSO-d6 to a final concentration of 40 mM and aliquoted into 1.5 mL microcentrifuge tubes. Two aliquots of each compound were frozen at -20°C for immediate use in cellular testing. Additional compound was frozen at -80°C for long term storage.

Sitagliptin phosphate was purchased as a powder and stored at -20°C. 8 mg of sitagliptin phosphate was dissolved in DMSO-d6 to a final concentration of 49.6 mM and aliquoted as 15 µL aliquots in 1.5 mL amber microcentrifuge tubes and frozen at -80°C. VH298 was purchased from Sigma Aldrich (catalog number SML1896-5MG) and dissolved to 40 mM in DMSO-d6. Aliquots of 15 µL were prepared in amber 1.5 mL microcentrifuge tubes and frozen at -80°C.

Chemical Synthesis

Synthesis of (3,5-dichloro-1H-indol-2-yl)(4-((3-isopropyl-1,2,4-oxadiazol-5-yl)methyl)piperidin-1-yl)methanone (CP4.29)

In a 20 mL vial, 53 mg (0.230 mmol) of 3,5-dichloro-1H-indole-2-carboxylic acid (Enamine Ltd., Kyiv, Ukraine; EN300-36960), 96.2 mg (0.218 mmol) BOP, 75.7 µL DIPEA (d=0.742 g/mL, 0.434 mmol) were combined and dissolved in 2 mL DMF. Solution was stirred at room temperature for 15 minutes at which time 53.4 mg (0.217 mmol) of 4-[[3-(propan-2-yl)-1,2,4-oxadiazol-5-yl]methyl]piperidine hydrochloride (Enamine Ltd; Kyiv, Ukraine; EN300-260977) were added. Reaction was allowed to run overnight at room temperature. The following morning, the DMF was removed using a rotary evaporator. Crude product was dissolved in ethyl acetate and filtered. Organic layer was washed with 1 N HCl followed by saturated sodium carbonate. Any precipitation was removed by filtration. The organic layer was dried with magnesium sulfate and filtered. Solvent was removed with a rotary evaporator before being dissolved back into DCM. Product was loaded onto a 40 g silica gel column equilibrated in DCM and eluted using a 0-10% MeOH gradient. Fractions containing product as determined by LC-MS were pooled and brought to dryness using a rotary evaporator. Product was brought up in ethyl acetate and washed with ammonium chloride followed by 1N HCl. The organic layer was then washed with saturated sodium carbonate followed by 1N NaOH. Product was assessed by LC-MS and brought to dryness in a clean vial using a rotary evaporator. Notably, this entire procedure was repeated a second time and final product was pooled. Final compound weight was 14.3 mg corresponding to a 7.9% yield.

Synthesis of (4-ethyl-1H-indol-2-yl)(4-((3-isopropyl-1,2,4-oxadiazol-5-yl)methyl)piperidin-1-yl)methanone (CP4.35)

In a 20 mL vial, 52.0 mg (0.275 mmol) of 4-ethyl-1H-indole-2-carboxylic acid (Enamine Ltd; Kyiv, Ukraine; EN300-321400), 205 mg (0.539 mmol) HATU, and 133 µL of DIPEA (d=0.742 g/mL, 0.764 mmol) were combined and dissolved in 2 mL DMF. Solution was stirred at room temperature for 15 minutes at which time 82.9 mg (0.337 mmol) of 4-[[3-(propan-2-yl)-1,2,4-oxadiazol-5-yl]methyl]piperidine hydrochloride (Enamine Ltd; Kyiv, Ukraine; EN300-260977) were added. Reaction was left to run overnight at room temperature. The following morning, the DMF was removed using a rotary evaporator. Crude product was dissolved in ethyl acetate and filtered. The organic layer was washed three times with saturated ammonium chloride and brine three times. The organic layer was transferred to a clean vial and solvent was removed using a rotary evaporator. The remaining product was brought up in a 95% DCM/5% MeOH mixture and a precipitate was noted and filtered into a separate vial. The vial containing the product remaining in solution was dried down on a rotary evaporator, brought up in a minimal amount of DCM, and purified through a 40 g silica gel column using a DCM/MeOH gradient (0-10% MeOH). Fractions containing product (as assessed by LC-MS) were combined and brought to dryness on a rotary evaporator. NMR analysis of product showed trace amine impurities, so the product was re-dissolved in DCM, washed twice with 1 N HCl, and the organic layer was dried with $MgSO_4$. The dried organic layer was transferred to a clean pre-weighed vial and solvent removed with a rotary evaporator. Final product was stored a -20°C for 1 week before being dried in a desiccator. LC-MS analysis was done to confirm purity of final product. Final product weighed 14.4 mg, corresponding to a 13.8% yield.

Synthesis of (4-ethyl-1H-indol-2-yl)(4-((4-methyl-4H-1,2,4-triazol-3-yl)methyl)piperidin-1-yl)methanone (CP4.36)

In a 20 mL vial, 50 mg (0.264 mmol) of 4-ethyl-1H-indole-2-carboxylic acid (Enamine Ltd; Kyiv, Ukraine; EN300-321400), 1 eq BOP, and 2 eq DIPEA were combined and dissolved in 3 mL DHF. Solution was stirred at room temperature for 15 minutes at which point 67 mg (0.265 mmol) of 4-[(4-methyl-4H-1,2,4-triazol-3-yl)methyl]piperidine dihydrochloride (Enamine Ltd.; Kyiv, Ukraine; EN300-697451) were added. Reaction was left to run overnight at room temperature. The following morning, the DMF was removed using a rotary evaporator. Crude product was dissolved in ethyl acetate and filtered. The organic layer was washed three times with saturated ammonium chloride and brine. The organic layer was subsequently transferred to a clean vial and solvent was removed using a rotary evaporator. Product was brought up in a minimal amount of DCM, and purified through a 40 g silica gel column using a DCM/MeOH gradient (0-10% MeOH). Fractions containing product (as assessed by LC-MS) were combined and brought to dryness on a rotary evaporator. Product was dried on a vacuum desiccator overnight and confirmed by LC-MS. Final product weighed 14.7 mg corresponding to a 15.8% yield.

Synthesis of (1-methyl-1H-indol-2-yl)(4-((4-methyl-4H-1,2,4-triazol-3-yl)methyl)piperidin-1-yl)methanone (CP4.40)

In a 20 mL vial, 52.5 mg (0.300 mmol) of 1-methylindole-2-carboxylic acid, 141.7 mg (0.320 mmol) of BOP, and 142 µL of DIPEA (d=0.742 g/mL, 0.815 mmol) were combined and dissolved in 3 mL DHF. Solution was stirred at room temperature for 15 minutes at which point 87.5 mg (0.346 mmol) of 4-[(4-methyl-4H-1,2,4-triazol-3-yl)methyl]piperidine dihydrochloride (Enamine Ltd.; Kyiv, Ukraine; EN300-697451) were added. Reaction was left to run overnight at room temperature. The following morning, 5 drops of 1N HCl were added and the DMF was removed using a rotary evaporator. Attempted to dissolve crude product in EtOAc, but product remained an insoluble oil. EtOAc was decanted off and the crude product was dissolved in MeOH. LC-MS confirmed product was present in MeOH solution. MeOH was removed by rotary evaporator and crude product (an oil) was washed with ethyl acetate and DCM. Washes were discarded. Solvent was removed by rotary evaporator and product was placed in a vacuum desiccator overnight. The following morning, product was dissolved into 1.5 mL of MeOH and purified by reverse phase HPLC on a C18 column using a water/acetonitrile gradient (0-100% acetonitrile). Fractions confirmed to

contain product (as determined by LC-MS) were pooled and solvent was removed by rotary evaporator. Final product was transferred to a clean vial and placed in a vacuum desiccator. Final product weighed 1.4 mg corresponding to a 1.38% yield.

Synthesis of (4-((4-methyl-4H-1,2,4-triazol-3-yl)methyl)piperidin-1-yl)(6-phenylpyridin-2-yl)methanone (CP4.41)

In a 20 mL vial, 53.3 mg of 6-phenyl-2-pyridinecarboxylic acid (0.268 mmol), 114.3 mg (0.258 mmol) BOP, 126.5 µL of DIPEA (d=0.742 g/mL, 0.726 mmol), and 3 mL of DMF were combined and allowed to stir for 15 minutes at room temperature. To the mixture, 85.4 mg (0.337 mmol) of 4-[(4-methyl-4H-1,2,4-triazol-3-yl)methyl]piperidine dihydrochloride (Enamine Ltd.; Kyiv, Ukraine; EN300-697451) were added. The reaction was allowed to run overnight at room temperature. The following morning, 5 drops of 1N HCl were added and solvent was removed using a rotary evaporator. Attempted to dissolve crude product in EtOAc, but product remained an insoluble oil. EtOAc was decanted off and the crude product was dissolved in MeOH. LC-MS confirmed product was present in MeOH solution. MeOH was removed by rotary evaporator and crude product (an oil) was washed with ethyl acetate and DCM. Washes were discarded. Solvent was removed by rotary evaporator and product was placed in a vacuum desiccator overnight. The following day, the product was dissolved in EtOH/EtOAc (1:1) mixture and heated. Product was found to be soluble in the EtOH/EtOAc solution by LC-MS. Transferred product to clean vial and removed solvent with rotary evaporator. The product was subsequently dissolved in MeOH and purified using reverse phase HPLC on a C18 column using a water/acetonitrile gradient (0-100% acetonitrile). Fractions confirmed to contain product (as determined by LC-MS) were pooled and solvent was removed by rotary evaporator. Final product was transferred to a clean vial and placed in a vacuum desiccator. Final product weighed 3.7 mg corresponding to a 4.0% yield.

Synthesis of (S)-2-(6-methoxynaphthalen-2-yl)-1-(4-((4-methyl-4H-1,2,4-triazol-3-yl)methyl)piperidin-1-yl)propan-1-one (CP4.42)

In a 20 mL vial, 47.6 mg (0.207 mmol) of (S)-2-(6-methoxynaphthalen-2-yl)propanoic acid, 94.0 mg (0.213 mmol) BOP, 104.8 µL of DIPEA (d=0.742 g/mL, 0.602 mmol), and 3 mL of DMF were combined and allowed to stir for 15 minutes at room temperature. To the mixture, 62.7 mg (0.248 mmol) of 4-[(4-methyl-4H-1,2,4-triazol-3-yl)methyl]piperidine dihydrochloride (Enamine Ltd.; Kyiv, Ukraine; EN300-697451) were added. The reaction was allowed to run overnight at room temperature. The following morning, 5 drops of 1N HCl were added and solvent was removed using a rotary evaporator. Attempted to dissolve crude product in EtOAc, but product remained an insoluble oil. Washed oil a second time with EtOAc and collected washings. Residual solvent was removed from the oil with a rotary evaporator. The oil was dissolved in MeOH and a sample was used to run LC-MS. Solvent was removed from remaining product using a rotary evaporator and the vial was placed in a desiccator. Final product weighed 94.1 mg corresponding to a 116% yield.

Synthesis of benzofuran-2-yl(4-((3-isopropyl-1,2,4-oxadiazol-5-yl)methyl)piperidin-1-yl)methanone (CP4.43)

In a 20 mL vial, 50 mg (0.277 mmol) of benzofuran-2-carbonyl chloride, 136 mg (0.554 mmol) of 4-[[3-(propan-2-yl)-1,2,4-oxadiazol-5-yl]methyl]piperidine hydrochloride (Enamine Ltd; Kyiv, Ukraine; EN300-260977), and 3 mL pyridine were combined. Reaction was allowed to run overnight at room temperature. The following morning, the crude product was filtered and solvent was removed by a rotary evaporator. The crude product was dissolved in MeOH and a sample was analyzed by LC-MS. Product was purified using reverse phase HPLC on a C18 column using a water/acetonitrile gradient (0-100% acetonitrile). Fractions confirmed to contain product (as determined by LC-MS) were pooled and solvent was removed by rotary evaporator. Final product was transferred to a clean vial and placed in a vacuum desiccator. Final product weighed 31.8 mg corresponding to a 32.5% yield.

Synthesis of (5-bromofuran-2-yl)(4-((3-isopropyl-1,2,4-oxadiazol-5-yl)methyl)piperidin-1-yl)methanone (CP4.44)

In a 20 mL vial, 50 mg (0.262 mmol) of 5-bromofuran-2-carboxylic acid, 99.5 mg (0.262 mmol) HATU, 137 µL of DIPEA (d=0.742 g/mL, 0.787 mmol), and 3 mL of DMF were combined and allowed to stir for 15 minutes at room temperature. To the mixture, 64.3 mg (0.262 mmol) of 4-[[3-(propan-2-yl)-1,2,4-oxadiazol-5-yl]methyl]piperidine hydrochloride (Enamine Ltd; Kyiv, Ukraine; EN300-260977) were added. The reaction was allowed to run overnight at room temperature. The following morning, the crude product was filtered, and solvent was removed by a rotary evaporator. The crude product was dissolved in MeOH, a sample of which was analyzed by LC-MS. Product was purified using reverse phase HPLC on a C18 column using a water/acetonitrile gradient (0-100% acetonitrile). Fractions confirmed to contain product (as determined by LC-MS) were pooled and solvent was removed by rotary evaporator. Final product was transferred to a clean vial and placed in a vacuum desiccator. Final product weighed 21.3 mg corresponding to a 21.3% yield.

Synthesis of (4-ethyl-1H-indol-2-yl)(piperidin-1-yl)methanone (CP4.45)

In a 20 mL vial, 50 mg (0.264 mmol) of 4-ethyl-1H-indole-2-carboxylic acid (Enamine Ltd; Kyiv, Ukraine; EN300-321400), 116.8 mg (0.264 mmol) BOP, 92 µL DIPEA (d=0.742 g/mL, 0.528 mmol), and 3 mL of DMF were combined and allowed to stir for 15 minutes at room temperature. To the mixture, 26.7 µL of piperidine (d=0.862 g/mL, 23 mg, 0.270 mmol) were added. The reaction was allowed to run overnight at room temperature. The following morning, the DMF was removed using a rotary evaporator. Crude product was dissolved in ethyl acetate and filtered. Organic layer was washed with 1 N HCl followed by saturated sodium carbonate. Any precipitation was removed by filtration. The organic layer was dried with sodium sulfate and filtered. Solvent was removed with a rotary evaporator before being dissolved back into DCM. Product was loaded onto a 40 g silica gel column equilibrated in DCM and eluted using a 0-10% MeOH gradient. Fractions containing product as determined by LC-MS were pooled and brought to dryness using a rotary evaporator. Product was assessed by LC-MS and brought to dryness in a clean vial using a rotary evaporator. Final product weighed 22.0 mg corresponding to a 32.5% yield.

Synthesis of (4-ethyl-1H-indol-2-yl)(morpholino)methanone (CP4.46)

In a 20 mL vial, 50 mg (0.264 mmol) of 4-ethyl-1H-indole-2-carboxylic acid (Enamine Ltd; Kyiv, Ukraine; EN300-321400), 116.8 mg (0.264 mmol) BOP, 92 µL DIPEA (d=0.742 g/mL, 0.528 mmol), and 3 mL of DMF were combined and allowed to stir for 15 minutes at room temperature. To the mixture, 22.8 µL of morpholine (d=1.007 g/mL, 0.264 mmol) were added. The reaction was allowed to run overnight at room temperature. The following morning, the reaction was filtered and allowed to continue for 1 additional day. Following the second day of the reaction, DMF was removed using a rotary evaporator. Crude product was dissolved in ethyl acetate and filtered. Organic layer was washed with saturated ammonium chloride. The organic layer was dried with sodium sulfate and filtered. Solvent was removed with a rotary evaporator before being dissolved back into DCM. Product was loaded onto a 40 g silica gel column equilibrated in DCM and eluted using a 0-10% MeOH gradient. Fractions containing product as determined by LC-MS were pooled and brought to dryness using a rotary evaporator. Product was assessed by LC-MS and brought to dryness in a clean vial using a rotary evaporator. Final product weighed 22.2 mg corresponding to a 32.5% yield.

Synthesis of (3,5-dichloro-1H-indol-2-yl)(4-((3-ethyl-1,2,4-oxadiazol-5-yl)methyl)piperidin-1-yl)methanone (CP4.29.1)

In a 20 mL vial, 52.7 mg (0.229 mmol) of 3,5-dichloro-1H-indole-2-carboxylic acid (Enamine Ltd., Kyiv, Ukraine; EN300-36960), 104.7 mg (0.275 mmol) HATU, 120 µL DIPEA (d=0.742 g/mL, 0.687 mmol) and 3 mL of dry dimethylformamide were added and allowed to mix with rapid stirring for 15 minutes. To the mixture, 61.6 mg of 4-[(3-ethyl-1,2,4-oxadiazol-5-yl)methyl]piperidine (0.315 mmol; Enamine Ltd., Kyiv, Ukraine; EN300-304609) were added and reaction was allowed to stir overnight at room temperature. Crude product was filtered, transferred to a 40 mL vial, and DMF removed using a rotary evaporator. Product was partitioned between water and dichloromethane (DMC). Organic layer was washed twice with water, dried with sodium sulfate, and transferred to a new vial. DCM was removed with a rotary evaporator and product was brought up in methanol

(MeOH) for LC-MS analysis. MeOH was removed in similar fashion and product left dry overnight. Product was brought up in 1-3 mL of DCM and purified using normal phase chromatography on a 4 g silica column and a DCM/MeOH (0-10%) gradient. Fractions were allowed to dry via evaporation in the hood and pulled up in MeOH for LC-MS analysis. Product was dried using a rotary evaporator, dissolved in DMSO, and purified using reverse phase HPLC on a C18 column using a linear water/acetonitrile gradient (with 0.1% formic acid). Fractions containing product as assessed by LC-MS were pooled into a weighed vial and dried using a Genevac with maximum temperature set to 60°C. Product was dissolved in $CDCl_3$ and analyzed by 1H NMR on a Bruker 400 MHz NMR spectrometer. Sample was returned to vial and $CDCl_3$ was allowed to evaporate in the hood. Product was re-dissolved in 85% acetonitrile/15% water mixture and dried on Genevac overnight on the same settings. Product was dissolved in DCM and transferred to a new pre-weighed 4 mL vial and solvent allowed to evaporate overnight in the hood. Vial was covered with a Kim wipe and placed in a vacuum desiccator overnight. Final compound dry weight was 7.3 mg which corresponded to a 7.8% yield. 1H NMR ($CDCl_3$, 400 MHz): δ 9.27 (s, 1H), 7.38 (d, 1H, J=1.92Hz), 7.08 (dd, 1H, J=8.76 Hz, 0.32 Hz), 7.04 (residual $CHCl_3$), 7.03 (dd, 1H, J=8.72 Hz, 1.92 Hz), 4.20 (br, 2H), 2.80 (br, 2H), 2.64 (d, 2H, J=7.08 Hz), 2.54 (q, 2H, J=7.6 Hz), 2.00 (m, 1H), 1.66 (br, 2H), 1.22 (qd, 2H, J=12.52 Hz, 3.84 Hz), 1.11 (t, 3H, J= 7.56 Hz). Found m/z = 407.1 $(M+H)^+$.

Synthesis of (4-((3-cyclobutyl-1,2,4-oxadiazol-5-yl)methyl)piperidin-1-yl)(3,5-dichloro-1H-indol-2-yl)methanone (CP4.29.3)

In a 20 mL vial, 53.2 mg (0.231 mmol) of 3,5-dichloro-1H-indole-2-carboxylic acid (Enamine Ltd., Kyiv, Ukraine; EN300-36960), 107.4 mg (0.283 mmol) HATU, 121 µL DIPEA (d=0.742 g/mL, 0.694 mmol) and 3 mL of dry dimethylformamide were added and allowed to mix with rapid stirring for 15 minutes. To the resulting mixture, 80.6 mg of 4-[(3-cyclobutyl-1,2,4-oxadiazol-5-yl)methyl]piperidine hydrochloride (0.313 mmol; Enamine Ltd., Kyiv, Ukraine; EN300-262395) were added and the reaction was left to stir overnight at room temperature. Product was purified as described above for CP4.29.1. Final dry compound weight was 7.8 mg which corresponded to an 7.8% yield as well. 1H NMR ($CDCl_3$, 400 MHz): δ 9.75 (s, 1H), 7.50 (d, 1H, J=1.92 Hz), 7.20 (d, 1H, J= 8.72 Hz), 7.19 (residual $CHCl_3$), 7.14 (dd, 1H, J= 8.76 Hz, 1.96 Hz), 4.30 (br, 2H), 3.58 (qd, 1H, J= 17.04 Hz, 0.92 Hz), 3.00 (br, 2H), 2.79 (d, 2H), 2.30 (m, 4H), 2.14 (m, 1H), 2.03 (m, 1H), 1.90 (m, 1H), 1.80 (br, 2H), 1.37 (m, 2H). Found m/z = 433.1 $(M+H)^+$.

Synthesis of (4-((3-cyclopentyl-1,2,4-oxadiazol-5-yl)methyl)piperidin-1-yl)(3,5-dichloro-1H-indol-2-yl)methanone (CP4.29.4)

In a 20 mL vial, 54.1 mg (0.235 mmol) of 3,5-dichloro-1H-indole-2-carboxylic acid (Enamine Ltd., Kyiv, Ukraine; EN300-36960), 108.9 mg (0.286 mmol) HATU, 123 µL DIPEA (d=0.742 g/mL, 0.705 mmol) and 3 mL of dry dimethylformamide were added and allowed to mix with rapid stirring for 15 minutes. To the resulting mixture, 77.8 mg of 4-[(3-cyclopentyl-1,2,4-oxadiazol-5-yl)methyl]piperidine hydrochloride (0.286 mmol; Enamine Ltd., Kyiv, Ukraine; EN300-313578) were added and the reaction was left to stir overnight at room temperature. Product was purified as described above for CP4.29.1. Final dry compound weight was 4.6 mg which corresponded to a 4.38% yield. 1H NMR ($CDCl_3$, 400 MHz): δ 9.20 (s, 1H), 7.53 (d, 1H, J=1.88 Hz), 7.22 (d, 1H, J= 8.48 Hz), 7.19 (residual $CHCl_3$), 7.17 (dd, 1H, J = 8.72 Hz, 1.92 Hz), 4.25 (br, 2H), 2.90 (br, 2H), 3.12 (p, 2H, J=7.8 Hz), 2.78 (d, 2H, J=7.04 Hz), 2.14 (m, 1H), 1.98 (m, 2H), 1.75 (m, 7H), 1.62 (m, 5H), 1.35 (qd, 2H, J=12.6 Hz, 3.96 Hz). Found m/z = 447.1 $(M+H)^+$.

Synthesis of (4-((3-cyclohexyl-1,2,4-oxadiazol-5-yl)methyl)piperidin-1-yl)(3,5-dichloro-1H-indol-2-yl)methanone (CP4.29.5)

In a 20 mL vial, 53.8 mg (0.234 mmol) of 3,5-dichloro-1H-indole-2-carboxylic acid (Enamine Ltd., Kyiv, Ukraine; EN300-36960), 108.2 mg (0.285 mmol) HATU, 122 µL DIPEA (d=0.742 g/mL, 0.702 mmol) and 3 mL of dry dimethylformamide were added and allowed to mix with rapid stirring for 15 minutes. To the resulting mixture, 85.3 mg of 4-[(3-cyclohexyl-1,2,4-oxadiazol-5-yl)methyl]piperidine hydrochloride (0.298 mmol; Enamine Ltd., Kyiv, Ukraine; EN300-312344) were added and the reaction was left to stir overnight at room temperature. Product was purified as described above for CP4.29.1. Final dry weight of the product was 3.4 mg which corresponded to

a 3.1% yield. 1H NMR ($CDCl_3$, 400 MHz): δ 9.28 (s, 1H), 7.52 (d, 1H, J=1.88 Hz), 7.21 (d, 1H, J=8.72 Hz), 7.19 (residual $CHCl_3$), 7.17 (dd, 1H, J=8.72 Hz, 1.92 Hz), 4.30 (br, 2H), 3.00 (br, 2H), 2.78 (d, 2H, J=7.08 Hz), 2.71 (tt, 1H, J=11.48 Hz, 3.56 Hz), 2.14 (m, 1H), 1.92 (m, 2H), 1.77 (m, 5H), 1.64 (m, 4H), 1.50 (qd, 3H, J=11.92 Hz), 1.40 (m, 7H). Found m/z = 461.1 $(M+H)^+$.

Synthesis of (3,5-dichloro-1H-indol-2-yl)(4-((3-(tetrahydro-2H-pyran-4-yl)-1,2,4-oxadiazol-5-yl)methyl)piperidin-1-yl)methanone (CP4.29.6)

In a 20 mL vial, 53.3 mg (0.232 mmol) of 3,5-dichloro-1H-indole-2-carboxylic acid (Enamine Ltd., Kyiv, Ukraine; EN300-36960), 113.7 mg (0.299 mmol) HATU, 121 µL DIPEA (d=0.742 g/mL, 0.696 mmol) and 3 mL of dry dimethylformamide were added and allowed to mix with rapid stirring for 15 minutes. To the resulting mixture, 82.7 mg of 4-[[3-(oxan-4-yl)-1,2,4-oxadiazol-5-yl]methyl]piperidine hydrochloride (0.287 mmol; Enamine Ltd., Kyiv, Ukraine; EN300-318107) were added and the reaction was left to stir overnight at room temperature. Product was purified as described above for CP4.29.1. Final compound weight was 6.7 mg which corresponded to a 6.2% yield. 1H NMR ($CDCl_3$, 400 MHz): δ 9.39 (s, 1H), 7.62 (d, 1H), 7.31 (d, 1H, J= 8.72 Hz), 7.28 (residual $CHCl_3$), 7.26 (dd, 1H, J = 8.72 Hz, 1.92 Hz), 4.40 (br, 2H), 4.05 (dt, 2H, J = Hz), 3.55 (td, 2H, J = Hz), 3.1 (br, 2H), 3.05 (septet, 1H, J = Hz), 2.88 (d, 2H, J = Hz), 2.23 (m, 1H), 1.94 (m, 7H), 1.68 (s, 2H), 1.46 (qd, 2H, J = Hz). Found m/z = 463.1 $(M+H)^+$.

Synthesis of (3,5-dichloro-1H-indol-2-yl)(4-(piperidin-1-ylmethyl)piperidin-1-yl)methanone (CP4.29.9)

In a 20 mL vial, 47.7 mg (0.207 mmol) of 3,5-dichloro-1H-indole-2-carboxylic acid (Enamine Ltd., Kyiv, Ukraine; EN300-36960), 102 mg (0.268 mmol) HATU, 108 µL DIPEA (d=0.742 g/mL, 0.621 mmol) and 3 mL of dry dimethylformamide were added and allowed to mix with rapid stirring for 15 minutes. To the resulting mixture, 65.2 mg of 4-[(piperidin-1-yl)methyl]piperidine dihydrochloride (0.255 mmol; Enamine Ltd., Kyiv, Ukraine; EN300-54899) were added and the reaction was left to stir overnight at room temperature. Product was purified as described above for CP4.29.1. Final compound dry weight was 2.7 mg corresponding to a yield of 3.3%. 1H NMR ($CDCl_3$, 400 MHz): δ 10.27 (s, 1H), 8.48 (s, 1H), 8.04 (s, 0.2 H), 7.60 (d, 1H, J = 1.84 Hz), 7.35 (d, 1H, J = 8.76 Hz), 7.28 (residual $CHCl_3$), 7.23 (dd, 1H, J = 8.72 Hz, 2.0 Hz), 4.50 (br, 6H), 2.98 (m, 5H), 2.91 (s, 1H), 2.79 (br, 2H), 2.64 (s, 0.3H), 2.18 (m, 1H), 2.11 (s, 0.17H), 2.02 (m, 2H), 1.89 (m, 5H), 1.61 (br, 2H), 1.41 (qd, 2H, J = 12.56 Hz, 3.52 Hz). Found m/z = 394 $(M+H)^+$.

Synthesis of (3,5-dichloro-1H-indol-2-yl)(4-(morpholinomethyl)piperidin-1-yl)methanone (CP4.29.10)

In a 20 mL vial, 50.2 mg (0.218 mmol) of 3,5-dichloro-1H-indole-2-carboxylic acid (Enamine Ltd., Kyiv, Ukraine; EN300-36960), 105.3 mg (0.277 mmol) HATU, 114 µL DIPEA (d=0.742 g/mL, 0.654 mmol) and 3 mL of dry dimethylformamide were added and allowed to mix with rapid stirring for 15 minutes. To the resulting mixture, 68.3 mg of 4-[(piperidin-4-yl)methyl]morpholine (0.371 mmol; Enamine Ltd., Kyiv, Ukraine; EN300-42119) were added and the reaction was left to stir overnight at room temperature. Product was purified as described above for CP4.29.1 with several slight modifications. During aqueous workup, the organic layer was washed once with water and once with saturated brine. Additionally, the aqueous layer was reverse extracted with DCM and the resulting organic layer pooled with the original organic layer. Final compound dry weight was 18.2 mg corresponding to a yield of 21.1%. 1H NMR ($CDCl_3$, 400 MHz): δ 10.25 (s, 1H), 8.27 (s, 3H), 7.60 (d, 1H, J =1.6 Hz), 7.32 (dd, 1H, J = 8.76 Hz, 0.36 Hz), 7.28 (residual $CHCl_3$), 7.24 (dd, 1H, J = 8.76 Hz, 2.0 Hz), 4.40 (br, 2H), 3.85 (t, 4H, J = Hz), 3.00 (br, 2H), 2.99 (s, 0.4H), 2.91 (s, 0.4H), 2.56 (d, 2H, J=6.72 Hz), 2.00 (m, 3H), 1.35 (qd, 2H, J=12.12 Hz, 2.96 Hz). Found m/z = 396.1 $(M+H)^+$.

Synthesis of (3,5-dichloro-1H-indol-2-yl)(4-(pyridin-3-ylmethyl)piperidin-1-yl)methanone (CP4.29.11)

In a 20 mL vial, 49.9 mg (0.217 mmol) of 3,5-dichloro-1H-indole-2-carboxylic acid (Enamine Ltd., Kyiv, Ukraine; EN300-36960), 107.8 mg (0.284 mmol) HATU, 113 µL DIPEA (d=0.742 g/mL, 0.651 mmol) and 3 mL of dry dimethylformamide were added and allowed to mix with rapid stirring for 15 minutes. To the resulting mixture, 61.1 mg of 3-[(piperidin-4-yl)methyl]pyridine (0.347 mmol;

Enamine Ltd., Kyiv, Ukraine; EN300-122729) were added and the reaction was left to stir overnight at room temperature. Product was purified as described above for CP4.29.10. Final compound dry weight was 5.5 mg corresponding to a yield of 6.5%. 1H NMR ($CDCl_3$, 400 MHz): δ 9.49 (s, 1H), 8.53 (s, 2H), 7.60 (m, 2H), 7.36 (br, 1H), 7.32 (d, 1H, J=8.72 Hz), 7.28 (residual $CHCl_3$), 7.26 (dd, 1H, J = 8.72 Hz, 1.96 Hz), 4.40 (br, 2H), 3.00 (br, 2H), 2.65 (d, 2H, J = Hz), 2.50 (br, 2H), 1.90 (m, 2H), 1.38 (qd, 2H, J = 12.32 Hz, 3.64 Hz). Found m/z = 388 $(M+H)^+$.

Synthesis of (4-(cyclopentylmethyl)piperidin-1-yl)(3,5-dichloro-1H-indol-2-yl)methanone (CP4.29.12)

In a 20 mL vial, 49.5 mg (0.215 mmol) of 3,5-dichloro-1H-indole-2-carboxylic acid (Enamine Ltd., Kyiv, Ukraine; EN300-36960), 103.9 mg (0.273 mmol) HATU, 112 µL DIPEA (d=0.742 g/mL, 0.645 mmol) and 3 mL of dry dimethylformamide were added and allowed to mix with rapid stirring for 15 minutes. To the resulting mixture, 52.0 mg of 4-(cyclopentylmethyl)piperidine hydrochloride (0.255 mmol; Enamine Ltd., Kyiv, Ukraine; EN300-240902) were added and the reaction was left to stir overnight at room temperature. Product was purified as described above for CP4.29.10. Final compound dry weight was 3.5 mg corresponding to a yield of 4.3%. 1H NMR ($CDCl_3$, 400 MHz): δ 9.62 (s, 1H), 7.61 (d, 1H, J = 1.96 Hz), 7.31 (d, 1H, J = 8.76 Hz), 7.28 (residual $CHCl_3$), 7.24 (dd, 1H, J= 8.76 Hz, 2.0 Hz), 4.30 (br, 2H), 3.10 (br, 2H), 1.80 (m, 6H), 1.6 (m, 7H), 1.30 (m, 5H), 1.10 (m, 2H). Found m/z = 379.1 $(M+H)^+$.

Synthesis of (4-((1H-pyrrol-1-yl)methyl)piperidin-1-yl)(3,5-dichloro-1H-indol-2-yl)methanone (CP4.29.13)

In a 20 mL vial, 49.2 mg (0.214 mmol) of 3,5-dichloro-1H-indole-2-carboxylic acid (Enamine Ltd., Kyiv, Ukraine; EN300-36960), 101.7 mg (0.267 mmol) HATU, 112 µL DIPEA (d=0.742 g/mL, 0.642 mmol) and 3 mL of dry dimethylformamide were added and allowed to mix with rapid stirring for 15 minutes. To the resulting mixture, 114 mg of 4-[(1H-pyrrol-1-yl)methyl]piperidine (0.694 mmol; Enamine Ltd., Kyiv, Ukraine; EN300-262763) were added and the reaction was left to stir overnight at room temperature. Product was purified as described above for CP4.29.10. Final compound dry weight was 3.3 mg corresponding to a yield of 4.1%. 1H NMR ($CDCl_3$, 400 MHz): δ 9.58 (s, 1H), 7.61 (d, 1H, J = 1.92 Hz), 7.29 (dd, 1H, J = 8.76 Hz, 0.4 Hz), 7.28 (residual $CHCl_3$), 7.25 (dd, 1H, J = 8.72 Hz, 1.96 Hz), 6.64 (t, 2H, J = 2.04 Hz), 6.18 (t, 2H, J = 2.12 Hz), 4.40 (br, 2H), 3.81 (d, 2H, J = 7.2 Hz), 3.10 (br, 2H), 2.04 (m, 1H), 1.73 (d, 4H, J = 10.44 Hz), 1.34 (qd, 2H, J = 12.52 Hz, 3.8 Hz). Found m/z = 376.1 $(M+H)^+$.

Synthesis of (3,5-dimethyl-1H-indol-2-yl)(4-((3-isopropyl-1,2,4-oxadiazol-5-yl)methyl)piperidin-1-yl)methanone (CP4.29.14)

In a 20 mL vial, 99.5 mg (0.526 mmol) of 3,5-dimethyl-1H-indole-2-carboxylic acid (Enamine Ltd., Kyiv, Ukraine; EN300-103388), 246.5 mg (0.648 mmol) HATU, 275 µL DIPEA (d=0.742 g/mL, 1.578 mmol) and 3 mL of dry dimethylformamide were added and allowed to mix with rapid stirring for 10 minutes. To the resulting mixture, 155.3 mg of 4-[[3-(propan-2-yl)-1,2,4-oxadiazol-5-yl]methyl]piperidine hydrochloride (0.632 mmol; Enamine Ltd., Kyiv, Ukraine; EN300-260977) were added and the reaction was left to stir overnight at room temperature. The following day, the DMF was removed using a rotary evaporator and the crude product was washed with 10 mL of water twice (washings were saved). 5-10 mL of ethyl acetate were added to the crude product but the product remained insoluble. Ethyl acetate was removed using a rotary evaporator and the product was dissolved in 10 mL of dichloromethane. The resulting solution was added to the saved initial aqueous washes and product was partitioned between the DCM and water layers.

After removal of the aqueous layer, the organic layer was washed once with 10 mL of 2N HCl, once with 10 mL of saturated sodium bicarbonate, and once with 10 mL of brine. Remaining product in the combined aqueous waste was reverse extracted using 10 mL of DCM and the washes repeated before combining the organic layers together. The organic layer was dried with sodium sulfate and transferred to new vials at which point the DCM was removed with a rotary evaporator. 5 mL of methanol (MeOH) was added to the crude product at which point a white solid crashed out of solution. Methanol solution was removed and placed into a second vial leaving behind the white

solid. The remaining white solid was washed twice more with methanol and the methanol washes were pooled. A sample of the white solid was dissolved in 1 mL of DMSO and analyzed by LC-MS which confirmed the compound identity as product.

The remaining product had solubility tested in 10 mL of hot methanol after which it was dried on a rotary evaporator and dissolved in 3 mL of DCM. A small sample of the resulting solution was transferred to a new vial and the DCM was removed by evaporation. The sample was dissolved in 1 mL of DMSO and analyzed using LC-MS. Remaining product was dissolved in $CDCl_3$ and analyzed by 1H NMR spectroscopy on a Bruker 400 MHz NMR spectrometer. The product was recovered and the $CDCl_3$ was removed via evaporation in the hood. Product was dissolved in DMSO and purified further using reverse phase HPLC on a C18 column with a water/acetonitrile gradient (with 0.1% formic acid). Fractions containing product were pooled and dried down on the Genevac with a maximum temperature of 60°C. The resulting product was once again dissolved in $CDCl_3$ and analyzed by 1H NMR. After evaporation of $CDCl_3$, the product was dissolved in DCM and transferred to a clean 4 mL vial, covered with a Kim wipe, and left in a vacuum desiccator overnight. Final compound weight was 11.8 mg which corresponded to a 5.9% yield. 1H NMR ($CDCl_3$, 400 MHz): δ 8.55 (s, 1H), 7.38 (s, 1H), 7.27 (d, 1H, J = 9.48 Hz), 7.10 (dd, 1H, J = 8.4 Hz, 1.32 Hz), 4.38 (s, 2H), 3.10 (m, 3H), 2.85 (d, 2H, J = Hz), 2.48 (s, 3H), 2.35 (s, 3H), 2.20 (m, 1H), 1.84 (d, 2H, J = 12.8 Hz), 1.38 (m, 8H). Found m/z = 381.2 $(M+H)^+$.

Synthesis of (3,5-dimethylbenzofuran-2-yl)(4-((3-isopropyl-1,2,4-oxadiazol-5-yl)methyl)piperidin-1-yl)methanone (CP4.29.16)

In a 20 mL vial, 100.7 mg (0.529 mmol) of 3,5-dimethyl-1-benzofuran-2-carboxylic acid (Enamine Ltd., Kyiv, Ukraine; EN300-12940), 261.9 mg (0.689 mmol) HATU, 277 µL DIPEA (d=0.742 g/mL, 1.587 mmol) and 3 mL of dry dimethylformamide were added and allowed to mix with rapid stirring for 10 minutes. To the resulting mixture, 159.6 mg of 4-[[3-(propan-2-yl)-1,2,4-oxadiazol-5-yl]methyl]piperidine hydrochloride (0.649 mmol; Enamine Ltd., Kyiv, Ukraine; EN300-260977) were added and the reaction was left to stir overnight at room temperature. Product was purified in a similar manner as CP4.29.14 with a few differences. Following acid/base workup, the organic layer was dried down and dissolved in MeOH. A sample of the MeOH soluble solution was used for LC-MS analysis. Remaining product was dried down on a rotary evaporator, dissolved in 1-3 mL DCM, and purified using normal phase chromatography on a 12 g silica column. Fractions containing product were left in hood to evaporate. These fractions were later dissolved in hot methanol and a sample of each was run on LC-MS. Highest purity fractions were pooled in a 20 mL vial and dried on rotary evaporator. The product was subsequently dissolved in $CDCl_3$ and a 1H NMR was taken. The sample was recovered and $CDCl_3$ was evaporated in the hood. Remaining sample was dissolved in hot DMSO, allowed to cool to room temperature, and purified via reverse phase HPLC on a C18 column using the same gradient already described. Fractions containing product were pooled and dried on the Genevac. From this point, compound was dried as already described for CP4.29.14. Final compound weight was 53.0 mg corresponding to a yield of 26.2%. 1H NMR ($CDCl_3$, 400 MHz): δ 7.34 (m, 2H), 7.28 (residual $CHCl_3$), 7.18 (dd, 1H, J = 8.44 Hz, 1.32 Hz), 4.50 (br, 2H), 3.08 (septet, 1H, J = 7.0 Hz), 2.86 (d, 2H, J = 7.12 Hz), 2.20 (m, 1H), 1.85 (br, 2H), 1.42 (qd, 2H, J = 12.84 Hz, 4.12 Hz), 1.35 (d, 6H, J = 6.92 Hz). Found m/z = 382.2 $(M+H)^+$.

Synthesis of 2-(4-((3-isopropyl-1,2,4-oxadiazol-5-yl)methyl)piperidine-1-carbonyl)-1H-indole-4-carbonitrile (CP4.29.17)

In a 20 mL vial, 99.7 mg (0.535 mmol) of 4-cyano-1H-indole-2-carboxylic acid (Enamine Ltd., Kyiv, Ukraine; EN300-321079), 268.4 mg (0.706 mmol) HATU, 280 µL DIPEA (d=0.742 g/mL, 1.605 mmol) and 3 mL of dry dimethylformamide were added and allowed to mix with rapid stirring for 10 minutes. To the resulting mixture, 159.4 mg of 4-[[3-(propan-2-yl)-1,2,4-oxadiazol-5-yl]methyl]piperidine hydrochloride (0.649 mmol; Enamine Ltd., Kyiv, Ukraine; EN300-260977) were added and the reaction was left to stir overnight at room temperature. Product was purified in a similar way to CP4.29.16 with a few changes. Following purification via reverse phase HPLC, a contaminant from the instrument co-eluted with the product. The resulting product was re-run through the same reverse phase HPLC after cleaning the instrument, but contaminant was still

present. Fractions were dried using the Genevac at a maximum temperature of 45°C. Remaining product was purified from the contaminant using normal phase chromatography with a 4 g silica column and a DCM/MeOH (up to 10%) linear gradient. Fractions were left to partially evaporate overnight in the hood and the following morning, fractions corresponding to single peak were pooled. Product was transferred to a clean pre-weighed vial and dried on a rotary evaporator. The resulting solid was dissolved in $CDCl_3$ and used for 1H NMR analysis. Sample was returned to the original vial and $CDCl_3$ removed by evaporation in the hood. Product was dissolved in DCM, transferred to 4 mL vial, and dried with a rotary evaporator. Finally, the vial was covered with a Kim wipe and left overnight in a vacuum desiccator. Final compound weight was 2.2 mg corresponding to a 1.1% yield. 1H NMR ($CDCl_3$, 400 MHz): δ 9.72 (s, 1H), 7.58 (d, 1H, J = 8.36 Hz), 7.45 (dd, 1H, J = 7.32 Hz, 0.68 Hz), 7.25 (t, 1H, J = 7.44 Hz), 7.19 (s, 2H), 6.87 (d, 1H, J = 1.28 Hz), 4.66 (d, 2H, J = 13.32 Hz), 3.42 (s, 0.6H), 3.01 (septet, 1H, J = 6.96 Hz), 2.81 (m, 3H), 2.19 (m, 1H), 1.87 (d, 2H, J = 11.36 Hz), 1.51 (br, 3H), 1.35 (qd, 3H, J = 8.36 Hz, 3.96 Hz), 1.25 (m, 11H). Found m/z = 378.2 $(M+H)^+$.

Synthesis of 2-(4-((3-isopropyl-1,2,4-oxadiazol-5-yl)methyl)piperidine-1-carbonyl)-1H-indole-3-carbonitrile (CP4.29.18)

In a 20 mL vial, 98.0 mg (0.526 mmol) of 3-cyano-1H-indole-2-carboxylic acid (Enamine Ltd., Kyiv, Ukraine; EN300-344668), 247.2 mg (0.650 mmol) HATU, 275 µL DIPEA (d=0.742 g/mL, 1.578 mmol) and 3 mL of dry dimethylformamide were added and allowed to mix with rapid stirring for 10 minutes. To the resulting mixture, 148.5 mg of 4-[[3-(propan-2-yl)-1,2,4-oxadiazol-5-yl]methyl]piperidine hydrochloride (0.604 mmol; Enamine Ltd., Kyiv, Ukraine; EN300-260977) were added and the reaction was left to stir overnight at room temperature. Product was purified in the same manner as described for CP4.29.17. Final compound weight was 3.6 mg corresponding to a 1.8% yield. 1H NMR ($CDCl_3$, 400 MHz): δ 10.26 (s, 1H), 7.68 (d, 1H, J = 8.12 Hz), 7.39 (d, 1H, 8.24 Hz), 7.30 (td, 1H, J = 7.04 Hz, 1.12 Hz), 7.23 (m, 1H), 7.19 (s, 1H), 4.43 (br, 2H), 3.17 (br, 2H), 3.01 (septet, 1H, J = 6.92 Hz), 2.80 (d, 2H, J = 7.12 Hz), 2.17 (m, 1H), 1.86 (br, 2H), 1.50 (m, 6H), 1.20 (m, 8H). Found m/z = 378.2 $(M+H)^+$.

Synthesis of (4-cyclopropyl-1H-indol-2-yl)(4-((3-isopropyl-1,2,4-oxadiazol-5-yl)methyl)piperidin-1-yl)methanone (CP4.29.19)

In a 20 mL vial, 94.6 mg (0.470 mmol) of 4-cyclopropyl-1H-indole-2-carboxylic acid (Enamine Ltd., Kyiv, Ukraine; EN300-323048), 219.7 mg (0.578 mmol) HATU, 246 µL DIPEA (d=0.742 g/mL, 1.41 mmol) and 3 mL of dry dimethylformamide were added and allowed to mix with rapid stirring for 10 minutes. To the resulting mixture, 142.9 mg of 4-[[3-(propan-2-yl)-1,2,4-oxadiazol-5-yl]methyl]piperidine hydrochloride (0.581 mmol; Enamine Ltd., Kyiv, Ukraine; EN300-260977) were added and the reaction was left to stir overnight at room temperature. Product was purified in the same manner as described for CP4.29.17. Final compound weight was 4.2 mg corresponding to a 2.3% yield. 1H NMR ($CDCl_3$, 400 MHz): δ 9.12 (s, 1H), 7.14 (m, 3H), 6.86 (d, 1H, J = 1.32 Hz), 6.64 (d, 1H, 7.0 Hz), 4.70 (d, 2H, J = 13.4 Hz), 3.01 (m, 3H), 2.80 (d, 2H, J = 7.12 Hz), 2.15 (m, 2H), 1.84 (br, 2H), 1.57 (br, 1H), 1.36 (qd, 2H, J = 12.6 Hz, 3.96 Hz), 1.20 (m, 8H), 0.93 (m, 2H), 0.75 (m, 2H). Found m/z = 393.2 $(M+H)^+$.

Synthesis of (3-cyclopropyl-1H-indol-2-yl)(4-((3-isopropyl-1,2,4-oxadiazol-5-yl)methyl)piperidin-1-yl)methanone (CP4.29.20)

In a 20 mL vial, 101.2 mg (0.503 mmol) of 3-cyclopropyl-1H-indole-2-carboxylic acid (Enamine Ltd., Kyiv, Ukraine; EN300-6764589), 237.3 mg (0.624 mmol) HATU, 263 µL DIPEA (d=0.742 g/mL, 1.509 mmol) and 3 mL of dry dimethylformamide were added and allowed to mix with rapid stirring for 10 minutes. To the resulting mixture, 152.5 mg of 4-[[3-(propan-2-yl)-1,2,4-oxadiazol-5-yl]methyl]piperidine hydrochloride (0.620 mmol; Enamine Ltd., Kyiv, Ukraine; EN300-260977) were added and the reaction was left to stir overnight at room temperature. Product was purified in the same manner as described for CP4.29.17. Final compound weight was 30.3 mg corresponding to a 15.3% yield. 1H NMR ($CDCl_3$, 400 MHz): δ 9.08 (s, 1H), 7.60 (d, 1H, J = 7.96 Hz),

7.26 (d, 1H, J = 8.2 Hz), 7.13 (td, 1H, J = 7.04 Hz, 1.0 Hz), 7.02 (t, 1H, J = 7.92 Hz), 4.42 (br, 2H), 3.39 (s, 1H), 2.99 (m, 3H), 2.74 (d, 2H, J = 7.08 Hz), 2.10 (m, 1H), 1.80 (m, 4H), 1.30 (m, 9H), 0.83 (m, 2H), 0.65 (m, 2H). Found m/z = 393.2 $(M+H)^+$.

Synthesis of (4-((3-isopropyl-1,2,4-oxadiazol-5-yl)methyl)piperidin-1-yl)(3-phenyl-1H-indol-2-yl)methanone (CP4.29.21)

In a 20 mL vial, 100.8 mg (0.425 mmol) of 3-phenyl-1H-indole-2-carboxylic acid (Enamine Ltd., Kyiv, Ukraine; EN300-7536218), 195.9 mg (0.515 mmol) HATU, 223 µL DIPEA (d=0.742 g/mL, 1.275 mmol) and 3 mL of dry dimethylformamide were added and allowed to mix with rapid stirring for 10 minutes. To the resulting mixture, 126.9 mg of 4-[[3-(propan-2-yl)-1,2,4-oxadiazol-5-yl]methyl]piperidine hydrochloride (0.516 mmol; Enamine Ltd., Kyiv, Ukraine; EN300-260977) were added and the reaction was left to stir overnight at room temperature. Product was purified in the same manner as described for CP4.29.17. Final compound weight was 10.3 mg corresponding to a 5.7% yield. 1H NMR ($CDCl_3$, 400 MHz): δ 9.14 (s, 1H), 7.56 (d, 1H, J = 2.2 Hz), 7.28 (m, 5H), 7.17 (tt, 1H, J = 6.52 Hz, 1.4 Hz), 7.10 (m, 1H), 7.07 (s, 1H), 6.97 (m, 1H), 4.00 (br, 2H), 2.85 (septet, 1H, J = 6.96 Hz), 2.39 (m, 4H), 1.69 (m, 1H), 1.56 (br, 2H), 1.11 (m, 8H), 0.00 (br, 1H). Found m/z = 429.2 $(M+H)^+$.

Synthesis of (4-((3-isopropyl-1,2,4-oxadiazol-5-yl)methyl)piperidin-1-yl)(1H-pyrrolo[2,3-b]pyridin-2-yl)methanone (CP4.29.22)

In a 20 mL vial, 97.0 mg (0.598 mmol) of 1H-pyrrolo[2,3-b]pyridine-2-carboxylic acid (Enamine Ltd., Kyiv, Ukraine; EN300-33541), 299.8 mg (0.788 mmol) HATU, 312 µL DIPEA (d=0.742 g/mL, 1.794 mmol) and 3 mL of dry dimethylformamide were added and allowed to mix with rapid stirring for 10 minutes. To the resulting mixture, 180.6 mg of 4-[[3-(propan-2-yl)-1,2,4-oxadiazol-5-yl]methyl]piperidine hydrochloride (0.735 mmol; Enamine Ltd., Kyiv, Ukraine; EN300-260977) were added and the reaction was left to stir overnight at room temperature. Product was purified in the same manner as described for CP4.29.17. Final compound weight was 7.7 mg corresponding to a 3.6% yield. 1H NMR ($CDCl_3$, 400 MHz): δ 8.43 (d, 1H, J = 4.0 Hz), 7.93 (dd, 1H, J = 7.96 Hz, 1.44 Hz), 7.19 (s, 1H), 7.08 (dd, 1H, J = 4.76 Hz, 3.2 Hz), 6.65 (s, 1H), 4.63 (d, 2H, J = 12.68 Hz), 3.42 (s, 2H), 3.01 (m, 3H), 2.80 (d, 2H, 7.08), 2.18 (m, 1H), 1.83 (d, 2H, J = 12.04 Hz), 1.25 (m, 9H). Found m/z = 354.2 $(M+H)^+$.

Supporting Tables

ID	Structure	SMILES
CP1	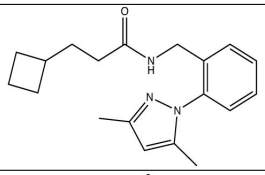	CC1=NN(C2=C(CNC(CCC3CCC3)=O)C=CC=C2)C(C)=C1
CP2	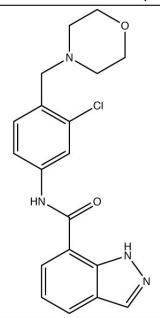	ClC1=C(CN2CCOCC2)C=CC(NC(C3=C4NN=CC4=CC=C3)=O)=C1
CP3	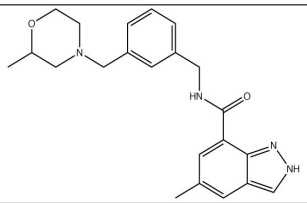	CC1CN(CCO1)CC2=CC(CNC(C3=CC(C)=CC4=CNN=C34)=O)=CC=C2
CP4	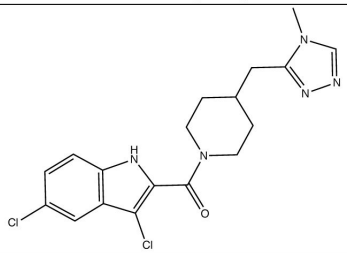	CN1C=NN=C1CC2CCN(C(C3=C(Cl)C4=C(C=CC(Cl)=C4)N3)=O)CC2
CP5	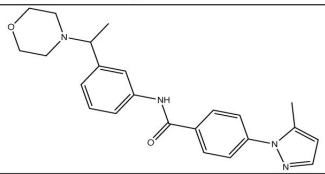	CC(C1=CC(NC(C2=CC=C(N3N=CC=C3C)C=C2)=O)=CC=C1)N4CCOCC4

CP6	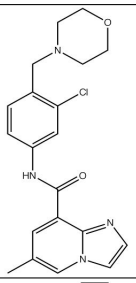	CC1=CN2C=CN=C2C(C(NC3=CC(Cl)=C(CN4CCOCC4)C=C3)=O)=C1
CP7	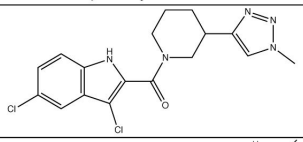	CN1C=C(C2CCCN(C(C3=C(Cl)C4=C(C=CC(Cl)=C4)N3)=O)C2)N=N1
CP8	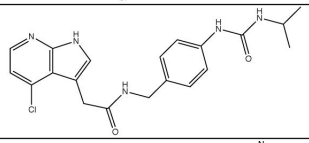	CC(NC(NC1=CC=C(CNC(CC2=CNC3=C2C(Cl)=CC=N3)=O)C=C1)=O)C
CP9	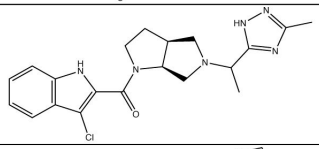	CC(C1=NC(C)=NN1)N2C[C@@H]3CCN(C(C4=C(Cl)C5=C(C=CC=C5)N4)=O)[C@@H]3C2
CP10	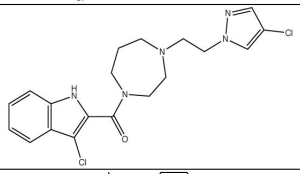	ClC1=CN(CCN2CCCN(C(C3=C(Cl)C4=C(C=CC=C4)N3)=O)CC2)N=C1
CP11	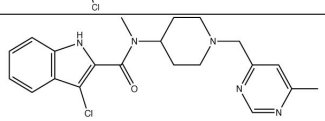	CN(C1CCN(CC=2C=C(C)N=CN2)CC1)C(=O)C=3NC=4C=CC=CC4C3Cl
CP12	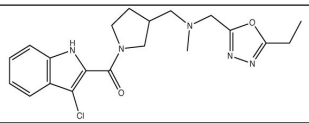	CCC1=NN=C(O1)CN(CC2CCN(C(C3=C(Cl)C4=C(C=CC=C4)N3)=O)C2)C
CP13	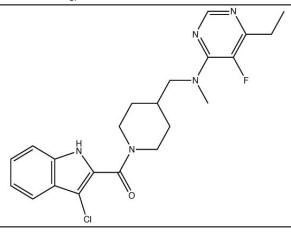	CCC1=C(F)C(N(CC2CCN(C(C3=C(Cl)C4=C(C=CC=C4)N3)=O)CC2)C)=NC=N1

CP14	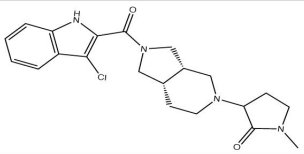	CN1CCC(C1=O)N2CC[C@@H]3CN(C(C4=C(Cl)C5=C(C=CC=C5)N4)=O)C[C@@H]3C2
CP15	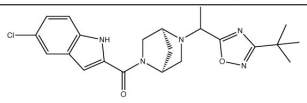	CC(C1=NC(C(C)(C)C)=NO1)N2C[C@@H]3C[C@H]2CN3C(C4=CC5=C(N4)C=CC(Cl)=C5)=O
CP16	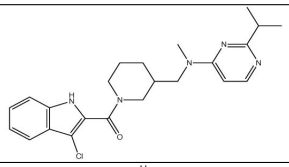	CC(C1=NC(N(CC2CCCN(C(C3=C(Cl)C4=C(C=CC=C4)N3)=O)C2)C)=CC=N1)C
CP17	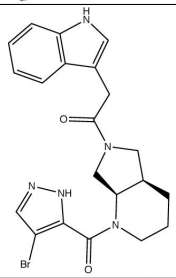	BrC1=C(C(N2CCC[C@@H]3CN(C(CC4=CNC5=C4C=CC=C5)=O)C[C@@H]32)=O)NN=C1
CP18	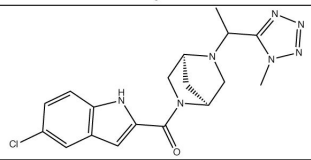	CC(C1=NN=NN1C)N2C[C@@H]3C[C@H]2CN3C(C4=CC5=C(N4)C=CC(Cl)=C5)=O

Table S1. **Structures of compounds included in initial screen (CP1 to CP18).**

ID	Structure	SMILES
CP4.1	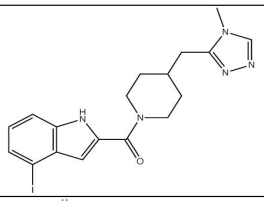	CN1C=NN=C1CC2CCN(C(C3=CC4=C(N3)C=CC=C4I)=O)CC2
CP4.2	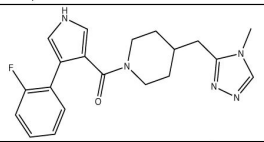	O=C(C1=CNC=C1C2=C(F)C=CC=C2)N(CC3)CCC3CC4=NN=CN4C
CP4.3	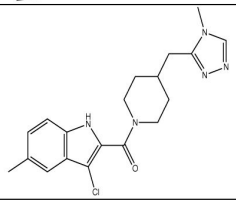	CC1=CC2=C(NC(C(N3CCC(CC3)CC4=NN=CN4C)=O)=C2Cl)C=C1
CP4.4	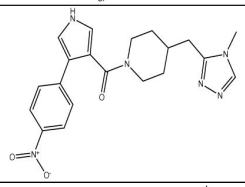	O=C(C1=CNC=C1C2=CC=C([N+]([O-])=O)C=C2)N(CC3)CCC3CC4=NN=CN4C
CP4.5	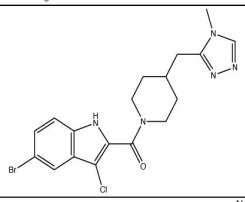	CN1C=NN=C1CC2CCN(C(C3=C(Cl)C4=C(C=CC(Br)=C4)N3)=O)CC2
CP4.6	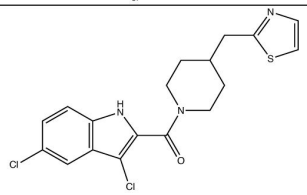	ClC1=C(C(N2CCC(CC2)CC3=NC=CS3)=O)NC4=C1C=C(Cl)C=C4

Table S2. Structures of CP4 derivatives included in second screen (CP4.1 to CP4.46).

CP4.7	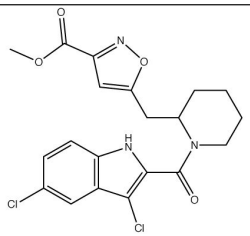	COC(C1=NOC(CC2CCCCN2C(C3=C(Cl)C4=C(C=CC(Cl)=C4)N3)=O)=C1)=O
CP4.8	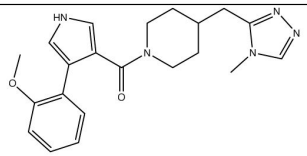	COC1=C(C2=CNC=C2C(N3CCC(CC3)CC4=NN=CN4C)=O)C=CC=C1
CP4.9	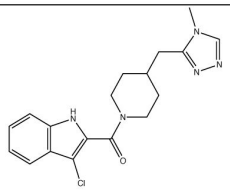	CN1C=NN=C1CC2CCN(C(C3=C(Cl)C4=C(C=CC=C4)N3)=O)CC2
CP4.10	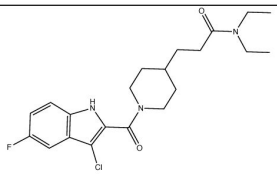	CCN(C(CCC1CCN(C(C2=C(Cl)C3=C(C=CC(F)=C3)N2)=O)CC1)=O)CC
CP4.11	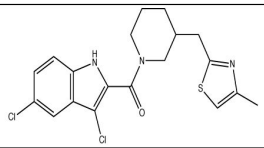	CC1=CSC(CC2CCCN(C(C3=C(Cl)C4=C(C=CC(Cl)=C4)N3)=O)C2)=N1
CP4.12	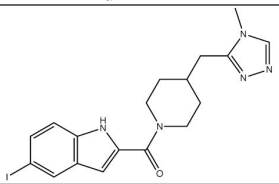	CN1C=NN=C1CC2CCN(C(C3=CC4=C(N3)C=CC(I)=C4)=O)CC2
CP4.13	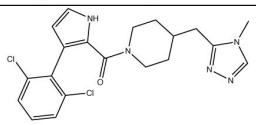	CN1C=NN=C1CC2CCN(CC2)C(C3=C(C=CN3)C4=C(C=CC=C4Cl)Cl)=O

Table S2. (continued)

CP4.14	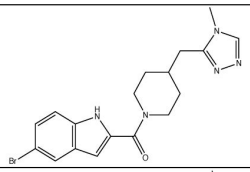	CN1C=NN=C1CC2CCN(C(C3=CC4=C(N3)C=CC(Br)=C4)=O)CC2
CP4.15	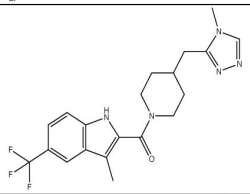	CC1=C(C(N2CCC(CC2)CC3=NN=CN3C)=O)NC4=C1C=C(C(F)(F)F)C=C4
CP4.16	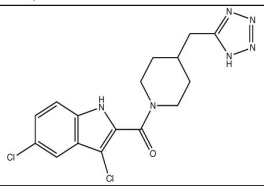	ClC1=C(C(N2CCC(CC2)CC3=NN=NN3)=O)NC4=C1C=C(Cl)C=C4
CP4.17	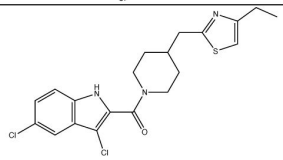	CCC1=CSC(CC2CCN(C(C3=C(Cl)C4=C(C=CC(Cl)=C4)N3)=O)CC2)=N1
CP4.18	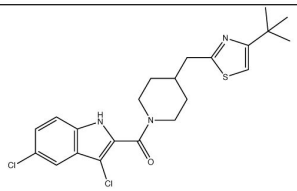	CC(C)(C1=CSC(CC2CCN(C(C3=C(Cl)C4=C(C=CC(Cl)=C4)N3)=O)CC2)=N1)C
CP4.19	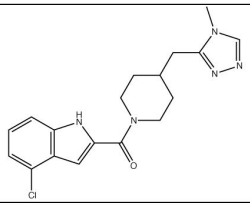	CN1C=NN=C1CC2CCN(C(C3=CC4=C(N3)C=CC=C4Cl)=O)CC2
CP4.20	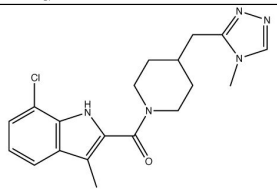	CC1=C(C(N2CCC(CC2)CC3=NN=CN3C)=O)NC4=C1C=CC=C4Cl
CP4.21	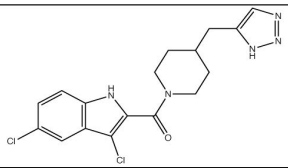	ClC1=C(C(N2CCC(CC2)CC3=CN=NN3)=O)NC4=C1C=C(Cl)C=C4

Table S2. (continued)

CP4.22	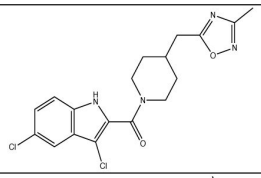	CC1=NOC(CC2CCN(C(C3=C(Cl)C4=C(C=CC(Cl)=C4)N3)=O)CC2)=N1
CP4.23	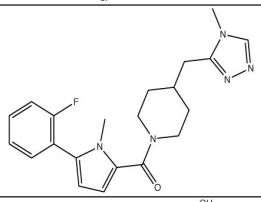	CN1C=NN=C1CC2CCN(C(C3=CC=C(N3C)C4=C(F)C=CC=C4)=O)CC2
CP4.24	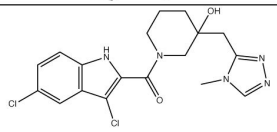	CN1C=NN=C1CC2(CCCN(C(C3=C(Cl)C4=C(C=CC(Cl)=C4)N3)=O)C2)O
CP4.25	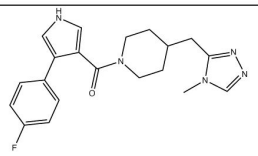	CN1C=NN=C1CC2CCN(C(C3=CNC=C3C4=CC=C(F)C=C4)=O)CC2
CP4.26	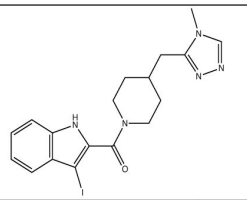	CN1C=NN=C1CC2CCN(C(C3=C(I)C4=C(C=CC=C4)N3)=O)CC2
CP4.27	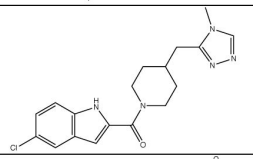	CN1C=NN=C1CC2CCN(C(C3=CC4=C(N3)C=CC(Cl)=C4)=O)CC2
CP4.28	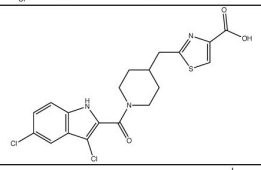	OC(C1=CSC(CC2CCN(C(C3=C(Cl)C4=C(C=CC(Cl)=C4)N3)=O)CC2)=N1)=O
CP4.29	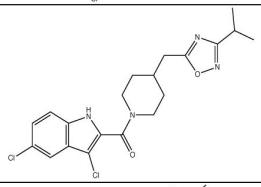	CC(C1=NOC(CC2CCN(C(C3=C(Cl)C4=C(C=CC(Cl)=C4)N3)=O)CC2)=N1)C
CP4.30	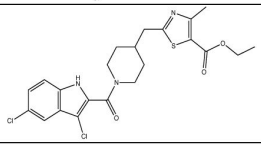	CCOC(C1=C(C)N=C(CC2CCN(C(C3=C(Cl)C4=C(C=CC(Cl)=C4)N3)=O)CC2)S1)=O

Table S2. (continued)

CP4.31	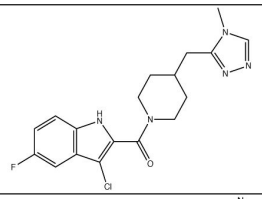	CN1C=NN=C1CC2CCN(C(C3=C(Cl)C4=C(C=CC(F)=C4)N3)=O)CC2
CP4.32	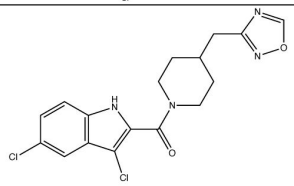	ClC1=C(C(N2CCC(CC2)CC3=NOC=N3)=O)NC4=C1C=C(Cl)C=C4
CP4.35	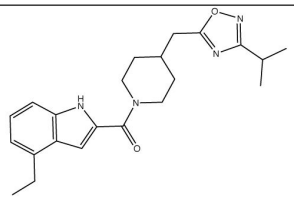	O=C(C(N1)=CC2=C1C=CC=C2CC)N3CCC(CC4=NC(C(C)C)=NO4)CC3
CP4.36	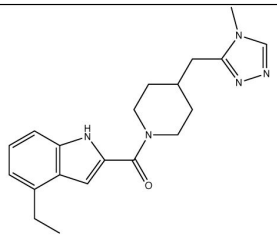	O=C(C(N1)=CC2=C1C=CC=C2CC)N3CCC(CC4=NN=CN4C)CC3
CP4.40	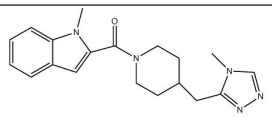	O=C(N1CCC(CC2=NN=CN2C)CC1)C3=CC4=CC=CC=C4N3C
CP4.41	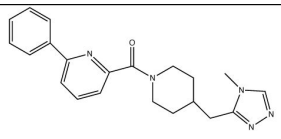	O=C(C1=NC(C2=CC=CC=C2)=CC=C1)N3CCC(CC4=NN=CN4C)CC3
CP4.42	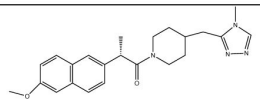	O=C(N1CCC(CC2=NN=CN2C)CC1)[C@@H](C)C3=CC4=C(C=C(OC)C=C4)C=C3

Table S2. (continued)

CP4.43	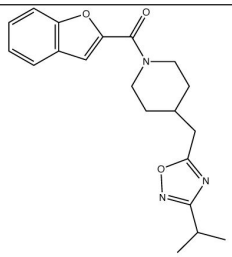	O=C(N1CCC(CC2=NC(C(C)C)=NO2)CC1)C(O3)=C C4=C3C=CC=C4
CP4.44	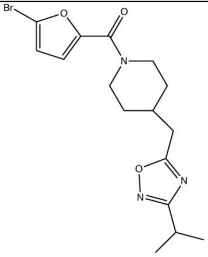	BrC1=CC=C(C(N2CCC(CC3=NC(C(C)C)=NO3)CC2) =O)O1
CP4.45	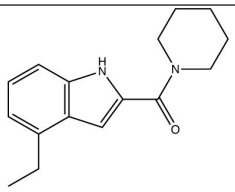	O=C(C(N1)=CC2=C1C=CC=C2CC)N3CCCCC3
CP4.46	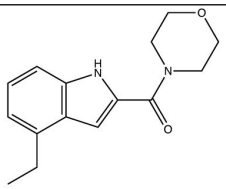	O=C(C(N1)=CC2=C1C=CC=C2CC)N3CCOCC3

Table S2. (continued)

ID	Structure	SMILES
CP4.29.1	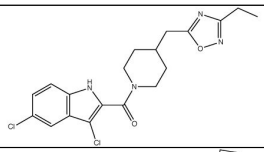	O=C(C1=C(Cl)C2=C(C=CC(Cl)=C2)N1)N(CC3)CCC3CC4=NC(CC)=NO4
CP4.29.3	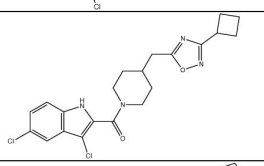	O=C(C1=C(Cl)C2=C(C=CC(Cl)=C2)N1)N(CC3)CCC3CC4=NC(C5CCC5)=NO4
CP4.29.4	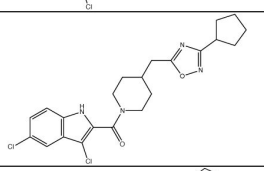	O=C(C1=C(Cl)C2=C(C=CC(Cl)=C2)N1)N(CC3)CCC3CC4=NC(C5CCCC5)=NO4
CP4.29.5	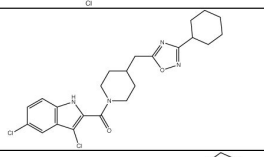	O=C(C1=C(Cl)C2=C(C=CC(Cl)=C2)N1)N(CC3)CCC3CC4=NC(C5CCCCC5)=NO4
CP4.29.6	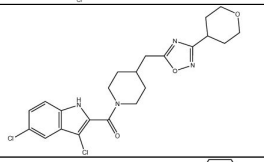	O=C(C1=C(Cl)C2=C(C=CC(Cl)=C2)N1)N(CC3)CCC3CC4=NC(C5CCOCC5)=NO4
CP4.29.9	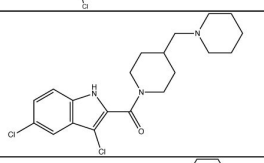	O=C(N1CCC(CN2CCCCC2)CC1)C3=C(Cl)C4=C(C=CC(Cl)=C4)N3
CP4.29.10	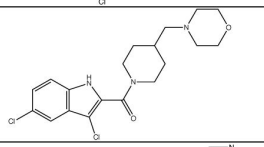	O=C(N1CCC(CC1)CN2CCOCC2)C3=C(Cl)C4=C(C=CC(Cl)=C4)N3
CP4.29.11	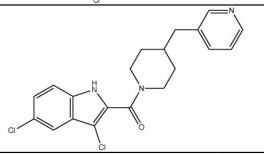	O=C(N1CCC(CC2=CC=CN=C2)CC1)C3=C(Cl)C4=C(C=CC(Cl)=C4)N3
CP4.29.12	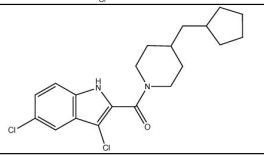	O=C(N1CCC(CC2CCCC2)CC1)C3=C(Cl)C4=C(C=CC(Cl)=C4)N3

Table S3. Structures of CP4.29 derivatives included in third screen (CP4.29.1 to CP4.29.22).

CP4.29.13	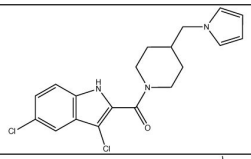	O=C(N(CC1)CCC1CN2C=CC=C2)C3=C(Cl)C4=C(C=CC(Cl)=C4)N3
CP4.29.14	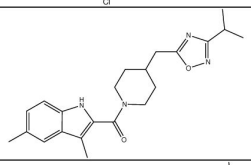	O=C(N1CCC(CC2=NC(C(C)C)=NO2)CC1)C3=C(C)C4=CC(C)=CC=C4N3
CP4.29.16	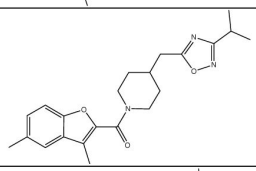	O=C(N1CCC(CC2=NC(C(C)C)=NO2)CC1)C3=C(C)C4=CC(C)=CC=C4O3
CP4.29.17	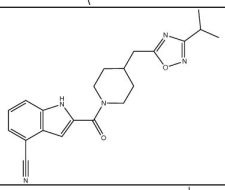	O=C(N1CCC(CC2=NC(C(C)C)=NO2)CC1)C3=CC4=C(C=CC=C4C#N)N3
CP4.29.18	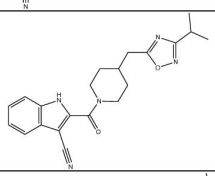	N#CC1=C(C(N2CCC(CC3=NC(C(C)C)=NO3)CC2)=O)NC4=C1C=CC=C4
CP4.29.19	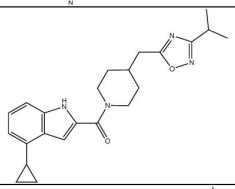	O=C(N1CCC(CC2=NC(C(C)C)=NO2)CC1)C3=CC4=C(C=CC=C4C5CC5)N3
CP4.29.20	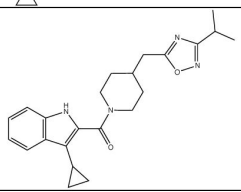	O=C(N1CCC(CC2=NC(C(C)C)=NO2)CC1)C(NC3=C4C=CC=C3)=C4C5CC5
CP4.29.21	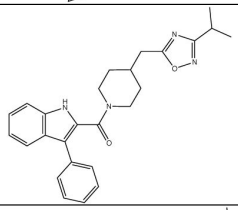	O=C(N1CCC(CC2=NC(C(C)C)=NO2)CC1)C3=C(C4=CC=CC=C4)C(C=CC=C5)=C5N3
CP4.29.22	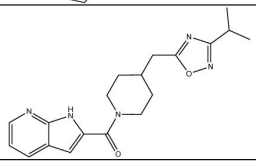	O=C(N1CCC(CC2=NC(C(C)C)=NO2)CC1)C3=CC4=CC=CN=C4N3

Table S3. (continued)

Supporting Figures

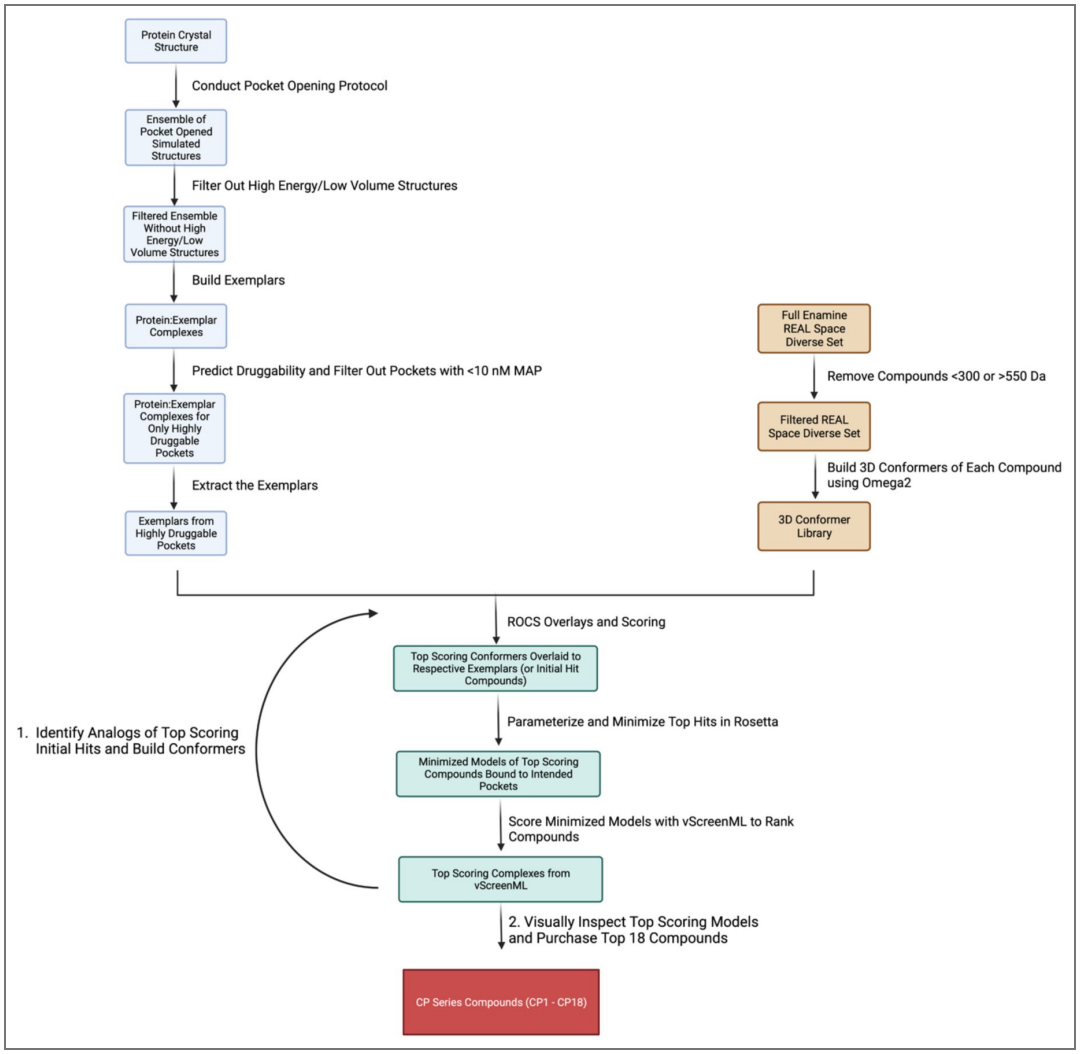

Figure S1. **Summary of computational workflow used to identify initial hit compounds CP1 to CP18.**

Figure S2. ^{1}H NMR of CP4 in DMSO-d6 at 295K obtained on Bruker 600 MHz NMR.

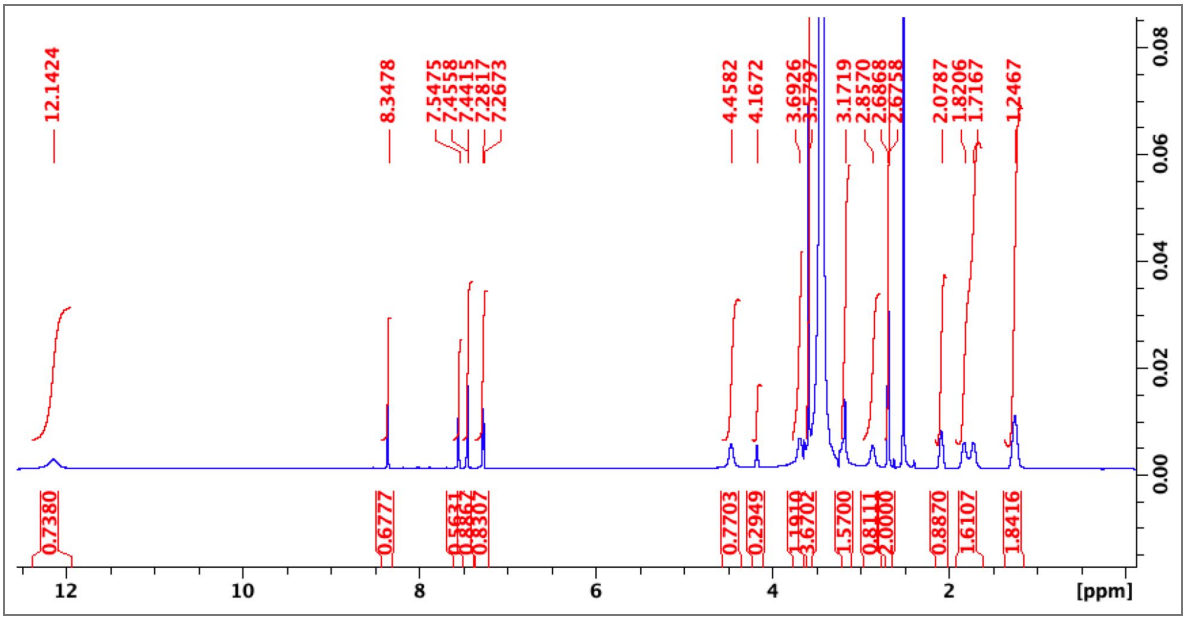

Figure S3. ^{13}C NMR of CP4 in DMSO-d6 at 295K obtained on Bruker 600 MHz NMR.

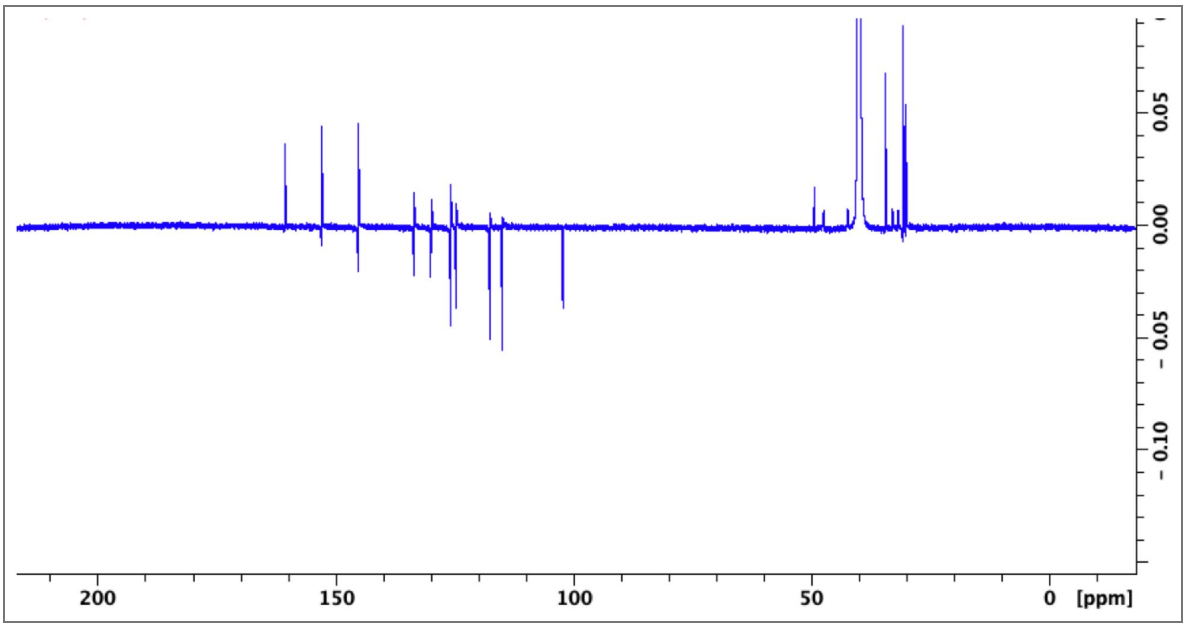

Figure S4. ^{1}H NMR with water suppression (ZGESGP) of 100 µM CP4 (*blue*), 100 µM sitagliptin (*red*), or 100 µM VH298 (*green*) in 50 mM sodium phosphate buffer, 10% D_2O, pH=6.95, 1% DMSO-d6.

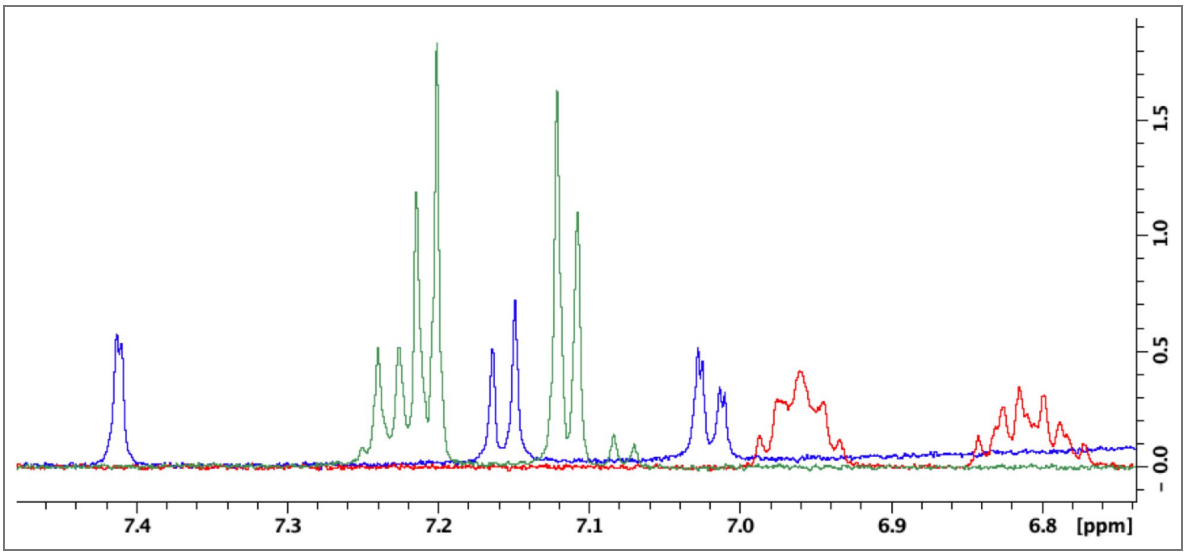

Figure S5. Full STD NMR spectrum for 100 µM CP4 / 100 µM Sitagliptin / 100 µM VH298 / 1% DMSO-d6 in the absence (*blue*) and presence (*red*) of 7.7 µM VCB protein complex.

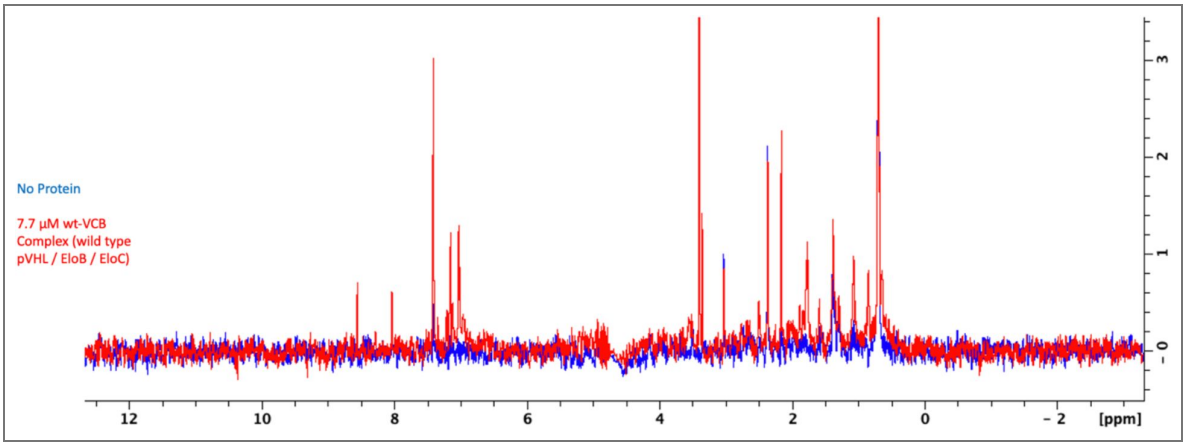

Figure S6. Full WaterLOGSY NMR spectrum for 100 µM CP4 / 100 µM Sitagliptin / 100 µM VH298 / 1% DMSO-d6 in the absence (*blue*) and presence (*red*) of 7.7 µM VCB protein complex.

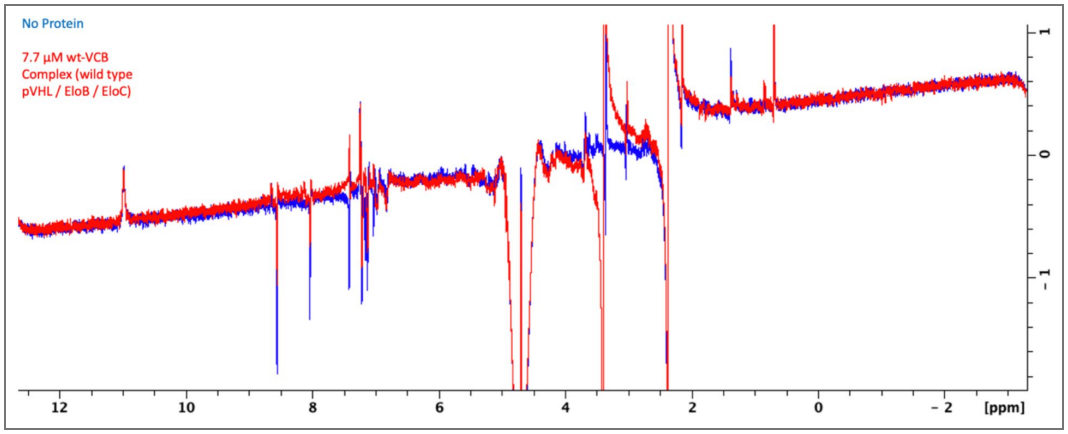

Figure S7. **Full CPMG NMR spectrum for 100 µM CP4 / 100 µM Sitagliptin / 100 µM VH298 / 1% DMSO-d6 in the absence (*blue*) and presence (*red*) of 7.7 µM VCB protein complex.**

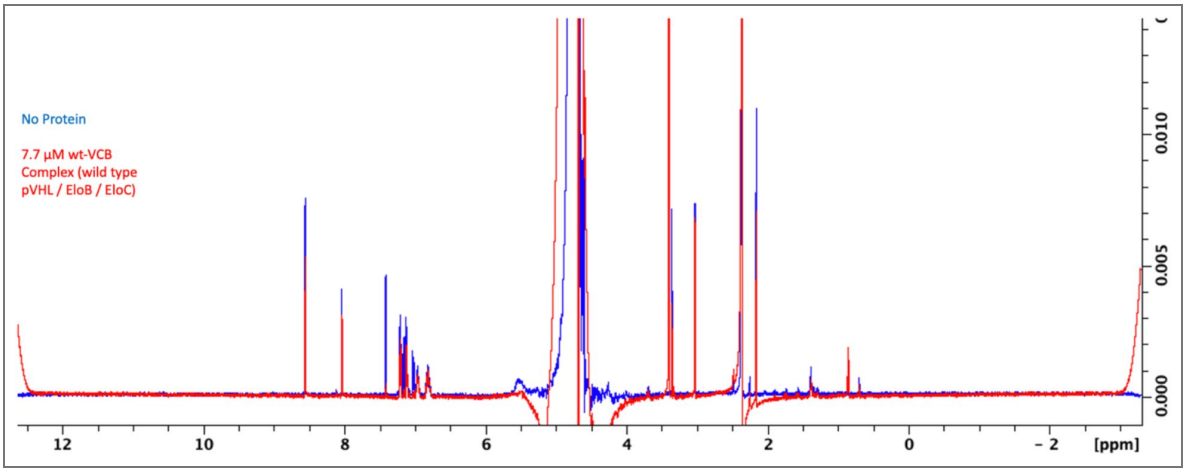

Figure S8. **Full STD NMR spectrum for 100 µM CP4 / 100 µM Sitagliptin / 100 µM VH298 / 1% DMSO-d6 in the presence of 7.7 µM WT VCB protein complex (*red*) or 7.7 µM $V_{D197K}CB$ (*green*).**

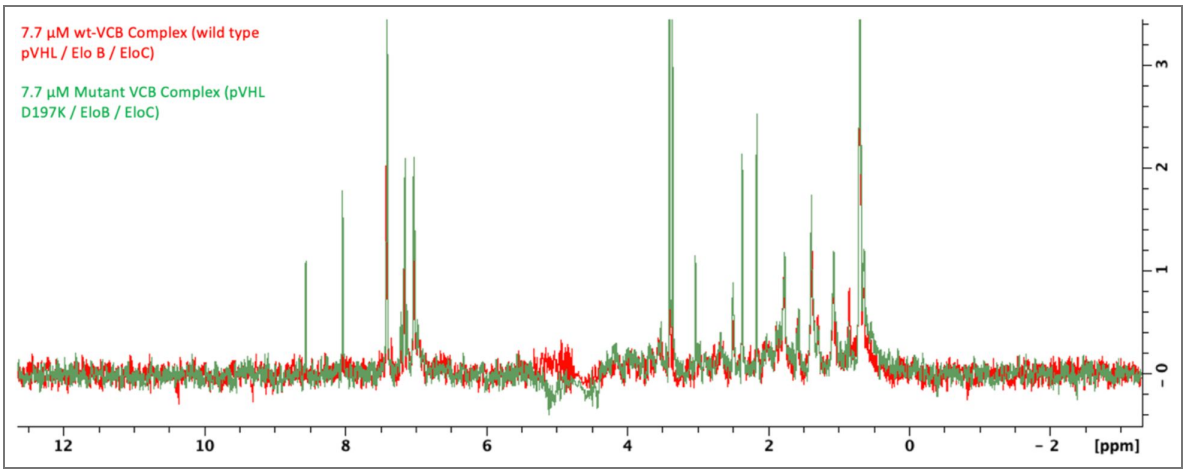

Figure S9. **Full WaterLOGSY NMR spectrum for 100 µM CP4 / 100 µM Sitagliptin / 100 µM VH298 / 1% DMSO-d6 in the presence of 7.7 µM WT VCB protein complex (*red*) or 7.7 µM $V_{D197K}CB$ (*green*).**

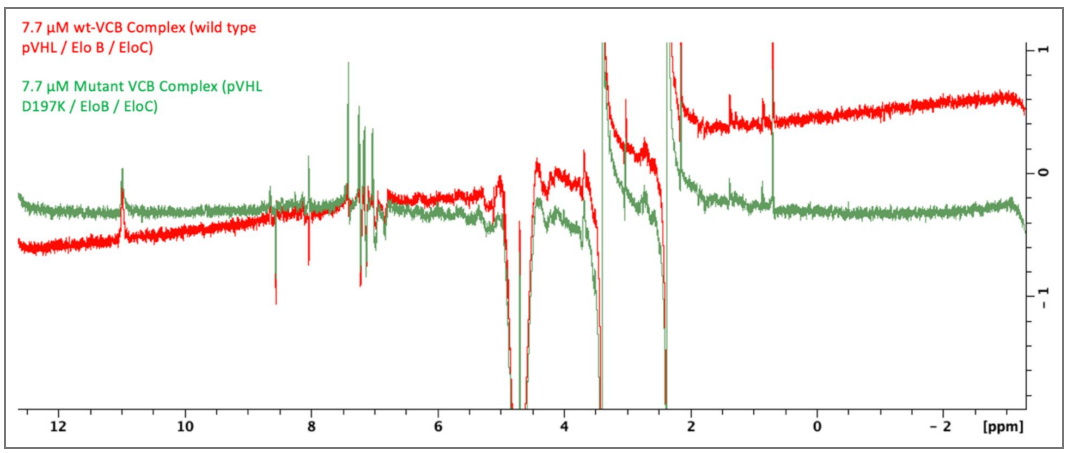

Figure S10. **Full CPMG NMR spectrum for 100 µM CP4 / 100 µM Sitagliptin / 100 µM VH298 / 1% DMSO-d6 in the presence of 7.7 µM WT VCB protein complex (*red*) or 7.7 µM $V_{D197K}CB$ (*green*).**

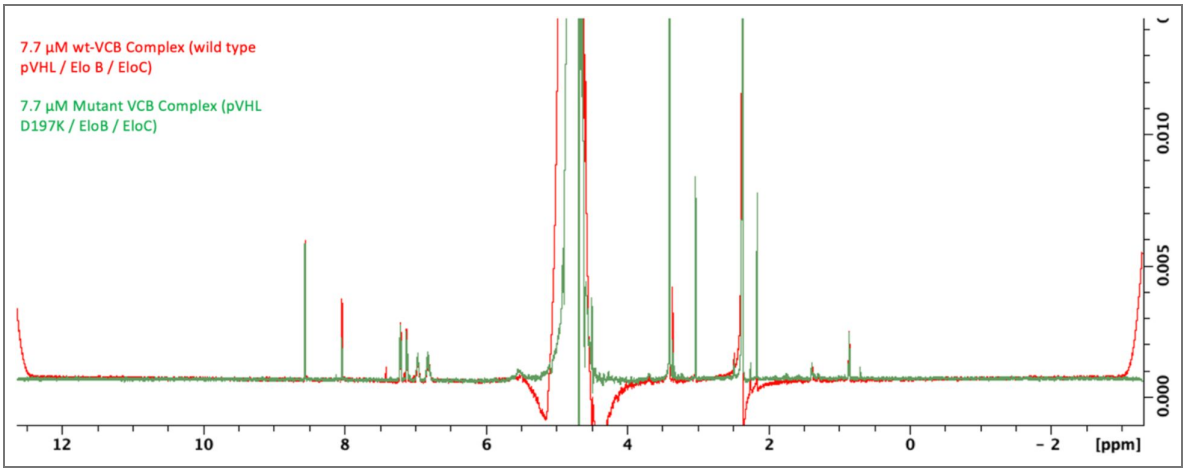

Figure S11. **Treatment with CP4.29 (but not CP4) led to depletion of HIF-1α in RCC4, RCC-MF, and 769-P cells.**

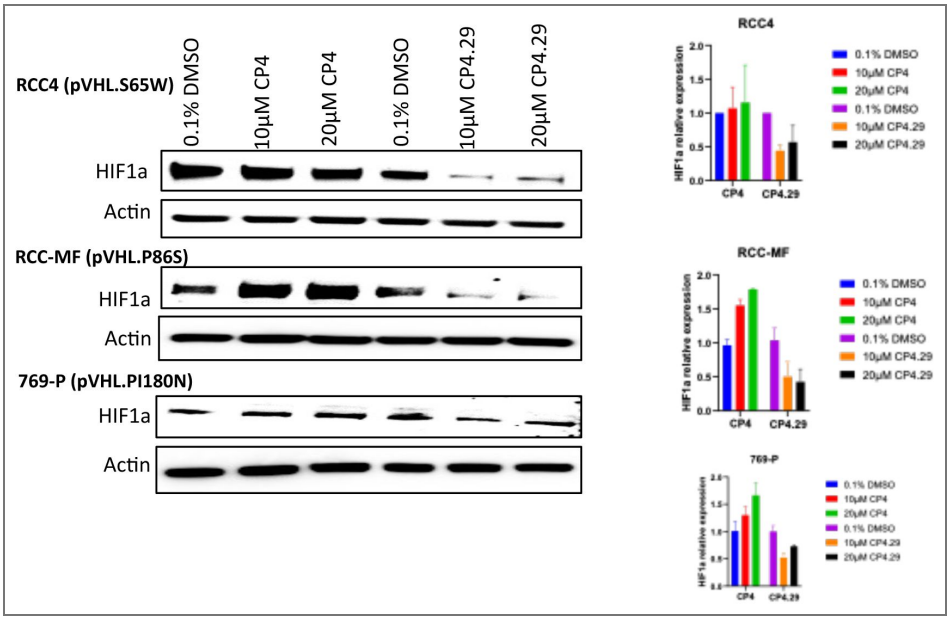

Figure S12. In RCC4 cells, (A) treatment with CP4.29 reduced the cellular abundance of HIF-2α.

However, the activity of CP4.29 on HIF-2α could be reversed by co-treatment with either **(B)** proteasome inhibitor MG132, **(C)** VHL inhibitor VH298, or **(D)** neddylation inhibitor MLN4924.

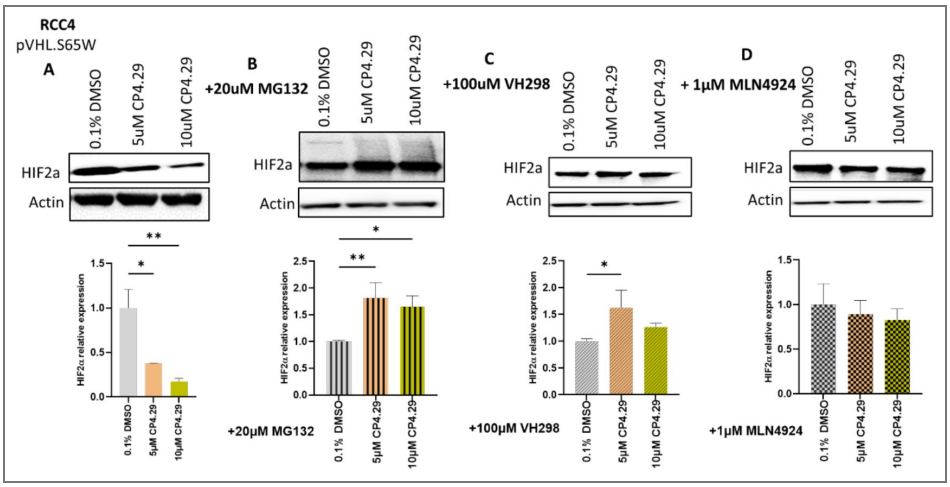

Figure S13. In RCC4 cells, (A) treatment with CP4.29 reduced the cellular abundance of Aurora A.

However, the activity of CP4.29 on Aurora A could be reversed by co-treatment with **(B)** proteasome inhibitor MG132, or **(C)** VHL inhibitor VH298.

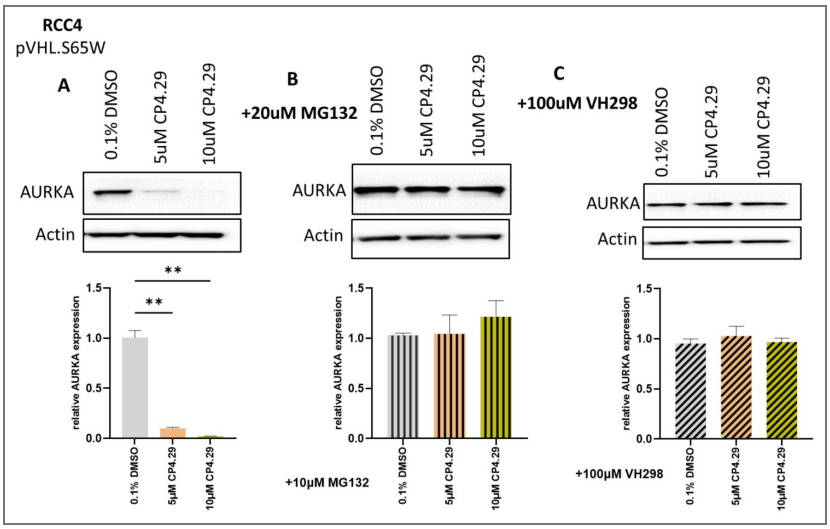

Figure S14. Parental cell lines RCC-MF, RCC4, and 769-P were each transfected with plasmids of pLenti-Cas9-GFP and were either provided with control sg-RNA or with sg-RNA for *VHL*.

The loss of pVHL expression each *VHL* KO cell line was confirmed by Western blot.

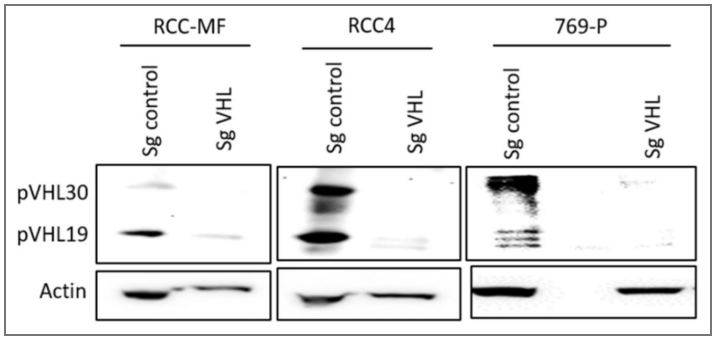

Figure S15. Immunoprecipitation (under non-denaturing conditions) of HIF-2α (*left*), AURKA (*middle*), or ZHX2 (*right*) followed by Western blot analysis for Ub-1.

769-P cells (or isogenic 769-P *VHL* KO cells) were treated with 20 μM proteasome inhibitor MG132, and with 10 μM CP4.29 for 2 hours in the HIF-2α experiment or for 24 hours in the AURKA and ZHX2 experiments.

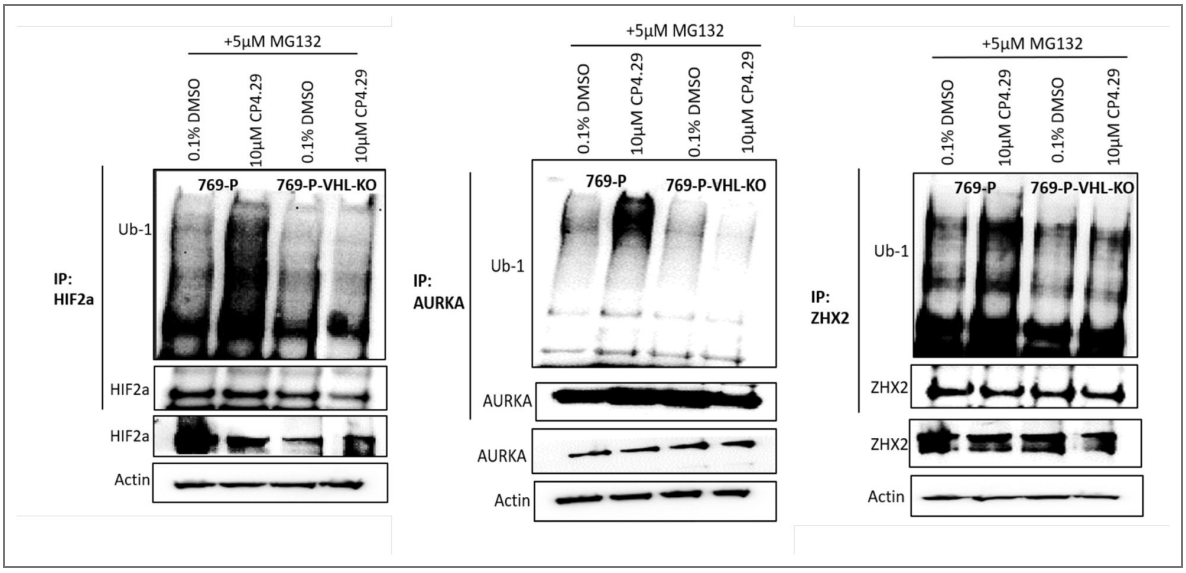

Figure S16. First-tier ADME characterization of CP4.29 indicates that further optimization is warranted prior to advancement into *in vivo* studies.

Alias	Solubility	Mouse Microsome Stability			Human Microsome Stability			Mouse plasma protein binding		Mouse liver microsome partitioning		hCYP 3A4	hCYP2D6	hCYP2C9
	PBS (7.4)	t1/2	Clint	w/o NADPH	t1/2	Clint	w/o NADPH	Bound	Stable 20 hrs 37 C	Bound	Stable 20 hrs 37 C	IC50	IC50	IC50
	uM	min	uL/min/mg	% Stable	min	uL/min/mg	% Stable	%	%	%	%	nM	nM	nM
CP4.29	2.5	15.6	88.6	78	26.7	51.9	89	99.1	107	97.9	131	2880	> 10000	> 10000

Figure S17. ^{1}H NMR of CP4.29 in DMSO-d6 at 295K obtained on Bruker 600 MHz NMR.

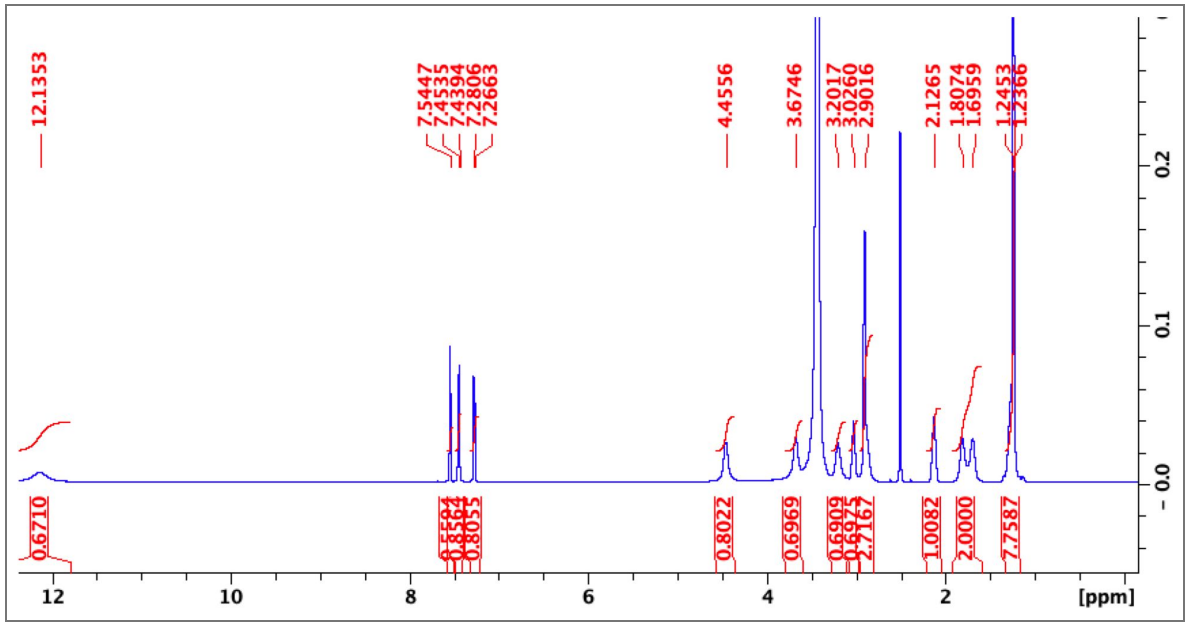

Figure S18. ^{13}C NMR of CP4.29 in DMSO-d6 at 295K obtained on Bruker 600 MHz NMR.

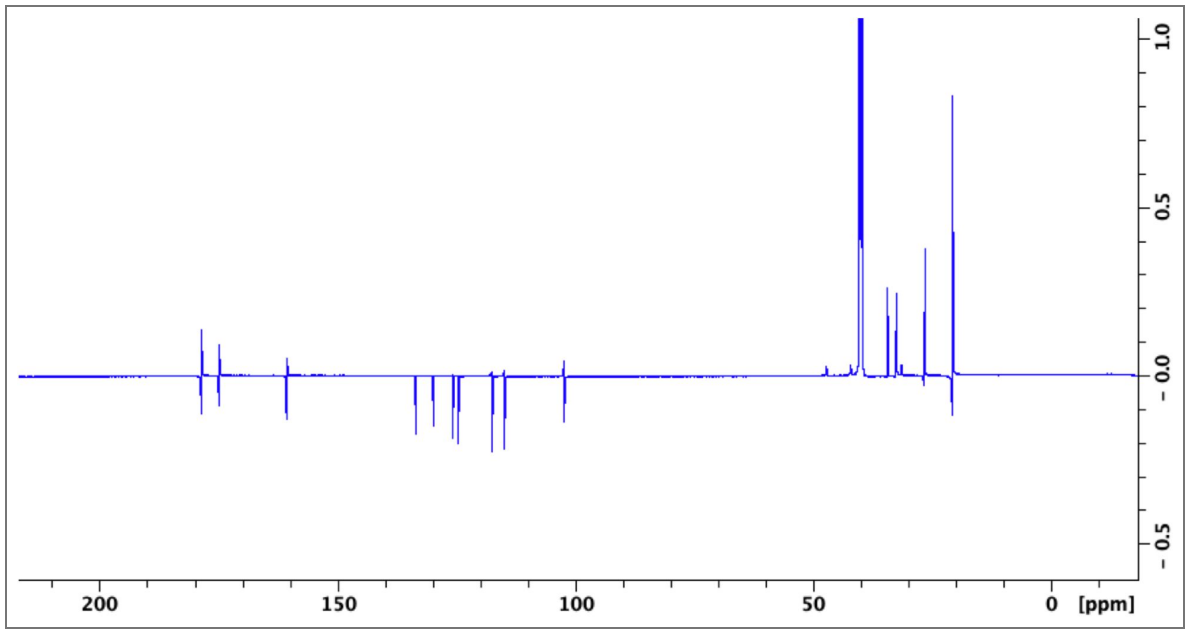

Acknowledgements

This work made use of Fox Chase Cancer Center's CCSG shared resources, specifically the Cell Culture Facility (CCF), Cell Sorting Facility (CSF), Genomics Facility (GF), and Spectroscopy Facility.

This work was supported by grants from DOD (W81XWH-20-1-0844) and the NIH National Institute of General Medical Sciences (R01GM112736, R01GM141513). This research was also funded in part through the NIH/NCI Cancer Center Support Grant P30CA006927, TUFCCC/HC Regional Comprehensive Cancer Health Disparities Partnership U54CA221705, and through Fox Chase / Moulder Center Pilot Funds.

This work used the Extreme Science and Engineering Discovery Environment (XSEDE) allocation MCB130049, which is supported by National Science Foundation grant number 1548562. This work also used computational resources through allocation MCB130049 from the Advanced Cyberinfrastructure Coordination Ecosystem: Services & Support (ACCESS) program, which is supported by National Science Foundation grants 2138259, 2138286, 2138307, 2137603, and 2138296.

Additional information

Funding

Funder	Grant reference number	Author
DOD | MHS | CDMRP | DOD Peer Reviewed Cancer Research Program (PRCRP)	W81XWH-20-1-0844	John Karanicolas
HHS | NIH | National Institute of General Medical Sciences (NIGMS)	R01GM112736	John Karanicolas
HHS | NIH | National Cancer Institute (NCI)	P30CA006927	John Karanicolas
HHS | NIH | National Cancer Institute (NCI)	U54CA221705	John Karanicolas
National Science Foundation (NSF)	1548562	John Karanicolas
HHS | NIH | National Institute of General Medical Sciences (NIGMS)	R01GM141513	John Karanicolas

Author ORCID iDs

John Karanicolas: https://orcid.org/0000-0003-0300-726X

References

1. **Chernoff J** (2021) The two-hit theory hits 50. *Mol Biol Cell* **32**:rt1 https://doi.org/10.1091/mbc.e21-08-0407 | PubMed
2. **Lipsick J** (2020) A History of Cancer Research: Tumor Suppressor Genes. *Cold Spring Harb Perspect Biol* **12** https://doi.org/10.1101/cshperspect.a035907 | PubMed
3. **Knudson AG Jr** (1971) Mutation and cancer: statistical study of retinoblastoma. *Proc Natl Acad Sci U S A* **68**:820-3 https://doi.org/10.1073/pnas.68.4.820 | PubMed
4. **Maher ER,** Yates JR, Ferguson-Smith MA (1990) Statistical analysis of the two stage mutation model in von Hippel-Lindau disease, and in sporadic cerebellar haemangioblastoma and renal cell carcinoma. *J Med Genet* **27**:311-4 https://doi.org/10.1136/jmg.27.5.311 | PubMed
5. **Latif F,** Tory K, Gnarra J, Yao M, Duh FM, Orcutt ML, Stackhouse T, Kuzmin I, Modi W, Geil L, *et al.* (1993) Identification of the von Hippel-Lindau disease tumor suppressor gene. *Science* **260**:1317-20 https://doi.org/10.1126/science.8493574 | PubMed
6. **Kaelin WG Jr** (2007) The von Hippel-Lindau tumor suppressor protein and clear cell renal carcinoma. *Clin Cancer Res* **13**:680s-4s https://doi.org/10.1158/1078-0432.ccr-06-1865 | PubMed

7. **Gossage L,** Eisen T, Maher ER (2015) VHL, the story of a tumour suppressor gene. *Nat Rev Cancer* **15**:55-64 https://doi.org/10.1038/nrc3844 | PubMed

8. **Lai Y,** Song M, Hakala K, Weintraub ST, Shiio Y (2011) Proteomic dissection of the von Hippel-Lindau (VHL) interactome. *J Proteome Res* **10**:5175-82 https://doi.org/10.1021/pr200642c | PubMed

9. **Frew IJ,** Krek W (2008) pVHL: a multipurpose adaptor protein. *Sci Signal* **1**:e30 https://doi.org/10.1126/scisignal.124pe30 | PubMed

10. **Iwai K,** Yamanaka K, Kamura T, Minato N, Conaway RC, Conaway JW, Klausner RD, Pause A (1999) Identification of the von Hippel-Lindau tumor-suppressor protein as part of an active E3 ubiquitin ligase complex. *Proc Natl Acad Sci U S A* **96**:12436-41 https://doi.org/10.1073/pnas.96.22.12436 | PubMed

11. **Jaakkola P,** Mole DR, Tian Y-m, Wilson MI, Gielbert J, Gaskell SJ, Kriegsheim AV, Hebestreit HF, Mukherji M, Schofield CJ, *et al.* (2001) Targeting of HIF-α to the von Hippel-Lindau Ubiquitylation Complex by O2-Regulated Prolyl Hydroxylation. *Science* **292**:468-72 https://doi.org/10.1126/science.1059796 | PubMed

12. **Ivan M,** Kondo K, Yang H, Kim W, Valiando J, Ohh M, Salic A, Asara JM, Lane WS, Kaelin WG (2001) HIFalpha targeted for VHL-mediated destruction by proline hydroxylation: implications for O2 sensing. *Science* **292**:464-8 https://doi.org/10.1126/science.1059817 | PubMed

13. **Lisztwan J,** Imbert G, Wirbelauer C, Gstaiger M, Krek W (1999) The von Hippel-Lindau tumor suppressor protein is a component of an E3 ubiquitin-protein ligase activity. *Genes Dev* **13**:1822-33 https://doi.org/10.1101/gad.13.14.1822 | PubMed

14. **Schofield CJ,** Ratcliffe PJ (2004) Oxygen sensing by HIF hydroxylases. *Nat Rev Mol Cell Biol* **5**:343-54 https://doi.org/10.1038/nrm1366 | PubMed

15. **Zhang J,** Wu T, Simon J, Takada M, Saito R, Fan C, Liu XD, Jonasch E, Xie L, Chen X, *et al.* (2018) VHL substrate transcription factor ZHX2 as an oncogenic driver in clear cell renal cell carcinoma. *Science* **361**:290-5 https://doi.org/10.1126/science.aap8411 | PubMed

16. **Xue J,** Lv DD, Jiao S, Zhao W, Li X, Sun H, Yan B, Fan L, Hu RG, Fang J (2012) pVHL mediates K63-linked ubiquitination of nCLU. *PLoS One* **7**:e35848 https://doi.org/10.1371/journal.pone.0035848 | PubMed

17. **Wang Y,** Zhao W, Gao Q, Fan L, Qin Y, Zhou H, Li M, Fang J (2016) pVHL mediates K63-linked ubiquitination of IKKbeta, leading to IKKbeta inactivation. *Cancer Lett* **383**:1-8 https://doi.org/10.1016/j.canlet.2016.09.009 | PubMed

18. **Hasanov E,** Chen G, Chowdhury P, Weldon J, Ding Z, Jonasch E, Sen S, Walker CL, Dere R (2017) Ubiquitination and regulation of AURKA identifies a hypoxia-independent E3 ligase activity of VHL. *Oncogene* **36**:3450-63 https://doi.org/10.1038/onc.2016.495 | PubMed

19. **Kuznetsova AV,** Meller J, Schnell PO, Nash JA, Ignacak ML, Sanchez Y, Conaway JW, Conaway RC, Czyzyk-Krzeska MF (2003) von Hippel-Lindau protein binds hyperphosphorylated large subunit of RNA polymerase II through a proline hydroxylation motif and targets it for ubiquitination. *Proc Natl Acad Sci U S A* **100**:2706-11 https://doi.org/10.1073/pnas.0436037100 | PubMed

20. **Mikhaylova O,** Ignacak ML, Barankiewicz TJ, Harbaugh SV, Yi Y, Maxwell PH, Schneider M, Van Geyte K, Carmeliet P, Revelo MP, *et al.* (2008) The von Hippel-Lindau tumor suppressor protein and Egl-9-Type proline hydroxylases regulate the large subunit of RNA polymerase II in response to oxidative stress. *Mol Cell Biol* **28**:2701-17 https://doi.org/10.1128/mcb.01231-07 | PubMed

21. **Okuda H,** Saitoh K, Hirai S, Iwai K, Takaki Y, Baba M, Minato N, Ohno S, Shuin T (2001) The von Hippel-Lindau tumor suppressor protein mediates ubiquitination of activated atypical protein kinase C. *J Biol Chem* **276**:43611-7 https://doi.org/10.1074/jbc.m107880200 | PubMed

22. **Grosfeld A,** Stolze IP, Cockman ME, Pugh CW, Edelmann M, Kessler B, Bullock AN, Ratcliffe PJ, Masson N (2007) Interaction of hydroxylated collagen IV with the von hippel-lindau tumor suppressor. *J Biol Chem* **282**:13264-9 https://doi.org/10.1074/jbc.m611648200 | PubMed

23. **Kurban G,** Duplan E, Ramlal N, Hudon V, Sado Y, Ninomiya Y, Pause A (2008) Collagen matrix assembly is driven by the interaction of von Hippel-Lindau tumor suppressor protein with hydroxylated collagen IV alpha 2. *Oncogene* **27**:1004-12 https://doi.org/10.1038/sj.onc.1210709 | PubMed

24. **Bluyssen HA,** Lolkema MP, van Beest M, Boone M, Snijckers CM, Los M, Gebbink MF, Braam B, Holstege FC, Giles RH, *et al.* (2004) Fibronectin is a hypoxia-independent target of the tumor suppressor VHL. *FEBS Lett* **556**:137-42 https://doi.org/10.1016/s0014-5793(03)01392-9 | PubMed

25. **Motzer RJ,** Michaelson MD, Redman BG, Hudes GR, Wilding G, Figlin RA, Ginsberg MS, Kim ST, Baum CM, DePrimo SE, *et al.* (2006) Activity of SU11248, a multitargeted inhibitor of vascular endothelial growth factor receptor and platelet-derived growth factor receptor, in patients with metastatic renal cell carcinoma. *J Clin Oncol* **24**:16-24 https://doi.org/10.1200/jco.2005.02.2574 | PubMed

26. **Jonasch E,** McCutcheon IE, Waguespack SG, Wen S, Davis DW, Smith LA, Tannir NM, Gombos DS, Fuller GN, Matin SF (2011) Pilot trial of sunitinib therapy in patients with von Hippel-Lindau disease. *Ann Oncol* **22**:2661-6 https://doi.org/10.1093/annonc/mdr011 | PubMed

27. **Jonasch E,** McCutcheon IE, Gombos DS, Ahrar K, Perrier ND, Liu D, Robichaux CC, Villarreal MF, Weldon JA, Woodson AH, *et al.* (2018) Pazopanib in patients with von Hippel-Lindau disease: a single-arm, single-centre, phase 2 trial. *Lancet Oncol* **19**:1351-9 https://doi.org/10.1016/s1470-2045(18)30487-x | PubMed

28. **Jonasch E,** Donskov F, Iliopoulos O, Rathmell WK, Narayan VK, Maughan BL, Oudard S, Else T, Maranchie JK, Welsh SJ, *et al.* (2021) Belzutifan for Renal Cell Carcinoma in von Hippel-Lindau Disease. *N Engl J Med* **385**:2036-46 https://doi.org/10.1056/nejmoa2103425 | PubMed

29. **Fallah J,** Brave MH, Weinstock C, Mehta GU, Bradford D, Gittleman H, Bloomquist EW, Charlab R, Hamed SS, Miller CP, *et al.* (2022) FDA Approval Summary: Belzutifan for von Hippel-Lindau Disease-Associated Tumors. *Clin Cancer Res* **28**:4843-8 https://doi.org/10.1158/1078-0432.ccr-22-1054 | PubMed

30. **Anonymous** (2023) Expanding "Practice-Changing" Belzutifan's Reach in RCC. *Cancer Discov* **13**:OF5 https://doi.org/10.1158/2159-8290.CD-NB2023-0080 | PubMed

31. **Choueiri TK,** Bauer TM, Papadopoulos KP, Plimack ER, Merchan JR, McDermott DF, Michaelson MD, Appleman LJ, Thamake S, Perini RF, *et al.* (2021) Inhibition of hypoxia-inducible factor-2alpha in renal cell carcinoma with belzutifan: a phase 1 trial and biomarker analysis. *Nat Med* **27**:802-5 https://doi.org/10.1038/s41591-021-01324-7 | PubMed

32. **Shmueli MD,** Levy-Kanfo L, Haj E, Schoenfeld AR, Gazit E, Segal D (2019) Arginine refolds, stabilizes, and restores function of mutant pVHL proteins in animal model of the VHL cancer syndrome. *Oncogene* **38**:1038-49 https://doi.org/10.1038/s41388-018-0491-x | PubMed

33. **Frew IJ,** Moch H (2015) A clearer view of the molecular complexity of clear cell renal cell carcinoma. *Annu Rev Pathol* **10**:263-89 https://doi.org/10.1146/annurev-pathol-012414-040306 | PubMed

34. **Xiao Y,** Thakkar KN, Zhao H, Broughton J, Li Y, Seoane JA, Diep AN, Metzner TJ, von Eyben R, Dill DL, *et al.* (2020) The m(6)A RNA demethylase FTO is a HIF-independent synthetic lethal partner with the VHL tumor suppressor. *Proc Natl Acad Sci U S A* **117**:21441-9 https://doi.org/10.1073/pnas.2000516117 | PubMed

35. **Bakouny Z,** Barbie DA (2020) TBK1 Activation by VHL Loss in Renal Cell Carcinoma: A Novel HIF-Independent Vulnerability. *Cancer Discov* **10**:348-50 https://doi.org/10.1158/2159-8290.cd-19-1525 | PubMed

36. **Nicholson HE,** Tariq Z, Housden BE, Jennings RB, Stransky LA, Perrimon N, Signoretti S, Kaelin WG (2019) HIF-independent synthetic lethality between CDK4/6 inhibition and VHL loss across species. *Sci Signal* **12** https://doi.org/10.1126/scisignal.aay0482 | PubMed

37. **Ding Z,** German P, Bai S, Feng Z, Gao M, Si W, Sobieski MM, Stephan CC, Mills GB, Jonasch E (2012) Agents that stabilize mutated von Hippel-Lindau (VHL) protein: results of a high-throughput screen to identify compounds that modulate VHL proteostasis. *J Biomol Screen* **17**:572-80 https://doi.org/10.1177/1087057112436557 | PubMed

38. **Yang C,** Huntoon K, Ksendzovsky A, Zhuang Z, Lonser RR (2013) Proteostasis modulators prolong missense VHL protein activity and halt tumor progression. *Cell Rep* **3**:52-9 https://doi.org/10.1016/j.celrep.2012.12.007 | PubMed

39. **Sato Y,** Yoshizato T, Shiraishi Y, Maekawa S, Okuno Y, Kamura T, Shimamura T, Sato-Otsubo A, Nagae G, Suzuki H, *et al.* (2013) Integrated molecular analysis of clear-cell renal cell carcinoma. *Nat Genet* **45**:860-7 https://doi.org/10.1038/ng.2699 | PubMed

40. **Tate JG,** Bamford S, Jubb HC, Sondka Z, Beare DM, Bindal N, Boutselakis H, Cole CG, Creatore C, Dawson E, *et al.* (2019) COSMIC: the Catalogue Of Somatic Mutations In Cancer. *Nucleic Acids Res* **47**:D941-D7 https://doi.org/10.1093/nar/gky1015 | PubMed

41. **Min JH,** Yang H, Ivan M, Gertler F, Kaelin WG, Pavletich NP (2002) Structure of an HIF-1alpha - pVHL complex: hydroxyproline recognition in signaling. *Science* **296**:1886-9 https://doi.org/10.1126/science.1073440 | PubMed

42. **Hon WC,** Wilson MI, Harlos K, Claridge TD, Schofield CJ, Pugh CW, Maxwell PH, Ratcliffe PJ, Stuart DI, Jones EY (2002) Structural basis for the recognition of hydroxyproline in HIF-1 alpha by pVHL. *Nature* **417**:975-8 https://doi.org/10.1038/nature00767 | PubMed

43. **Sutovsky H,** Gazit E (2004) The von Hippel-Lindau tumor suppressor protein is a molten globule under native conditions: implications for its physiological activities. *J Biol Chem* **279**:17190-6 https://doi.org/10.1074/jbc.m311225200 | PubMed

44. **Schoenfeld AR,** Davidowitz EJ, Burk RD (2000) Elongin BC complex prevents degradation of von Hippel-Lindau tumor suppressor gene products. *Proc Natl Acad Sci U S A* **97**:8507-12 https://doi.org/10.1073/pnas.97.15.8507 | PubMed

45. **Liu J,** Nussinov R (2008) Allosteric effects in the marginally stable von Hippel-Lindau tumor suppressor protein and allostery-based rescue mutant design. *Proc Natl Acad Sci U S A* **105**:901-6 https://doi.org/10.1073/pnas.0707401105 | PubMed

46. **Knauth K,** Cartwright E, Freund S, Bycroft M, Buchberger A (2009) VHL mutations linked to type 2C von Hippel-Lindau disease cause extensive structural perturbations in pVHL. *J Biol Chem* **284**:10514-22 https://doi.org/10.1074/jbc.m809056200 | PubMed

47. **Knauth K,** Bex C, Jemth P, Buchberger A (2006) Renal cell carcinoma risk in type 2 von Hippel-Lindau disease correlates with defects in pVHL stability and HIF-1alpha interactions. *Oncogene* **25**:370-7 https://doi.org/10.1038/sj.onc.1209062 | PubMed

48. **Serghini A,** Portelli S, Troadec G, Song C, Pan Q, Pires DEV, Ascher DB (2023) Characterizing and predicting ccRCC-causing missense mutations in Von Hippel-Lindau disease. *Hum Mol Genet* https://doi.org/10.1093/hmg/ddad181 | PubMed

49. **Brown SP,** Hajduk PJ (2006) Effects of conformational dynamics on predicted protein druggability. *ChemMedChem* **1**:70-2 https://doi.org/10.1002/cmdc.200500013 | PubMed

50. **Johnson DK,** Karanicolas J (2013) Druggable protein interaction sites are more predisposed to surface pocket formation than the rest of the protein surface. *PLoS Comput Biol* **9**:e1002951 https://doi.org/10.1371/journal.pcbi.1002951 | PubMed

51. **Johnson DK,** Karanicolas J (2015) Selectivity by small-molecule inhibitors of protein interactions can be driven by protein surface fluctuations. *PLoS Comput Biol* **11**:e1004081 https://doi.org/10.1371/journal.pcbi.1004081 | PubMed

52. **Leaver-Fay A,** Tyka M, Lewis SM, Lange OF, Thompson J, Jacak R, Kaufman K, Renfrew PD, Smith CA, Sheffler W, *et al.* (2011) ROSETTA3: an object-oriented software suite for the simulation and design of macromolecules. *Methods Enzymol* **487**:545-74 https://doi.org/10.1016/b978-0-12-381270-4.00019-6 | PubMed

53. **Malhotra S,** Andrianov GV, Karanicolas J (no date) A Quantitative View of Protein Surface Druggability: Predicting Maximum Achievable Potency.

54. **Malhotra S,** Karanicolas J (2020) https://github.com/ShipraMalhotra/PocketDruggability

55. **Malhotra S** (2019) Predicting the Most Tractable Protein Surfaces in the Human Proteome for Developing New Therapeutics. University of Kansas.

56. **Johnson DK,** Karanicolas J (2016) Ultra-High-Throughput Structure-Based Virtual Screening for Small-Molecule Inhibitors of Protein-Protein Interactions. *J Chem Inf Model* **56**:399-411 https://doi.org/10.1021/acs.jcim.5b00572 | PubMed

57. **Adeshina YO,** Deeds EJ, Karanicolas J (2020) Machine learning classification can reduce false positives in structure-based virtual screening. *Proc Natl Acad Sci U S A* **117**:18477-88 https://doi.org/10.1073/pnas.2000585117 | PubMed

58. **Davis B** (2013) Screening protein-small molecule interactions by NMR. *Methods Mol Biol* **1008**:389-413 https://doi.org/10.1007/978-1-62703-398-5_14 | PubMed

59. **Aguirre C,** Cala O, Krimm I (2015) Overview of Probing Protein-Ligand Interactions Using NMR. *Curr Protoc Protein Sci* **81**:17 8 1-8 24 https://doi.org/10.1002/0471140864.ps1718s81 | PubMed

60. **Dias DM,** Van Molle I, Baud MG, Galdeano C, Geraldes CF, Ciulli A (2014) Is NMR Fragment Screening Fine-Tuned to Assess Druggability of Protein-Protein Interactions?. *ACS Med Chem Lett* **5**:23-8 https://doi.org/10.1021/ml400296c | PubMed

61. **Lucas X,** Van Molle I, Ciulli A (2018) Surface Probing by Fragment-Based Screening and Computational Methods Identifies Ligandable Pockets on the von Hippel-Lindau (VHL) E3 Ubiquitin Ligase. *J Med Chem* **61**:7387-93 https://doi.org/10.1021/acs.jmedchem.8b00842 | PubMed

62. **Frost J,** Galdeano C, Soares P, Gadd MS, Grzes KM, Ellis L, Epemolu O, Shimamura S, Bantscheff M, Grandi P, *et al.* (2016) Potent and selective chemical probe of hypoxic signalling downstream of HIF-alpha hydroxylation via VHL inhibition. *Nat Commun* **7**:13312 https://doi.org/10.1038/ncomms13312 | PubMed

63. **Soares P,** Gadd MS, Frost J, Galdeano C, Ellis L, Epemolu O, Rocha S, Read KD, Ciulli A (2018) Group-Based Optimization of Potent and Cell-Active Inhibitors of the von Hippel-Lindau (VHL) E3 Ubiquitin Ligase: Structure-Activity Relationships Leading to the Chemical Probe (2S,4R)-1-((S)-2-(1-Cyanocyclopropanecarboxamido)-3,3-dimethylbutanoyl)-4-hydroxy -N-(4-(4-methylthiazol-5-yl)benzyl)pyrrolidine-2-carboxamide (VH298). *J Med Chem* **61**:599-618 https://doi.org/10.1021/acs.jmedchem.7b00675 | PubMed

64. **Walpole S,** Monaco S, Nepravishta R, Angulo J (2019) STD NMR as a Technique for Ligand Screening and Structural Studies. *Methods Enzymol* **615**:423-51 https://doi.org/10.1016/bs.mie.2018.08.018 | PubMed

65. **Calabrese DR,** Connelly CM, Schneekloth JS (2019) Ligand-observed NMR techniques to probe RNA-small molecule interactions. *Methods Enzymol* **623**:131-49 https://doi.org/10.1016/bs.mie.2019.05.030 | PubMed

66. **Hajduk P,** Olejniczak E, Fesik SW (1997) One-Dimensional Relaxation- and Diffusion-Edited NMR Methods for Screening Compounds That Bind to Macromolecules. *J Am Chem Soc* **119**:12257-61 https://doi.org/10.1021/ja9715962

67. **Almeida TB,** Panova S, Walser R (2021) NMR Reporter Assays for the Quantification of Weak-Affinity Receptor-Ligand Interactions. *SLAS Discov* **26**:1020-8 https://doi.org/10.1177/24725552211009782 | PubMed

68. **Osborne J,** Panova S, Rapti M, Urushima T, Jhoti H (2020) Fragments: where are we now?. *Biochem Soc Trans* **48**:271-80 https://doi.org/10.1042/bst20190694 | PubMed

69. **Zhu S,** Cohen MB, Bjorge JD, Mier JW, Cho DC (2013) PI3K inhibition potentiates Bcl-2-dependent apoptosis in renal carcinoma cells. *J Cell Mol Med* **17**:377-85 https://doi.org/10.1111/jcmm.12019 | PubMed

70. **Peng S,** Wang Z, Tang P, Wang S, Huang Y, Xie Q, Wang Y, Tan X, Tang T, Yan X, *et al.* (2023) PHF8-GLUL axis in lipid deposition and tumor growth of clear cell renal cell carcinoma. *Sci Adv* **9**:eadf3566 https://doi.org/10.1126/sciadv.adf3566 | PubMed

71. **Iliopoulos O,** Ohh M, Kaelin WG (1998) pVHL19 is a biologically active product of the von Hippel-Lindau gene arising from internal translation initiation. *Proc Natl Acad Sci U S A* **95**:11661-6 https://doi.org/10.1073/pnas.95.20.11661 | PubMed

72. **Kondo K,** Kim WY, Lechpammer M, Kaelin WG (2003) Inhibition of HIF2alpha is sufficient to suppress pVHL-defective tumor growth. *PLoS Biol* **1**:E83 https://doi.org/10.1371/journal.pbio.0000083 | PubMed

73. **Choueiri TK,** Kaelin WG (2020) Targeting the HIF2-VEGF axis in renal cell carcinoma. *Nat Med* **26**:1519-30 https://doi.org/10.1038/s41591-020-1093-z | PubMed

74. **Budiardjo SJ,** Licknack TJ, Cory MB, Kapros D, Roy A, Lovell S, Douglas J, Karanicolas J (2016) Full and Partial Agonism of a Designed Enzyme Switch. *ACS Synth Biol* **5**:1475-84 https://doi.org/10.1021/acssynbio.6b00097 | PubMed

75. **Deckert K,** Budiardjo SJ, Brunner LC, Lovell S, Karanicolas J (2012) Designing allosteric control into enzymes by chemical rescue of structure. *J Am Chem Soc* **134**:10055-60 https://doi.org/10.1021/ja301409g | PubMed

76. **Wallace EM,** Rizzi JP, Han G, Wehn PM, Cao Z, Du X, Cheng T, Czerwinski RM, Dixon DD, Goggin BS, *et al.* (2016) A Small-Molecule Antagonist of HIF2alpha Is Efficacious in Preclinical Models of Renal Cell Carcinoma. *Cancer Res* **76**:5491-500 https://doi.org/10.1158/0008-5472.CAN-16-0473 | PubMed

77. **Soucy TA,** Smith PG, Milhollen MA, Berger AJ, Gavin JM, Adhikari S, Brownell JE, Burke KE, Cardin DP, Critchley S, *et al.* (2009) An inhibitor of NEDD8-activating enzyme as a new approach to treat cancer. *Nature* **458**:732-6 https://doi.org/10.1038/nature07884 | PubMed

78. **Barrett TD,** Palomino HL, Brondstetter TI, Kanelakis KC, Wu X, Haug PV, Yan W, Young A, Hua H, Hart JC, *et al.* (2011) Pharmacological characterization of 1-(5-chloro-6-(trifluoromethoxy)-1H-benzoimidazol-2-yl)-1H-pyrazole-4-carboxylic acid (JNJ-42041935), a potent and selective hypoxia-inducible factor prolyl hydroxylase inhibitor. *Mol Pharmacol* **79**:910-20 https://doi.org/10.1124/mol.110.070508 | PubMed

79. **Tsubuki S,** Saito Y, Tomioka M, Ito H, Kawashima S (1996) Differential inhibition of calpain and proteasome activities by peptidyl aldehydes of di-leucine and tri-leucine. *J Biochem* **119**:572-6 https://doi.org/10.1093/oxfordjournals.jbchem.a021280 | PubMed

80. **Lee DH,** Goldberg AL (1998) Proteasome inhibitors: valuable new tools for cell biologists. *Trends Cell Biol* **8**:397-403 https://doi.org/10.1016/s0962-8924(98)01346-4 | PubMed

81. **Tetko IV,** Poda GI (2004) Application of ALOGPS 2.1 to predict log D distribution coefficient for Pfizer proprietary compounds. *J Med Chem* **47**:5601-4 https://doi.org/10.1021/jm049509l | PubMed

82. **Ding Z,** German P, Bai S, Reddy AS, Liu XD, Sun M, Zhou L, Chen X, Zhao X, Wu C, *et al.* (2014) Genetic and pharmacological strategies to refunctionalize the von Hippel Lindau R167Q mutant protein. *Cancer Res* **74**:3127-36 https://doi.org/10.1158/0008-5472.can-13-3213 | PubMed

83. **Chittiboina P,** Mandal D, Bugarini A, Asuzu DT, Mullaney D, Mastorakos P, Stoica S, Alvarez R, Scott G, Maric D, *et al.* (2023) Proteostasis Modulation in Germline Missense von Hippel Lindau Disease. *Clin Cancer Res* **29**:2199-209 https://doi.org/10.1158/1078-0432.ccr-22-3651 | PubMed

84. **Kenakin T** (2024) Bias translation: The final frontier?. *Br J Pharmacol* https://doi.org/10.1111/bph.16335 | PubMed

85. **Kenakin T** (2009) Biased agonism. *F1000 Biol Rep* **1**:87 https://doi.org/10.3410/b1-87 | PubMed

86. **Vogelstein B,** Papadopoulos N, Velculescu VE, Zhou S, Diaz LA, Kinzler KW (2013) Cancer genome landscapes. *Science* **339**:1546-58 https://doi.org/10.1126/science.1235122 | PubMed

87. **Morris LG,** Chan TA (2015) Therapeutic targeting of tumor suppressor genes. *Cancer* **121**:1357-68 https://doi.org/10.1002/cncr.29140 | PubMed

88. **Cagiada M,** Johansson KE, Valanciute A, Nielsen SV, Hartmann-Petersen R, Yang JJ, Fowler DM, Stein A, Lindorff-Larsen K (2021) Understanding the Origins of Loss of Protein Function by Analyzing the Effects of Thousands of Variants on Activity and Abundance. *Mol Biol Evol* **38**:3235-46 https://doi.org/10.1093/molbev/msab095 | PubMed

89. **Fayer S,** Horton C, Dines JN, Rubin AF, Richardson ME, McGoldrick K, Hernandez F, Pesaran T, Karam R, Shirts BH, *et al.* (2021) Closing the gap: Systematic integration of multiplexed functional data resolves variants of uncertain significance in BRCA1, TP53, and PTEN. *Am J Hum Genet* **108**:2248-58 https://doi.org/10.1016/j.ajhg.2021.11.001 | PubMed

90. **Elias R,** Tcheuyap VT, Kaushik AK, Singla N, Gao M, Reig Torras O, Christie A, Mulgaonkar A, Woolford L, Stevens C, *et al.* (2021) A renal cell carcinoma tumorgraft platform to advance precision medicine. *Cell Rep* **37**:110055 https://doi.org/10.1016/j.celrep.2021.110055 | PubMed

91. **Convertino M,** Das J, Dokholyan NV (2016) Pharmacological Chaperones: Design and Development of New Therapeutic Strategies for the Treatment of Conformational Diseases. *ACS Chem Biol* **11**:1471-89 https://doi.org/10.1021/acschembio.6b00195 | PubMed

92. **Chiti F,** Kelly JW (2022) Small molecule protein binding to correct cellular folding or stabilize the native state against misfolding and aggregation. *Curr Opin Struct Biol* **72**:267-78 https://doi.org/10.1016/j.sbi.2021.11.009 | PubMed

93. **Fischer ES,** Jones LH (2022) Small molecule modulation of protein polymerization. *Chem Soc Rev* **51**:2392-6 https://doi.org/10.1039/d2cs00070a | PubMed

S1. **Wells JA,** McClendon CL (2007) Reaching for high-hanging fruit in drug discovery at protein-protein interfaces. *Nature* **450**:1001-9 https://doi.org/10.1038/nature06526 | PubMed

S2. **Brown SP,** Hajduk PJ (2006) Effects of conformational dynamics on predicted protein druggability. *ChemMedChem* **1**:70-2 https://doi.org/10.1002/cmdc.200500013 | PubMed

S3. **Johnson DK,** Karanicolas J (2013) Druggable protein interaction sites are more predisposed to surface pocket formation than the rest of the protein surface. *PLoS Comput Biol* **9**:e1002951 https://doi.org/10.1371/journal.pcbi.1002951 | PubMed

S4. **Johnson DK,** Karanicolas J (2015) Selectivity by small-molecule inhibitors of protein interactions can be driven by protein surface fluctuations. *PLoS Comput Biol* **11**:e1004081 https://doi.org/10.1371/journal.pcbi.1004081 | PubMed

S5. **Min JH,** Yang H, Ivan M, Gertler F, Kaelin WG, Pavletich NP (2002) Structure of an HIF-1alpha - pVHL complex: hydroxyproline recognition in signaling. *Science* **296**:1886-9 https://doi.org/10.1126/science.1073440 | PubMed

S6. **Qian B,** Raman S, Das R, Bradley P, McCoy AJ, Read RJ, Baker D (2007) High-resolution structure prediction and the crystallographic phase problem. *Nature* **450**:259-64 https://doi.org/10.1038/nature06249 | PubMed

S7. **Combs SA,** Deluca SL, Deluca SH, Lemmon GH, Nannemann DP, Nguyen ED, Willis JR, Sheehan JH, Meiler J (2013) Small-molecule ligand docking into comparative models with Rosetta. *Nat Protoc* **8**:1277-98 https://doi.org/10.1038/nprot.2013.074 | PubMed

S8. **Johnson DK,** Karanicolas J (2016) Ultra-High-Throughput Structure-Based Virtual Screening for Small-Molecule Inhibitors of Protein-Protein Interactions. *J Chem Inf Model* **56**:399-411 https://doi.org/10.1021/acs.jcim.5b00572 | PubMed

S9. **Malhotra S,** Andrianov GV, Karanicolas J (no date) A Quantitative View of Protein Surface Druggability: Predicting Maximum Achievable Potency.

S10. **Malhotra S,** Karanicolas J (2020) PocketDruggability. GitHub. https://github.com/ShipraMalhotra/PocketDruggability

S11. **Malhotra S** (2019) Predicting the Most Tractable Protein Surfaces in the Human Proteome for Developing New Therapeutics.

S12. **OpenEye Scientific Software** (no date) Omega2. version: 2.5.1.4

S13. **Hawkins PC,** Nicholls A (2012) Conformer generation with OMEGA: learning from the data set and the analysis of failures. *J Chem Inf Model* **52**:2919-36 https://doi.org/10.1021/ci300314k | PubMed

S14. **Hawkins PC,** Skillman AG, Warren GL, Ellingson BA, Stahl MT (2010) Conformer generation with OMEGA: algorithm and validation using high quality structures from the Protein Databank and Cambridge Structural Database. *J Chem Inf Model* **50**:572-84 https://doi.org/10.1021/ci100031x |

PubMed

S15. **Hawkins PC,** Skillman AG, Nicholls A (2007) Comparison of shape-matching and docking as virtual screening tools. *J Med Chem* **50**:74-82 https://doi.org/10.1021/jm0603365 | PubMed

S16. **OpenEye Scientific Software** (no date) ROCS. version: 3.2.1.4

S17. **OpenEye Scientific Software** (2017) OEChem Toolkit. version: 2.1.3

S18. **OpenEye Scientific Software** (no date) QUACPAC. version: . 1.7.0.2 ed

S19. **Adeshina YO,** Deeds EJ, Karanicolas J (2020) Machine learning classification can reduce false positives in structure-based virtual screening. *Proc Natl Acad Sci U S A* **117**:18477-88 https://doi.org/10.1073/pnas.2000585117 | PubMed

S20. **BioSolveIT** (2019) REAL Space Navigator.

S21. **BioSolveIT** (2021) infiniSee. version: 3.2 Andromeda

S22. **Tan S** (2001) A modular polycistronic expression system for overexpressing protein complexes in Escherichia coli. *Protein Expr Purif* **21**:224-34 https://doi.org/10.1006/prep.2000.1363 | PubMed

S23. **Davis B** (2013) Screening protein-small molecule interactions by NMR. *Methods Mol Biol* **1008**:389-413 https://doi.org/10.1007/978-1-62703-398-5_14 | PubMed

S24. **Duvaud S,** Gabella C, Lisacek F, Stockinger H, Ioannidis V, Durinx C (2021) Expasy, the Swiss Bioinformatics Resource Portal, as designed by its users. *Nucleic Acids Res* **49**:W216-W27 https://doi.org/10.1093/nar/gkab225 | PubMed

S25. **Calabrese DR,** onnelly CM, Schneekloth JS (2019) Ligand-observed NMR techniques to probe RNA-small molecule interactions. *Methods Enzymol* **623**:131-49 https://doi.org/10.1016/bs.mie.2019.05.030 | PubMed

S26. **Walpole S,** Monaco S, Nepravishta R, Angulo J (2019) STD NMR as a Technique for Ligand Screening and Structural Studies. *Methods Enzymol* **615**:423-51 https://doi.org/10.1016/bs.mie.2018.08.018 | PubMed

S27. **Huang R,** Leung IKH (2019) Protein-Small Molecule Interactions by WaterLOGSY. *Methods Enzymol* **615**:477-500 https://doi.org/10.1016/bs.mie.2018.08.020 | PubMed

S28. **Kao SH,** Wang WL, Chen CY, Chang YL, Wu YY, Wang YT, Wang SP, Nesvizhskii AI, Chen YJ, Hong TM, *et al.* (2015) Analysis of Protein Stability by the Cycloheximide Chase Assay. *Bio Protoc* **5** https://doi.org/10.21769/bioprotoc.1374 | PubMed

Peer reviews

Reviewer #1 (Public review):

[Editors' note: this version has been assessed by the Reviewing Editor without further input from the original reviewers. The authors have addressed some of comments raised in the previous round of review and have opted to proceed to a Version of Record without additional review.]

Summary:

This is an excellent and strong paper. The authors not only show the mechanisms of action of destabilizing mutations in VHL, but notably, they also go on to computationally design and experimentally test an inhibitor that restores wild-type pVHL function, offering starting points for a new class of kidney cancer drugs. The approach that the authors take here can be used to target destabilizing mutations in repressor proteins, common in diseases, including cancer.

Strengths:

This paper is the culmination of an extraordinary amount of work, over years, including method development and testing by a broad range of tools and experiments. It is thorough and comprehensive. It is also well-written and easy to follow.

https://doi.org/10.7554/eLife.110305.2.sa2

Reviewer #2 (Public review):

Summary:

Inactivating VHL mutations are common in clear cell renal cell carcinoma, and about half of those mutations unfold/destabilize the protein rather than directly interfering with critical protein-protein interactions. The authors identify a compound that can stabilize/refold mutant VHL and seemingly restore its ability to downregulate its major downstream targets.

Strengths:

The authors use a clever combination of virtual and cell-based screens, followed by suitable biophysical and cell-based validation assays, to arrive at a VHL refolder. This compound is suboptimal from an ADME point of view, but could be a starting point for further medicinal chemistry optimization. Success would have implications for other diseases linked to similar loss-of-function mutations.

Weaknesses:

In going from CP4 to CP4.29 the authors screened based on downregulation of HIF. This is logical but also introduces the danger of identifying chemicals that can downregulate HIF in an "off-target" manner i.e. non-specifically. It therefore essential to clearly show that CP4.29 downregulates steady-state levels of HIF and HIF target genes in cells with suitable (hydrophobic core) VHL mutants but not in isogenic cells lacking VHL.

https://doi.org/10.7554/eLife.110305.2.sa1

Author response:

The following is the authors' response to the original reviews.

We are most grateful to both reviewers for providing valuable feedback on our manuscript.

Reviewer 1 had solely favorable comments, with no suggestions for revision.

Reviewer 2 pointed out that experiment evaluating the effect of CP4 on pVHL half-life (originally included as Figure 3c) was difficult to evaluate because of CP4's effect on pVHL abundance prior to cycloheximide treatment. We agree with this assessment, and we opted to remove this experiment from the revised manuscript since it was not central to our overarching conclusions.

Reviewer 2 also pointed out that experiment evaluating the effect of CP4.29 on HIF-2α half-life (originally included as Figure 4g) was not very compelling. We agree with this assessment, and we opted to remove this experiment from the revised manuscript since it was not central to our overarching conclusions.

We agree with Reviewer 2's suggestion that additional experiments could further solidify that C4.29 downregulates HIF2 in a purely "on-target" manner, however we prefer to reserve such studies for the future.

Reviewer 2 also made several valuable suggestions for the text itself (awkward wordings / citations / clearer figure legends). We appreciate this feedback and have updated the text accordingly.

https://doi.org/10.7554/eLife.110305.2.sa0